Handling biological complexity:
as simple as possible but not simpler

Hanna Härdin

The research presented in this thesis was conducted at the department of Molecular Cell Physiology at the VU University Amsterdam, Amsterdam, the Netherlands, and at the Modeling, Analysis and Simulation cluster at Centrum Wiskunde & Informatica, Amsterdam, the Netherlands, and was funded by the Netherlands Organization for Scientific Research (NWO/EW/635.100.007).

This thesis has been reviewed by:
dr. B.M. Bakker, University of Groningen, Groningen
prof.dr.ir. J.J. Heijnen, Delft University of Technology, Delft
prof.dr. J. Heringa, VU University Amsterdam, Amsterdam
prof.dr. U. Kummer, University of Heidelberg, Heidelberg, Germany
prof.dr. H. Lill, VU University Amsterdam, Amsterdam
dr. R.M.H. Merks, Centrum Wiskunde & Informatica, Amsterdam
prof.dr. B. Teusink, VU University Amsterdam, Amsterdam

Printed by Gildeprint drukkerijen B.V., Enschede
ISBN 9789461080486

VRIJE UNIVERSITEIT

Handling biological complexity: as simple as possible but not simpler

ACADEMISCH PROEFSCHRIFT

ter verkrijging van de graad Doctor aan
de Vrije Universiteit Amsterdam,
op gezag van de rector magnificus
prof.dr. L.M. Bouter,
in het openbaar te verdedigen
ten overstaan van de promotiecommissie
van de faculteit der Aard- en Levenswetenschappen
op woensdag 30 juni 2010 om 11.45 uur
in de aula van de universiteit,
De Boelelaan 1105

door

Hanna Maria Härdin

geboren te Hägersten, Zweden

promotoren:	prof.dr. H.V. Westerhoff
	prof.dr.ir. J.H. van Schuppen
copromotoren:	dr. K. Krab
	dr. A. Zagaris

Make things as simple as possible, but not simpler

Albert Einstein, 1879–1955

Abbreviations

EI	enzyme I
EIIA	enzyme IIA
EIICB	enzyme IICB
Glc	glucose
HPr	histidine protein
MCA	metabolic control analysis
ODE	ordinary differential equation
P	phosphate group
PEP	phosphoenolpyruvate
PTS	phosphotransferase system
Pyr	pyruvate
QEA	quasi-equilibrium approximation
QSSA	quasi-steady-state approximation
SIM	slow invariant manifold
ZDP	zero-derivative principle

Contents

Chapter 1

Introduction

Because of the inherent complexity of biochemical systems in living cells, simple models of these systems often fail when tested by the multidimensional experimental data that is now available. On the other hand, more complex models which may reproduce the available data are in general hard to understand and to deal with mathematically. It is therefore of interest to explore methods to make these realistic models as tractable as possible without doing away with their essential complexity.

In this chapter we outline the various aspects of the complexity of biochemical models, we discuss the resulting difficulties with model analysis, and we motivate the need of simplifying biochemical models without oversimplifying them. Subsequently, we introduce the model reduction methods investigated in this thesis, *i.e.*, balanced truncation, a widely used method in the field of control theory, and a method based on the so-called zero-derivative principle which makes use of the fact that biochemical processes in cells occur on a wide variety of timescales. Finally, the aim of this thesis is described and an overview of the chapters is provided.

1.1 The use of models in systems biology

The use of mathematical models for investigating biochemical processes in living cells has accelerated rapidly during the last decade. Model analysis contributes to a better insight in the functional properties of cellular networks, facilitates drug development, and assists in experimental design. The use of modeling has been necessitated by the shift of focus in recent years from, on the one hand, studying the molecules in cells separately (*i.e.*, molecular biology) to, on the other hand, study the cell as a system in which function emerges from the interplay between the molecules—a field which has become known as *systems biology*.

The factors that have contributed to the development of systems biology are several. A major contribution comes from the increased knowledge about the organization of the genetic material which culminated in the accomplishment of the human genome project less than a decade ago and which has further stimulated the developments in functional genomics. This has enabled determination of concentrations and properties of virtually all mRNAs in a living organism, and the same is about to become possible for all proteins and metabolites. The large amount of information that hence can be retrieved is calling for the construction of models. Another contribution to the development comes from the discoveries made during the last century pertaining to the organization of living cells. In particular, the progress in the understanding of the arrangement of the cellular network into functional pathways constituting strongly connected subnetworks which operate relatively independent of each other has enabled the modeling of these processes separately from the rest of the cell as well as the experimental validation of these models. For historical reviews of the development of this field, see *e.g.* Westerhoff & Kell [131], Kitano [68, 69], and Westerhoff & Palsson [134].

1.2 The need for reduction of biochemical models

Mathematical models describing biochemical processes in living cells are often simple, because they have been made in reductionist ways and with the objective to make them tractable by simple mathematics. However, as the complexity of living matter becomes better understood—for instance, we now know that the simplest cell is encoded by more than 300 genes that cannot do without each other [31, 42]—and as experimental methods are developed for verification of the models, those simple models often prove too crude. As a consequence, models with increasing complexity are constructed which are more realistic but also more difficult to understand and to deal with mathematically. In this section we describe the modeling of biochemical systems, in what sense the biological complexity reflects on these models, and we motivate the need for model reduction without oversimplifying the models.

1.2.1 Complexity *in vivo*

One of the most striking features of the biochemical reaction networks underlying the functioning of living cells is their complexity: the processes of transcription, splicing, translation, proofreading of these processes, electron transfer, and signalling cascades

are just a few examples of the innumerable fascinating and highly intricate biochemical processes taking place in the cells. The complexity of living systems has several different aspects. One of these is the large number of molecular components involved in the intracellular processes: the smallest cell contains a few hundred genes [31] and, *e.g.*, the human genome contains between 20 000 and 25 000 genes [62]; according to the central dogma of molecular biology [22, 23], each gene is associated with at least one and in mammalian cells typically several mRNA and protein molecules, and, further, the number of metabolites *e.g.* in human are in the order of several thousands. In other words, the number of molecular species in a cell ranges from thousands up to hundreds of thousands depending on the cell type.

A second contribution to the complexity comes from the nonlinear dependence of the reaction rates on the concentrations of many of the reactants. These nonlinearities stem from the inherent chemical properties of the reactions—this is outlined in Section 1.2.3.

A third aspect of the complexity is the fact that each of the concentrations at one level of cellular organization, such as the metabolome, may well depend on *all* the concentrations of substances at another level, *e.g.* the transcriptome, and this in terms of a democratic hierarchy [133]: for example, exposing a cell to an external stimulus which induces the activation of a signal transduction cascade in the cell typically results in the regulation of the expression of a particular set of genes; the change in gene expression, in turn, may influence other processes and in this way the signal will further propagate and may eventually influence every single concentration in the entire cell [30, 39, 46, 130]. However, a particular stimulus tends to influence certain processes to much larger extents than others; the effect on a major fraction of the cellular processes is often negligible, at least when considering a specific timescale. This organization of the cell into strongly connected subnetworks is necessary for its biological functioning and enables the modeling of these subnetworks separately [16, 15, 53, 116, 119].

In the coming sections we describe how the complexity of biochemical systems *in vivo* reflects on the *in silico* models of these systems. To this end, we shall first give a brief background about the description of biochemical systems by ordinary differential equations (ODEs).

1.2.2 Biochemical systems described by ODEs

In this thesis we consider deterministic biochemical models which are described by ODEs. These models are suitable when the molecular copy numbers of the components involved are sufficiently high for stochasticity to be neglected. Further, this type of description assumes homogeneity of the concentrations in the compartment under consideration, which is approximately obtained when the diffusion is fast enough; then, the more general partial differential equations, which would account for the spacial factor, can be approximated by ODEs.

We will denote the time-dependent variables that describe the system at a given moment *state variables* (in the non-equilibrium thermodynamic context these are denoted *functions of state* [135]). These typically represent concentrations although in some models they may represent functions of some concentrations, *e.g.* a linear

combination or ratio of adenosine phosphates. The values of the n state variables at a given time t are collected in a vector which we denote $x(t)$. The time evolution of x is described by the ODEs

$$\dot{x}(t) = f(x(t)), \tag{1.1}$$

where f is a vector-valued function of n variables with n components. In this thesis, we will denote these ODEs *state equations*. Together with the n initial conditions, $x(0) = x_0$, these equations can be solved to yield the time evolution of the state variables, $x(t)$. The n-dimensional space in which x may assume values is denoted the *state space* and the curve that $x(t)$ follows in the state space is called a *trajectory*.

The rates of change of the state variables given by (1.1) can be expressed in an alternative way emphasizing their explicit dependence on the rates of the reactions in which the molecules are produced and consumed, *i.e.*,

$$\dot{x}(t) = Nv(x(t)) \tag{1.2}$$

where N is the so-called stoichiometric matrix, a constant matrix with n rows and m columns, and v is a vector containing the m reaction rates, which depend on the state variables. These equations are often referred to as the *balance equations* or *mass balances* since they express the law of conservation: the increase in a state variable must equal (or *balance*) the difference between production plus import and consumption plus export.

The entry on the i^{th} row and in the j^{th} column of the stoichiometric matrix N specifies how many molecules of the type represented by the state variable x_i are produced or (if negative) consumed in the reaction with rate v_j. We briefly illustrate this for an example of a small biochemical system with three reactions,

$$\begin{aligned} A &\xrightarrow{v_1} X_1, \\ B + X_1 &\xrightarrow{v_2} 2X_2, \\ X_1 + X_2 &\xrightarrow{v_3} C. \end{aligned} \tag{1.3}$$

We use the lower-case letters a, b, c, x_1, and x_2 to denote the concentrations of the molecules named by the corresponding upper-case letters (a formalism which will be used alternatingly with the common square bracket notation for concentrations in the sequel of this thesis). Here, a, b, and c are constant, the state of the system is given by the two time-dependent state variables x_1 and x_2, and we denote the rates of the three reactions by v_1, v_2, and v_3. The state equations of this system are

$$\begin{aligned} \dot{x}_1 &= v_1 - v_2 - v_3 \\ \dot{x}_2 &= 2v_2 - v_3 \end{aligned}$$

which may be written in the form (1.2),

$$\begin{pmatrix} \dot{x}_1 \\ \dot{x}_2 \end{pmatrix} = \begin{pmatrix} 1 & -1 & -1 \\ 0 & 2 & -1 \end{pmatrix} \begin{pmatrix} v_1 \\ v_2 \\ v_3 \end{pmatrix}.$$

The stoichiometric matrix above contains all information about the network structure given in the chemical equations (1.3)—these are two equivalent representations of the same information.

By writing the state equations in the form (1.2), repetition of the reaction rates occurring in several of the state equations is avoided. This representation is also natural from a biochemical point of view as it separates the network structure, represented by the stoichiometric matrix N, from the typically nonlinear reaction rates, specified in the vector v. The reaction rates typically depend on the concentrations of substrates, products, enzymes and effector molecules—which all may be modeled either as state variables or as constants—and on the constant kinetic parameters which have to be determined from experimental data. This dependence can be modeled in a variety of ways and the choice of kinetic description is guided by the properties of the reaction. Some of the common ways to model the rates are outlined in the following section.

1.2.3 Rate expressions

In this section we first discuss the most accurate way to model reaction rates by mass action kinetics and, subsequently, the approximate rate expressions used much more frequently in biochemistry. Our aim here is to briefly introduce some of the common rate expressions that are relevant for this thesis while for more extensive accounts of the subject we refer the reader to [112, 132].

Mass action kinetics and its limitations

The traditional and most exact way to model rates of chemical reactions is by mass action kinetics. This type of kinetics was first demonstrated empirically in the nineteenth century [47] and later on derived using statistical mechanics [64]. It has been extensively used in chemical engineering *e.g.* to describe the behavior of reacting gases and it is also used to model certain biochemical reactions in cells such as phosphorylation reactions, which are common in signal transduction [66, 99]. Further, it is the basis for the in biochemistry widely used Michaelis–Menten kinetics in the sense that the latter can be derived from mass action kinetics by imposing certain assumptions (see the following section).

According to mass action kinetics, the rate of an elementary reaction (*i.e.*, a reaction with a single mechanistic step) is proportional to the product of the concentrations of the participating molecules. In an example of an elementary reaction in which two different substrate molecules form two product molecules of the same type,

$$A + B \underset{k_r}{\overset{k_f}{\rightleftharpoons}} 2C, \tag{1.4}$$

the *rate in the forward direction*, *i.e.*, the net formation of C and net consumption of A and B, is given by

$$v = k_f ab - k_r c^2$$

where k_f and k_r are denoted *rate constants* and are independent of a, b, and c, but potentially dependent on temperature and pressure. The expressions $k_f ab$ and $k_r c^2$

are the so-called *forward* and *reverse rates*, *i.e.*, the chemical forces driving the forward and reverse reactions, respectively. The exponents of a, b, and c in the rate expression (one, one, and two, respectively) equals the corresponding stoichiometric coefficients in (1.4). This also holds in the general case, *i.e.*, if the stoichiometric coefficient of a molecule is α then its concentration appears with the exponent α in the rate expression. It follows that the rate expressions given by mass action kinetics are nonlinear when there is more than one time-dependent substrate or product (counted stoichiometrically). Since biochemical systems in general involve a large number of reactants they therefore typically exhibit nonlinear dynamics.

Although mass action kinetics serves as the most exact description of elementary reactions, it is nevertheless an inconvenient way to model many biochemical reactions since these typically consist of more than one mechanistic steps that all involve the same component—*i.e.*, the enzyme—plus a varying number of other components—*i.e.*, the sequel of compounds en route from substrates to products. To illustrate this, we consider one of the simplest reactions that may occur in a cell, *i.e.*, an irreversible enzymatic reaction with one substrate and one product,

$$S \xrightarrow{e} P. \tag{1.5}$$

Here, e above the reaction arrow denotes that an enzyme E catalyzes the reaction without being produced or consumed in it. This deceptively simple reaction can be dissected into the more involved elementary reactions of the substrate binding to the enzyme, the possibly effectively irreversible conversion of the substrate to product while in complex with the enzyme, and the subsequent release of the product, *i.e.*,

$$E + S \underset{k_{-1}}{\overset{k_1}{\rightleftharpoons}} ES \xrightarrow{k_2} EP \underset{k_{-3}}{\overset{k_3}{\rightleftharpoons}} E + P. \tag{1.6}$$

Applying mass action kinetics to the three elementary reaction steps yields

$$v_1 = k_1[E][S] - k_{-1}[ES],\ v_2 = k_2[ES],\ v_3 = k_3[EP] - k_{-3}[E][P], \tag{1.7}$$

and the rate of change of the concentrations of the five molecular species involved is then given by

$$\begin{aligned} \frac{d[S]}{dt} = -v_1,\ \frac{[E]}{dt} = -v_1 + v_3,\ \frac{[ES]}{dt} = v_1 - v_2, \\ \frac{[EP]}{dt} = v_2 - v_3,\ \frac{d[P]}{dt} = v_3. \end{aligned} \tag{1.8}$$

Hence, according to mass action kinetics, the behavior of the seemingly simple irreversible enzyme-catalyzed reaction (1.5) is given by the fairly involved set of equations (1.7)–(1.8).

Biochemical reactions often involve considerably more elaborate interactions than the irreversible reaction considered above and, consequently, their mass action kinetic expressions may be even more involved than the expressions (1.7)-(1.8). In fact, intracellular reactions with only one substrate and one product are relatively rare. The most common enzymatic reactions are the bi-bi reactions, involving two substrates

and two products, while even more elaborate reactions with as many as four or five substrates also occur [21]. Moreover, channeling reactions involve the formation of complexes of several enzymes and metabolites from the same pathway; in this way the metabolites can be readily transferred from one enzyme to another [25, 60, 89]. Further, reactions involving polynucleotides, such as translation and transcription, involve gigantic machineries of enzymes and reactants, often involving thousands of components if counting the separate nucleotides and tRNA molecules loaded with amino acids that take part in the formation of mRNA and proteins, respectively. In all these cases, mass action kinetics becomes cumbersome or sometimes even impracticable as this approach requires that the processes are dissected into their numerous elementary steps. It is also often the case that information about binding order and the values of the rate constants is lacking and sometimes not even all the molecules involved are identified. In particular, the determination of the rate constants is often difficult and requires specialized laboratory equipment. However, for many of these advanced biochemical processes one may neglect much of the complexity and treat the entire processes as single reactions and hence model them with simplified rate laws. For example, it may well be relevant to study the rate with which mRNA molecules are formed while neglecting the possibly thousands of elementary reactions involved in this process. Similarly, it is also useful to formulate an overall rate of the reaction (1.5) without taking the elementary steps in (1.6) into account. Some of the simplified—yet less precise—kinetic descriptions frequently used in biochemistry are described in the coming section.

Biochemical kinetics

For enzyme catalyzed reactions, a wide variety of approaches to model the rates have been developed. The best-known are the rate laws of Michaelis–Menten type which are valid when formulated in terms of free substrate and product concentrations, or when the enzyme concentrations are much lower than those of the reactants, as is the case in many metabolic reactions in living cells. The simplest of these rate laws is the famous *Michaelis–Menten equation* which describes the rate of the irreversible enzymatic reaction (1.5). It states that the reaction rate is a hyperbolic function of the substrate concentration, *i.e.*,

$$v = \frac{V_{max}[S]}{K_M + [S]}, \tag{1.9}$$

where V_{max} and K_M are constant parameters. Here, $[S]$ refers to the free concentration of S, *i.e.* the concentration of the substrate that is not bound to the enzyme, which becomes effectively equal to the total concentration of S when the latter is much larger than the total concentration of the enzyme. The expression (1.9) describes both the formation of P and consumption of S ($d[P]/dt = -d[S]/dt = v$) while the dynamics of the enzyme is implicitly described. It serves as an alternative to the kinetic equations (1.7)-(1.8) that are exact also when the total concentration of substrate is not much larger than the total concentration of enzyme. Due to the assumption of irreversibility, this rate expression does not depend on the concentration of product. The rate expression in (1.9) is both more and less complex than

the kinetic expressions in (1.7)-(1.8). It is less complex in the sense of containing fewer state variables whereas it is more complex in the sense that it is nonlinear in $[S]$. This nonlinear behavior dictated by the expression (1.9) is highly important for biochemistry and systems biology and although implicit in (1.7)-(1.8) it is not easily recognized in that equation: when $[S]$ is large ($[S] \to \infty$), the rate reaches a maximum value, V_{max}, and the half maximum rate is achieved for $[S] = K_M$. The *Michaelis constant* K_M provides a measure of the affinity of the substrate to the enzyme: a low value corresponds to a high affinity and *vice versa*. The maximum rate is proportional to the total enzyme concentration e, *i.e.* $V_{max} = k_{cat}e$, where k_{cat} is equal to k_2 in (1.6) and a measure of how quickly the enzyme converts substrate into product and therefore k_{cat} is sometimes referred to as the *turnover rate*. The constants V_{max} and K_M can be determined in enzyme assays in which the rate v is measured for different values of s—for instance by using spectroscopic techniques to monitor the change in concentration of product—and subsequently fitting the parameters to the data using (1.9). These experiments are often relatively easy in comparison with the more difficult ones needed for determining the rate constants in mass action kinetics.

The Michaelis–Menten equation above can be derived from mass action kinetics if two assumptions are made. First, the total enzyme concentration, $[E] + [ES]$, is assumed to be constant (in the sense of being independent of total substrate concentration and time) and, second, the substrate is assumed to be in large excess with respect to the enzyme. The latter assumption implies that when adding (the excess of) substrate to an enzyme assay there will be an initial short phase in which the enzyme binds quickly to the substrate while the concentration of free substrate, $[S]$, remains approximately constant. During this initial phase, the formation of free molecules of product is not yet commenced and hence $[P]$ is also approximatively constant and, consequently, one can then consider $[E]$, $[ES]$, and $[EP]$ as the only dynamic variables. In view of this fast timescale, a virtual steady state is reached in which it holds approximately that $d[ES]/dt = d[EP]/dt = 0$ (and hence also $d[E]/dt = 0$ since $[E]+[ES]$ is constant) and this then holds approximatively during a subsequent phase with slow dynamics. These are exactly the relations used for the derivation of Michaelis–Menten equation, which thus describes the dynamics in the second, slow phase. Similar rate laws to (1.9) can also be derived for more elaborate reactions by applying analogous assumptions—a comprehensive account of this type of rate laws for a large set of biochemical mechanisms is given in the book by Segel [112]. The derivation of a Michaelis–Menten expression from the corresponding mass action kinetics will be reproduced in Chapter 3 of this thesis. To the end of demonstrating the type of nonlinear forms that the biochemical equations can assume, we provide a few of the most common expressions below.

If in addition the irreversible reaction discussed above involves a mixed inhibitor, *i.e.*, an inhibitor I that decreases the apparent maximum rate of the enzyme V_{max}^{app} according to

$$V_{max}^{app} = \frac{V_{max}}{1 + [I]/K_{iu}}$$

and increases the apparent Michaelis constant K_M^{app} (corresponding to a decrease in

affinity) according to

$$K_M^{app} = \frac{K_M(1+[I]/K_{ic})}{1+[I]/K_{iu}}$$

(K_M and V_{max} correspond to the situation when the inhibitor is absent), the rate law assumes the form

$$v = \frac{V_{max}^{app}[S]}{K_M^{app}+[S]} = \frac{\frac{V_{max}}{1+[I]/K_{iu}}[S]}{\frac{K_M(1+[I]/K_{ic})}{1+[I]/K_{iu}}+[S]} = \frac{V_{max}[S]}{K_M(1+[I]/K_{ic})+[S](1+[I]/K_{iu})},$$

where K_{iu} and K_{ic} are inhibition constants.

For a reversible enzyme-catalyzed reaction with one substrate and one product,

$$S \overset{e}{\rightleftharpoons} P,$$

the rate of Michaelis–Menten type reads,

$$v = \frac{\frac{V_f}{K_f}[S] - \frac{V_r}{K_r}[P]}{1+\frac{[S]}{K_f}+\frac{[P]}{K_r}}, \tag{1.10}$$

where V_f and V_r are the maximum rates of the forward and reverse reactions, respectively, and K_f and K_r are Michaelis-type constants representing the inverse affinities of the substrate and the product for the enzyme. The equation (1.10) is sometimes referred to as the *reversible Michaelis–Menten equation.*

As mentioned earlier, the most common reactions in the cell are the bi-bi reactions,

$$A + B \overset{e}{\rightleftharpoons} C + D.$$

These reactions may proceed through various reaction mechanisms which each has its specific Michaelis–Menten type rate law. In the case when A binds before B and C is released before D, *i.e.*,

$$E + A + B \rightleftharpoons EA + B \rightleftharpoons EAB \rightleftharpoons ECD \rightleftharpoons ED + C \rightleftharpoons E + C + D,$$

the rate law becomes

$$v = \frac{\frac{V_f ab}{K_{iA}K_{MB}} - \frac{V_r cd}{K_{MC}K_{iD}}}{D(a,b,c,d)} \tag{1.11}$$

where the denominator D is given by the expression

$$\begin{aligned} D(a,b,c,d) = 1 &+ \frac{a}{K_{iA}} + \frac{K_{MA}b}{K_{iA}K_{MB}} + \frac{K_{MD}c}{K_{MC}K_{iD}} + \frac{d}{K_{iD}} \\ &+ \frac{ab}{K_{iA}K_{MB}} + \frac{K_{MD}ac}{K_{iA}K_{MC}K_{iD}} + \frac{K_{MA}bd}{K_{iA}K_{MB}K_{iD}} + \\ &\frac{cd}{K_{MC}K_{iD}} + \frac{abc}{K_{iA}K_{MB}K_{iC}} + \frac{bcd}{K_{iB}K_{mC}K_{iD}} \end{aligned} \tag{1.12}$$

and where V_f, V_r, K_{MA}, K_{MB}, K_{MC}, K_{MD}, K_{iA}, K_{iB}, K_{iC}, and K_{iD} are the maximum rates, the Michaelis constants, and substrate inhibition constants (deriving from the competition between the reactants for binding the enzyme), respectively. This rate expression can be approximated by a simpler one if it can be assumed that the substrates can bind and products can be released in random order. In this case, the denominator of (1.11) is given by

$$D(a,b,c,d) = 1 + \frac{a}{K_{iA}} + \frac{b}{K_{iB}} + \frac{c}{K_{iC}} + \frac{d}{K_{iD}} + \frac{ab}{K_{iA}K_{MB}} + \frac{cd}{K_{MC}K_{iD}},$$

i.e., also b and c may have inhibitory effects on the enzyme, with strengths modeled by K_{iB} and K_{iC}, while the effect of the third order terms diminishes.

Michaelis–Menten type rate laws may be derived for in principle any reaction mechanism, including cases with various types of inhibitions, regulation by coenzymes and other regulatory elements, reactions with various numbers of substrates and products, and for different binding orders [112]. Because these rate laws, as well as the mass action kinetic ones, are *mechanistic*, *i.e.*, directly derived from the underlying biochemical mechanisms, they are tractable for the investigation of the effects of drug molecules. However, for many biochemical reactions, the reaction mechanism is unknown or information is missing and hence the mechanistic rate laws can not be applied as such. This particularly applies to the more complex cellular processes such as transcription and translation, for which the dissection into elementary reactions is impracticable. Another constraint with Michaelis–Menten kinetics is that the assumptions on which they rely concerning large differences between substrate and enzyme concentrations do not always hold. Moreover, many of the Michaelis–Menten rate laws contain large numbers of parameters and therefore the experimental determination of their values may be time-consuming.

In the cases mentioned above when mechanistic rate laws are unsuitable, various approximate *phenomenological* rate laws may be used instead. These often contain fewer model parameters and require less information about the biochemical system but, however, do not allow for the straight-forward addition of drug molecule involvement as mechanistic rate laws do. Examples of phenomenological rate laws include approaches that model enzymatic reaction rates with *(mosaic) non-equilibrium thermodynamics*, also denoted *log–linear* or *lin–log kinetics* [85, 135, 128, 129], *i.e.*,

$$v = e(k_0 + \sum_{i=1}^{n} k_i \log x_i)$$

where e is the enzyme concentration, $k_0, \ldots, k_n$ are the kinetic constants and $x_1, \ldots, x_n$ are molecular concentrations, and *power law kinetics* [103, 104, 105, 106], *i.e.*,

$$v = ae^b \prod_{i=1}^{n} x_i^{k_i}$$

where a, b, $k_1, \ldots, k_n$ are kinetic constants, e enzyme concentration, and $x_1, \ldots, x_n$ molecular concentrations. Another rate law frequently used to describe various enzy-

matic reactions is the *Hill equation*, *i.e.*,

$$v = V\frac{x^n}{K + x^n},$$

where V and K are nonnegative real constants and n can assume any real number. When n takes on a positive integer value, the equation describes a reaction in which the enzyme must bind n molecules X before the reaction can proceed and when $n = 1$, it is equivalent with the Michaelis–Menten equation 1.9. The Hill equation has also been used to model the rate of gene transcription, in which case v represents the number of mRNA molecules produced per time unit and x is the concentration of a transcription factor [20, 41, 43].

In summary, the kinetic expressions used in the modeling of biochemical reactions have assumed a variety of different nonlinear forms. Common to the expressions of the Michaelis–Menten type is that they consist of ratios of polynomials. As outlined above, for a reaction with one substrate and one product these polynomials are of first order—in (1.10) the terms depend either on $[S]$ or on $[P]$. In the rate law for the much more abundant bi-bi reaction (1.11)-(1.12), the polynomial in the numerator is of second order (it contains terms with ab and cd) and that in the denominator is of third order (involving terms with abc and bcd) and hence the nonlinearities are strongly pronounced here. Naturally, for reactions with more reactants, the polynomials assume even higher orders. Also the phenomenological rate laws mentioned above typically exhibit highly nonlinear dynamics.

1.2.4 Size of the models

The large number of molecular species in living cells and their interdependencies could well result in models with large numbers of dynamic variables. However, the organization of biochemical systems into strongly connected subnetworks (discussed in Section 1.2.1) may enable modeling of these subnetworks separately, *i.e.*, describing only their internal behavior while neglecting or approximating that of the processes that connect them [16, 15, 53, 116, 119]. For example, it is likely, although no one proved this yet, that the concentrations of the metabolites and enzymes in glycolysis depend more strongly and directly on each other than that they depend on *e.g.* the transcription of the majority of the non-glycolytic genes in the cell. Because of this, glycolysis may be modeled with about a dozen of biochemical components, *i.e.*, its metabolites and possibly also the enzymes in this pathway, in stead of describing the dynamics of all the several thousands of molecular components present in the cell. However, with the increased knowledge about biochemical processes and the availability of high-throughput experimental data due to the progress in functional genomics, there has been a tendency in recent years to construct increasingly large models and to extend and join existing models and, consequently, models with hundreds of state variables appear [91, 111]. Several initiatives towards the construction of models describing the dynamic behavior of entire cells have been initiated. One of these is the Silicon Cell project managed by Snoep and Westerhoff (see www.siliconcell.net) in which models of cellular subnetworks are collected in a database. The ultimate aim of this project is to join these models together into a silicon cell, *i.e.*, a replica of a

living cell or a part thereof—such models will consist of thousands or possibly tens of thousands of state variables.

1.2.5 Timescale differences

Another characteristic of biochemical systems are the enormous disparities between the timescales at which different intracellular mechanisms proceed: for instance, Ca^{2+} signalling may occur at the timescale of microseconds to hours [10] while processes involving hormonal regulation may take place on timescales ranging between days to years [4, 44]. These differences are caused by the large differences in the inherent kinetic properties of the molecules, *i.e.*, their binding specificities and turnover rates. The timescale disparities also depend on the difference in abundance of various molecules as is the case in the example of an enzyme-catalyzed reaction where a high concentration of a substrate in comparison to that of its enzyme results in large differences between the rate of change of the substrate concentration, on the one hand, and the rate of change of complex formed between substrate and enzyme, on the other hand. Intracellular processes evolving on slower timescales pertain to changes in gene expression [33].

The timescale differences *in vivo* are reflected on the models by means of vast differences in the parameter values and large timescale separations in the model dynamics. These properties of the models have important implications on their computational tractability as well as on their reducibility—two issues we will return to later.

1.2.6 Problem formulation: the need for simplifications

In Sections 1.2.2-1.2.3 we showed that the state equations of biochemical models typically are highly nonlinear: their right hand sides often consist of ratios of polynomials, which are often of degree two or higher. Further, the models are often relatively large, with tens to hundreds of state variables. This complexity causes a range of different problems with *e.g.* the numerical and analytical computations and the determination of the parameter values—problems which all suggest the need of model simplification. On the other hand, biology is studied much because one wishes to appreciate the true complexity of living systems. Hence oversimplification that models the emergent properties away, is not desirable. Here we discuss the needs for *just enough* simplification.

First of all, the complexity of biochemical models outlined in the previous sections renders their behavior nonintuitive and the function of the underlying systems difficult to fathom [2, 55, 78, 99, 123]. It is therefore of interest to develop methods that enable the extraction of overall patterns from the mass of details, *i.e.* to obtain simplified descriptions of the dynamics which enable an over-all picture of the dynamics.

A second reason for simplification is that the large size, the highly nonlinear dynamics, and the timescale differences in these models sometimes render the times for numerical analysis of the models prohibitively long. When the timescale differences are large in a model, numerical integrators need to take short time steps in order to obtain accurate results also for the fastest changing variables, and this renders the

computation slow. There are nowadays efficient, stiff, integrators which adapt the length of the time steps to the extent of the changes of the state variables along the trajectory, taking short steps when they change quickly and longer steps when they change on a slower timescale [50]. Nevertheless, long computation times remain a problem *e.g.* when repeated calculations are needed for a large set of different parameter values or for different initial conditions. These limitations generate an interest in investigating and developing methods for reduction of these models.

A different aspect of the complexity of biochemical modeling and the need for simplification concerns the need of accurate, mechanism related, kinetic descriptions which are simpler than the corresponding mass action kinetic expressions. Although such descriptions have already been developed for many types of cellular reactions there are nevertheless also many reactions for which the available modeling methods are either prohibitively complicated or insufficiently accurate. In particular, the Michaelis–Menten type kinetics is suitable when its underlying assumptions hold, *i.e.*, when the reactants are present in much higher concentrations than the enzymes; these assumptions hold in many cellular reactions, primarily metabolic ones, but there are also numerous other reactions in which the concentrations of reactants are similar to those of the enzymes or even lower. For example, in signal transduction the product of one reaction may act as an enzyme of another reaction and hence the distinction between enzymes and reactants is often blurred. Therefore, modeling these processes by Michaelis–Menten kinetics may yield inaccurate or erroneous results. Also the phenomenological rate laws are often insufficiently accurate. Because of this, such reactions are often modeled by mass action kinetics in spite of the disadvantages with that [70, 76, 99]. Other cellular reaction mechanisms for which there are few accurate rate laws are those of channeling [86] and sequestration [5, 118]. The modeling of all these processes in perspicuous yet accurate ways constitutes an important challenge in the field of systems biology.

A variety of different approaches to resolve the problems mentioned above have already been developed, see, *e.g.*, the reviews [132, 125, 120]. In the following section we introduce the specific approaches to be taken in this thesis.

1.3 Reduction of biochemical models

Model reduction is the simplification of mathematical models resulting in simpler models that approximate the dynamics of the original ones well. In different fields of study, different types of model reduction have been developed. Accordingly, the term has a somewhat different meaning in different contexts; it may refer either to the reduction of the number of state variables [1] or to the simplification of the right hand side of state equations [109, 114], or both [79, 93]. Further, the approximation error, *i.e.*, the difference between the dynamics of the original and the reduced models may be defined in disparate ways [1, 114]. In this thesis, unless stated otherwise, we use the term model reduction to refer to its broader meaning, *i.e.*, *any* simplification leading to a reduced model which—in some sense (to be specified later)—approximates the behavior of the original model.

Model reduction has a long tradition in biochemistry starting in the beginning of

the twentieth century with the approximation of the mass action kinetic description of an irreversible enzyme-catalyzed reaction by the Michaelis–Menten equation, also known as the Henri–Michaelis–Menten equation. A rate law which is empirically indistinguishable from this equation was first derived by Henri [56, 57], based on the assumption that the free enzyme is at equilibrium with its complexes with substrate and product. A decade later, Michaelis and Menten derived their equation based on the assumption that the enzyme–substrate complex is at equilibrium with free enzyme and free substrate [88]. Such reduction based on equilibrium assumptions has later become known as quasi-equilibrium approximation (QEA). Later on, Briggs and Haldane showed that the Michaelis–Menten equation can be derived under relaxed conditions by assuming that the concentration of enzyme–substrate complex changes on a fast timescale as compared to the concentrations of substrate and product, *i.e.*, by application of a method now known as the quasi-steady-state approximation (QSSA) [12]. Both QEA and QSSA have been employed later in a more general setting to simplify biochemical systems [55]. Other well-known reduction methods include various lumping techniques [79, 93]. In this thesis, two different types of approximation methods are discussed extensively. The first one, consisting of so-called *balancing* and subsequent *truncation*, derives from the area of control theory and has been widely applied within the engineering sciences. The second method, based on the so-called zero-derivative principle (ZDP), is a nonlinear method which is a generalization of the QSSA and which yields reduced systems with higher accuracy than QSSA. In the two upcoming subsections we outline the essential ideas underlying these two model reduction methods.

We here remark that as a preparation, before any model reduction or model analysis is performed, it is useful and common practice first to identify the potential conservation relationships in the model and to use these to eliminate any linear dependencies between the state equations. This simplification procedure results in a system with fewer state variables but with *exactly* the same dynamics as the original system, *i.e.*, it brings about many benefits (including improvement of simulation times and often increased transparency) without any trade-off in accuracy. Accordingly, it is not a regular reduction method in the sense that it does not approximate the dynamics. The procedure is described for instance in [97]. In the appendix of Chapter 3 we apply it to a model of the phosphotransferase system prior to further reduction.

1.3.1 Methods deriving from control theory

As discussed in Section 1.2, the models treated in systems biology are increasing in size, now including models of hundreds of state variables [91, 111]. Models of that size are however not unique to systems biology but appear also in several fields of engineering, *e.g.*, in electronic chip design and for the construction of aerospace structures. Also the work with models in those fields has required model reduction techniques, mainly in order to decrease simulation times. Consequently, the subject of model reduction has already been treated for about thirty years in the area of control theory—a fact raising an interest in exploring the utility of these techniques in a biochemical context. (The area of control theory we refer to is a field distinct of that of

metabolic control theory, the latter more frequently called metabolic control analysis [17].) In most engineering sciences, the models are typically linear and therefore the focus of the development of model reduction techniques has been on linear systems. One of the best-known of these methods consists of balancing and truncation and is the first method that will be treated in this thesis. In this section, we outline some concepts used in the area of control theory that we will need later and we briefly describe the idea underlying balancing and truncation. For a broad introduction to model reduction from the control theory perspective we refer the reader to the book by Antoulas [1].

Control systems

The systems considered in control theory are dynamical systems—recall (1.1)—with additional time-dependent variables denoted *input* and *output* variables, collected in the vectors u and y with k and l variables, respectively. These variables are connected to the dynamical system according to

$$\begin{aligned} \dot{x}(t) &= f(x(t), u(t)), \\ y(t) &= g(x(t), u(t)) \end{aligned} \tag{1.13}$$

and we shall denote this a (nonlinear) *control system*. The state variables, collected in the vector x, are again the time-dependent variables that fully describe the state of the system at a given moment, also known as the functions of state [135].

For model reduction by control theoretical methods the model under study has to be of the form defined above, *i.e.*, input and output variables have to be defined by the investigator. In general, the input variables are one of two types: either they are variables possibly controlled by the experimentalist (in which case biochemists might call them parameters) or, alternatively, they are controlled by external time-dependent processes that are not included in the model (in this case they are more commonly called independent variables). The output variables are typically either time-dependent variables that are experimentally measurable or variables whose time evolution is of interest to study, or both, and as seen from (1.13) they may depend on the state variables. To concretize this, we consider an example of a chain of enzymatic reactions with reactants X_1, ..., X_n and enzymes e_1, ..., e_{n-1},

$$X_1 \underset{\nwarrow}{\overset{e_1}{\rightleftharpoons}} \dots \underset{\nwarrow}{\overset{e_{n-1}}{\rightleftharpoons}} X_n,$$

where this chain is part of a larger system of biochemical reactions and where only X_1 and X_n are involved in reactions with the surrounding system. Here, the input may be chosen as the time-dependent influence of the surrounding system on X_1 and X_n (which should itself be independent of the system that is modeled), modeled by the two functions u_1 and u_2, respectively. The output variables may then, for instance, be chosen as either or both of x_1 and x_n or as some function of these, such as the free energy drop across the pathway; these variables may be of interest to study due to their effect on the surrounding system. In case both x_1 and x_n are chosen, the model

becomes

$$\begin{aligned}
\dot{x}_1(t) &= u_1(t) - f_1(x(t)) \\
\dot{x}_2(t) &= f_2(x(t)) \\
&\vdots \\
\dot{x}_{n-1}(t) &= f_{n-1}(x(t)) \\
\dot{x}_n(t) &= f_n(x(t)) - u_n(t) \\
y(t) &= \begin{pmatrix} x_1(t) \\ x_n(t) \end{pmatrix},
\end{aligned}$$

where only the state variables x_1 and x_n depend directly on the input variables. For more general systems, the input and output variables may be chosen analogously, *i.e.*, based on their interactions with the surrounding system.

Linear control systems

As already mentioned, most of the systems treated in control theory are *linear*, *i.e.*, they are control systems in the form

$$\begin{aligned}
\dot{x}(t) &= Ax(t) + Bu(t) \\
y(t) &= Cx(t) + Du(t)
\end{aligned} \tag{1.14}$$

where x, u, and y are n-, k-, and l-dimensional vectors, respectively, and A, B, C, and D are constant matrices with dimensions $n \times n$, $n \times k$, $l \times n$, and $l \times k$. A nonlinear model in the form (1.13) may be *linearized*, *i.e.*, approximated by a linear model, in order to enable application of analysis and reduction techniques that require the models to be linear. Linearization is performed locally at a state x_p and for a given constant input function u_p and consists of determination of the matrices A, B, C, and D as functions of f, g, x_p, and u_p—this is described in the algorithm in Chapter 2. The state variables in the linearized system approximate the deviations from x_p in the nonlinear model and the input of the linear model is the deviation of the input in the nonlinear model from u_p.

Model reduction in control theory

In the field of control theory, model reduction of a system Σ in the form (1.13) is the determination of an approximant system $\hat{\Sigma}$ that has *fewer state variables* than Σ and that exhibits dynamics *similar* to that of Σ, in terms of some norm which measures the difference between the dynamics of the two systems. For most methods, the control system to be reduced, Σ, has to be linear and then the resulting system $\hat{\Sigma}$, is also linear. The number of state variables in the reduced system is to be determined by the investigator based on a trade-off between the desired simplicity and accuracy of the reduced system.

Reduction of linear control systems

Reduction techniques for linear control systems project the dynamics in the state space onto a lower-dimensional linear subspace by transformation and subsequent truncation. A transformation of the linear system (1.14) by a matrix S, *i.e.* a substitution $x_s = Sx$ of the state variables where S is $n \times n$ and of rank n (and hence x_s is an n-dimensional vector), results in the new linear system of the same size as the original one, *i.e.*,

$$\begin{aligned} \dot{x}_s(t) &= SAS^{-1}x_s(t) + SBu(t) \\ y(t) &= CS^{-1}x_s(t) + Du(t). \end{aligned}$$

Truncation, *i.e.* the elimination of the last $n - n_r$ transformed state variables, can then be performed by a transformation with an $n_r \times n$ truncation matrix $R = (I\ 0)$ where I is an $n_r \times n_r$ identity matrix and 0 is an $n_r \times n - n_r$ zero matrix. The resulting system is given by

$$\begin{aligned} \dot{x}_r(t) &= RSAS^{-1}R^T x_r(t) + RSBu(t) \\ y(t) &= CS^{-1}R^T x_r(t) + Du(t), \end{aligned}$$

where the new state vector x_r contains the first n_r state variables in x_s. We here use the superscript T to denote the transpose of a matrix and we will employ this notation in the sequel of this thesis. The new model matrices $RSAS^{-1}R^T$, SB, $CS^{-1}R^T$, and D have the dimensions $n_r \times n_r$, $n_r \times k$, $l \times n_r$, and $l \times k$, respectively.

The aim of the transformation step is to define the new state variables in such a way that the final truncated system, with only the first n_r transformed state variables, well approximates the dynamics of the full system. There are many strategies to design the transformation matrix S and one of the best-known ways is the procedure of balancing outlined below.

Balancing

The idea of balancing is based on the concept of the so-called *energies* of the input and output functions, which are defined as

$$\begin{aligned} E_r &= \int_0^\tau u^T(t)u(t)dt \\ E_o &= \int_0^\tau y^T(t)y(t)dt, \end{aligned}$$

respectively. We remark that these entities are not related to energy as the term is used in physical and biochemical contexts. For linear systems, it can be shown that the *minimal* energy of the input function ϵ_r required to steer the system from the steady state to any state $\bar{x}$ during a time τ and the *maximal* observation energy ϵ_o obtained when the initial state is $\bar{x}$ can be expressed as

$$\epsilon_r = \min E_r = \bar{x}^T P^{-1}\bar{x} \text{ and } \epsilon_o = \max E_o = \bar{x}^T Q\bar{x}, \tag{1.15}$$

respectively, where P and Q are the so-called reachability and observability Grammians which are defined as the matrices

$$P = \int_0^\infty e^{At} B B^T e^{A^T t} dt \text{ and } Q = \int_0^\infty e^{A^T t} C^T C e^{At} dt,$$

where A, B, are C are matrices of a linear system of the form (1.14). The minimum input energy of a state $\bar{x}$ is a measure of how much the input function needs to deviate from 0, integrated over time, in order for the system to assume the state $\bar{x}$ when time goes towards infinity ($u = 0$ corresponds to $u = u_p$ in the nonlinear model since the input in the linearized model represents the deviation from the reference input value u_p). The maximum output energy is a measure of how much the output function deviates from the steady output value upon starting in $\bar{x}$, also integrated over time. If only a small input energy is needed for the system to assume a given state, *i.e.* the state is easily reachable, and if starting in this state causes the output to change much from its reference value, *i.e.* the state is easily observable, then this state will be highly 'important' for the dynamics in the model and *vice versa*. In this notion of importance, balancing and truncation aims at extracting the model dynamics that is important; this is described in detail in Chapter 2.

Whether this notion of importance is appropriate depends on the model and what it is used for. It has shown proper for the many linear systems to which the method has successfully been applied. For linearizations of biological models this choice is less obvious; for instance, in non-equilibrium thermodynamics of biology, away from the Onsager region, one may have states quite far away from equilibrium that are difficult to achieve by random fluctuations but which play an important rule for the dynamics of the model. On the other hand, it is conceivable that there may be many cases in biology where the states that are easily reachable and observable indeed have a major influence on the dynamics.

The aim of extracting dynamics that is easily reachable and easily observable is achieved by first transforming the model such that every state variable has equal influence on the model in these two aspects, *i.e.*, balancing. A transformation of a linear system of the form (1.14) by a matrix K results in Grammians of the transformed system given by KPK^T and $K^{-T}QK^{-1}$. (The superscript $-T$ denotes that the matrix is both inverted and transposed.) A balancing transformation S of a linear system is a transformation which renders the reachability and observability Grammians equal and diagonal with the entries on the diagonals arranged in decreasing order, *i.e.*,

$$SPS^T = S^{-T}QS^{-1} = \begin{pmatrix} \sigma_1 & & 0 \\ & \ddots & \\ 0 & & \sigma_n \end{pmatrix},$$

where $\sigma_1 > \ldots > \sigma_n > 0$ are the eigenvalues of the balanced Grammians. There exist several algorithms to construct a balancing transformation matrix S with these properties given a linear system [1, 3].

Because the Grammians of the balanced system are diagonal, the state represented by the i^{th} unit vector (*i.e.*, a vector with a 1 in the i^{th} entry and zeros in all others) in the transformed basis requires a minimal input energy of $\epsilon_r = 1/\sigma_i$ to reach and

generates a maximal output energy of $\epsilon_o = \sigma_i$, *i.e.*, the values of the two energies are inverses of each other—cf. (1.15). In other words, the state variables in the balanced basis which requires much energy to reach, *i.e.*, is difficult to reach, also generates small output energy, *i.e.*, is difficult to observe. The ordering and equalization of the eigenvalues of the two Grammians thus ensures that the last state variables, which are eliminated in the truncation step, correspond to states which both are difficult to reach and difficult to observe and, with the notion of importance that was briefly outlined above, these variables hence have little influence on the dynamics.

In this section we have introduced several involved concepts in only brief terms; in Chapter 2 we describe these concepts and the idea behind balancing in detail.

1.3.2 Methods based on timescale separation

The second type of model reduction technique treated in this thesis, *i.e.* the ZDP, derives from geometric singular perturbation theory and dynamical systems theory, areas within applied mathematics. This method performs the reduction by extracting the slow behavior from models exhibiting timescale separation and it is based on the presence of slow manifolds in their state space towards which the trajectories are attracted.

Model reduction by approximation of SIMs

As discussed in Section 1.2.5, biochemical systems typically exhibit a wide range of timescales at which the processes in the system proceed [54, 95, 98]. During the course of the fast timescales (*i.e.*, over a short initial time span), certain processes are virtually stagnant while others proceed essentially independently of these. At slower timescales (*i.e.*, over longer time periods), the latter (*fast*) processes seem to evolve coherently with the former (*slower*) ones. In the example of the enzyme-catalyzed conversion of a substrate to a product, the fast timescale corresponds to an initial, short phase where the concentration of the enzyme–substrate complex quickly moves to a different value while the substrate concentration remains approximately constant, and the slow timescale to the subsequent, longer phase where both concentrations change slowly with the concentration of the complex constrained by that of the substrate. This behavior gives rise to the phenomenon that the trajectories in the state space quickly move towards, and subsequently reside close to, a type of attractors called *slow invariant manifolds* (SIMs)—a detailed description of this behavior is provided in Chapter 3. A manifold is a space embedded in a larger space, *e.g.* a 2-dimensional surface in a volume, or a 1-dimensional curve on a plane; in biochemical models the state spaces are often of higher dimensions than 3 and a SIM may be of any dimension smaller than that of the state space. The notion that the SIM is invariant refers to the fact that when the initial values of the state variables lie within the SIM, their values will remain within the SIM as the system develops over time.

Since the initial movement of the state variables towards the SIM is much faster than the subsequent movement along the manifold, the system will spend a large part of its time close to this manifold. Therefore, a simplified description of the system dynamics can be achieved by neglecting the fast dynamics and only incorporating the

dynamics of the behavior on the SIM into the model. In this way, one reduces the number of state variables to the same number as the dimension of the SIM.

The QSSA

The best-known model reduction method of the type described above is the QSSA. This method assumes that the fast state variables are in quasi-steady state with respect to the slow ones, *i.e.*, for a dynamical model with state variables $x = (x_s, x_f)$, where x_s and x_f are vectors containing the fast and slow variables, respectively, and with state equations

$$\begin{aligned} \dot{x}_s &= f_s(x_s, x_f) \\ \dot{x}_f &= f_f(x_s, x_f) \end{aligned} \tag{1.16}$$

the SIM can be approximated by the set of points in the state space fulfilling the equation

$$f_f(x_s, x_f) = 0. \tag{1.17}$$

The decomposition of the state vector into a slow component x_s and a fast component x_f is to be performed by the investigator and it is typically performed based on experience stemming from experimental results. If an analytical expression $x_f = g(x_s)$ fulfilling the equation (1.17) is available, it can be used to construct a reduced model by substitution into the state equation for x_s in 1.16.

The QSSA has proven highly accurate in cases when the timescale separation is large which can readily be the case in *e.g.* the enzyme catalysis example above. However, when the timescale separation is moderate, as is the case in *e.g.* many signal transduction pathways, this approximation may not be sufficiently accurate. Several extensions of the QSSA have been developed in order to achieve more accurate reduced models [32, 113, 110]. These extensions all require the identification of a small parameter which measures the timescale disparity. This identification is fairly involved already for small biochemical models with only a few state variables (see *e.g.* [115]) and for the large nonlinear models common to biology it readily becomes prohibitive.

The ZDP

The second reduction method treated in this thesis is based on the ZDP. It offers a sequel of increasingly accurate refinements of the QSSA [40, 139] which do not require the identification of the small parameter discussed above. For a model of the form (1.16) the ZDP approximation of order m is given by

$$\frac{d^m x_f}{dt^m} = 0$$

where the m^{th} time derivative of x_f is given by the $(m-1)^{st}$ time derivative of $f_f(x_s, x_f)$. The ZDP has been employed to obtain accurate, yet simplified descriptions of complex models arising in meteorology [81], computational physics [77, 126], and more general multiscale systems [138, 140], but not yet in the current biochemical context.

1.4 Aim and outline of this thesis

In this thesis, the reduction of biochemical models by two types of model reduction methods is explored. The aim is to investigate the performance of these methods in the biochemical context. The first method we shall investigate is the linear method of balancing and truncation widely used previously for various engineering purposes. This method primarily addresses the problem of long computation times discussed in Section 1.2.6. Subsequently, we shall explore the nonlinear method based on the ZDP and develop it for enzyme kinetics. With this method we shall address all the issues pertaining to complexity that were raised in Section 1.2.6.

In **Chapter 2** we treat the method of balancing and truncation which requires a linearization of the nonlinear biochemical model. We describe the method and outline its underlying idea. Then, we demonstrate the use of this method for a realistic model of glycolysis in yeast with thirteen state variables. We show that the method can reduce this model to a linear model with only five state variables which approximates the behavior of the original model when the values of the input function remain close to the steady state input. However, for deviations of the input from the point at which the linearization was performed, the linearization becomes inaccurate and hence the reduction fails. We also used the information obtained from the balancing procedure to extract information about the importance of the different state variables for the model dynamics and we then used this information to construct a reduced model with the least important state variables eliminated.

Because the method above is restricted by the inaccuracy of the linearization, a natural next step was to explore a nonlinear method such as the ZDP. In **Chapter 3** we develop a highly accurate enzyme kinetics based on the ZDP which is suitable for describing systems with moderate timescale separation such as many signal transduction pathways. We demonstrate the method for two systems: first, analytically, for a prototypical example with a reversible enzymatic reaction and, second, in a numerical setting, for a substantially more complex system, *i.e.* the phosphotransferase system (PTS). The PTS is a signal transduction pathway regulating and catalyzing glucose uptake in enteric bacteria and regulating a multitude of other processes in response to changes in glucose levels. In both cases, we demonstrate that our results are more accurate than those obtained by the QSSA. Moreover, this chapter also serves to present the theory underlying ZDP to a biochemically oriented readership including a detailed description of the formation of a SIM for a concrete example of a reversible enzyme reaction—previously, this theory has only been available in the more technical mathematical literature.

In **Chapter 4** we describe in detail the numerical algorithm that we used to reduce the phosphotransferase system in Chapter 3. In **Chapter 5**, we show that the numerically determined SIM of the phosphotransferase system can be used to retrieve interesting information about the slow dynamics of this system. Finally, in **Chapter 6** the main results are summarized and discussed and directions for future work are suggested.

Chapter 2

Simplification of a model of glycolysis in yeast based on balancing

The method of balancing and truncation is one of the best-known reduction methods deriving from the area of control theory. In this chapter we apply this method to a realistic nonlinear model of glycolysis in yeast with 13 state variables. Since this method is formulated for linear models, the glycolysis model first had to be approximated by a linear model. This approximation however resulted in relatively large errors when comparing the time courses of the linear model with those of the original one. These results suggest that important metabolic pathways may be inherently complex in the sense that they cannot be linearized without losing much dynamic information. We then employed the information obtained implicitly from the balancing procedure to estimate the relative importance of the various state variables for the dynamics of the model. To account for nonlinear effects, we performed this analysis at a variety of linearization points. We found, in particular, that the state variables representing the concentrations of NADH and acetaldehyde only have a very small influence on the dynamics of the model. Reducing the nonlinear model by approximating these state variables by their steady state values resulted in a nonlinear reduced model which accurately approximated the original model.

2.1 Introduction

One of the most established model reduction methods that originates from the area of control theory is the method of balancing and subsequent truncation. This method was developed in the early eighties by Moore [87] and has since then been widely used within the engineering sciences in order to reduce computation times for models describing *e.g.* electronic chips and aerospace structures. Yet, the performance of the method for reduction of biochemical models had not been explored at the time our work was initiated and hence this task was a natural first approach to the project on simplification of biochemical models presented in this thesis.

Balancing is a transformation of a model, rendering the state variables of the new linear model linear combinations of those in the original one. The objective of this transformation is to achieve a new model in which the state variables are ordered according to their importance for the dynamics. This is achieved through balancing the influence of input variables on state variables, on the one hand, with the influence of state variables on output variables on the other hand; this objective will be outlined in more detail in this chapter. Because the balancing results in ordering of the state variables according to their importance, it ensures that the subsequent truncation—*i.e.*, the elimination of the last state variables—amounts to a simplification that has the smallest possible effect om system dynamics, at least according to this criterion.

Similar to many of the methods deriving from control theory, balancing is a linear method, *i.e.*, it requires the model to be reduced to be linear, and the resulting reduced model also becomes linear albeit with fewer state variables than the original one. Since biochemical models typically are nonlinear they need to be linearized, *i.e.*, approximated with linear models, prior to the balancing and truncation. The dynamics of such a linear model accurately approximates that of the original nonlinear model when the input and state variables assume values close to the point at which the linearization was performed while with increasing deviations from this point, the accuracy decreases.

In this chapter we explore the usefulness of balancing for a realistic model with thirteen state variables of glycolysis in yeast [122]. The glycolysis is one of the most well-studied metabolic pathways and is present in nearly all organisms, with relatively small variations. It fulfills the important task to break down energy-rich glucose through a chain of reactions and use the resulting free energy to produce ATP from ADP plus phosphate and to reduce NAD into NADH. One of the last products in the chain of reactions is pyruvate which is a carbon substrate for growth and a substrate for further free energy harvest, aerobically. The glycolysis has been studied in particular detail in yeast since its glycolysis pathway has a high similarity to that in human while it is simpler to study. Many mathematical models of the glycolysis pathway have been made and several of those describe that in yeast [2, 24, 61, 100, 122]. The model that we study here is based on experimental measurements of a majority of the kinetic constants and is carefully validated by experimental data.

We first apply linearization, balancing, and truncation to the glycolysis model, which results in relatively large approximation errors already in cases when the input and state variables deviate only modestly from the point at which the model was linearized. Then, we turn the focus from reduction of simulation times to another

aim of simplifications, *i.e.*, achieving insight about a system; by interpreting the information given by the coefficients in the linear combinations defining the balanced state variables we estimate the importance of the different state variables for the dynamics of the model. We then use this information to construct a nonlinear reduced model which approximates the dynamics of the original nonlinear model with higher accuracy. Because our analysis of the importance of state variables is based on the interpretation of the information obtained from balancing, we put a relatively large emphasis on the theoretical idea underlying balancing in this chapter; this is provided in the next section.

Part of the work presented in this chapter has been presented in our publications [14, 51]. Whilst our work was performed, similar work was published [80] yet differing from ours as discussed in the Discussion chapter of this thesis.

2.2 The method of linearization, balancing, and truncation

In this section, we aim to provide a brief background about the method of linearization, balancing, and truncation for the reader with a background in biochemistry, systems biology, or similar. In the coming four subsections we describe the performance of the method and in the last two subsections we outline the idea behind it and briefly describe the properties of a balanced model. For further details about the method we refer the reader to Chapter 7 in the book by Antoulas [1] and the article from which the method originates [87].

2.2.1 The model to be reduced

The reduction method consisting of linearization, balancing, and truncation requires the biochemical model that is to be reduced to be expressed in terms of state, input, and output variables, as collected in the vectors $x(t)$, $u(t)$ and $y(t)$, respectively. The state variables $x(t)$ are variables that fully describe the state of the system and which in biochemical literature often are referred to as the internal variables and in the thermodynamics literature as the state functions. The input variables $u(t)$ are in general either of two types: either they are variables controlled by the experimentalist or, alternatively, they are controlled by external time-dependent processes that are not included in the model. The output variables $y(t)$ are typically either variables that are experimentally measurable or variables whose time evolution is of interest to study, or both, and they are mostly functions of the state and sometimes also of input variables. The model to be reduced needs to be on the form of a control system, *i.e.*,

$$\begin{aligned} \dot{x}(t) &= f(x(t), u(t)), \\ y(t) &= g(x(t), u(t)). \end{aligned} \tag{2.1}$$

An example of the reformulation of a biochemical model consisting of a set of ODEs—cf. (1.1)—into a control system of the form above was provided in the Introduction to this thesis and in the next section of this chapter we demonstrate it for a model of glycolysis in yeast.

For a given input function $u(t)$ and given initial conditions $x(0) = x_0$, the output function $y(t)$ is uniquely defined under the dynamics of the model (2.1) and hence this model describes how the dynamics of the output variables may be modified by the input function. Consequently, the model describes a map from input to output, which we will denote the *input-to-output map* without delving into technical details of its definition. Naturally, this map depends on the dynamics of the state variables; neglecting the direct influence of the input on the output (*i.e.*, the dependence of g on $u(t)$ in (2.1)) this map can be partitioned into one map from u to x, the *input-to-state map*, and another from x to y, the *state-to-output map*. The objective of reduction methods deriving from control theory is to approximate the dynamics of the input-to-output map by a simpler such map. The particular reduction method consisting of balancing and truncation achieves this goal by means of reducing the input-to-state and the state-to-output maps to equal extents: balancing ensures that each state variable in the balanced model influences the dynamics of the input-to-state map to the same extent as it influences the dynamics of the state-to-output map and truncation consists in elimination of those state variables with least influence on both of these maps. This idea behind balancing and truncation is described in detail in Section 2.2.5.

2.2.2 Linearization

Linearization is carried out at reference values u_s and x_s of the input and state variables, respectively. The reference value of the state (x_s) may for instance be set to a steady state determined for the constant input function $u(t) = u_s$, *i.e.*, a value x_s which fulfills $f(x_s, u_s) = 0$. The linear model which approximates the dynamics of the nonlinear model (2.1) when the input and state variables assume values close to the reference values is given by

$$\begin{aligned} \dot{x}_l(t) &= Ax_l(t) + Bu_l(t), \\ y_l(t) &= Cx_l(t) + Du_l(t) \end{aligned} \tag{2.2}$$

where $u_l(t)$ is the deviation of the input from its reference value, *i.e.* $u_l(t) = u(t) - u_s$, and A, B, C, and D are the Jacobians

$$\begin{aligned} A &= \left.\frac{df(x,u)}{dx}\right|_{(x_s,u_s)}, \; B = \left.\frac{df(x,u)}{du}\right|_{(x_s,u_s)}, \\ C &= \left.\frac{dg(x,u)}{dx}\right|_{(x_s,u_s)}, \; D = \left.\frac{dg(x,u)}{du}\right|_{(x_s,u_s)}.^{1} \end{aligned} \tag{2.3}$$

Denoting the dimensions of the vectors x, u, and y by n, m, and k, respectively, the dimensions of the constant (for a given reference state; they would vary when going to a different reference state) matrices A, B, C, and D are $n \times n$, $n \times m$, $k \times n$, and $k \times m$, respectively. The new state variables of the linearized system, x_l, approximate the deviation of the original variables from their reference state x_s, *i.e.*

[1] The vertical bars in the expressions of the Jacobians denote evaluation of the expressions to the left of the bars at the values specified at the bottom right of the bars.

$x_l(t) \approx x(t) - x_s$, and the new output variables $y_l(t)$ approximate the deviations from the steady output values of the nonlinear model achieved when applying the constant input u_s, *i.e.*, $y_l(t) \approx y(t) - y_s$ where $y_s = g(x_s, u_s)$. We remark that the linearized model is of the same *order* as the original model, *i.e.*, the new state vector x_l is of dimension n. Here, and in the sequel of this chapter, the notion *order of a model* refers to its number of state variables.

2.2.3 Balancing

The next step, *i.e.* the balancing, is a transformation of the linear model (2.2)–(2.3) into another linear model of the same order but with state variables given by $x_b(t) = Sx_l(t)$ where S is a nonsingular $n \times n$ matrix. The transformed, or *balanced*, model is given by substitution of $x_l(t) = S^{-1}x_b(t)$ into the linear model equations (2.2), yielding

$$\begin{aligned} \dot{x}_b(t) &= A_b x_b(t) + B_b u_l(t), \\ y_l(t) &= C_b x_b(t) + D_b u_l(t) \end{aligned} \tag{2.4}$$

where

$$A_b = SAS^{-1}, B_b = SB,\ C_b = CS^{-1},\ D_b = D.$$

The balancing transformation matrix S has specific properties which ensure that the final reduced model (which will be achieved after the subsequent truncation) efficiently approximates the dynamics of the linear (unbalanced) model (2.2). These properties pertain to the so-called reachability and observability Grammians of the balanced model. The reachability and observability Grammians for a linear model of the form (2.2) are defined as

$$P = \int_0^\infty e^{At}BB^T e^{A^T t}dt \text{ and } Q = \int_0^\infty e^{A^T t}C^T Ce^{At}dt, \text{ respectively.} \tag{2.5}$$

In the equation above, e^{At} and $e^{A^T t}$ are matrix exponentials and are hence both $n \times n$ matrices.[2] Consequently, also P and Q are of dimension $n \times n$. A flavor of the meaning of the Grammians is given by considering a case when the state, input, and output variables are all 1-dimensional. If $A = -k$, then P becomes $B^2/2k$. This Grammian gives an indication of the homeostatic capacity of the system, *i.e.*, how fast it is brought to a steady state, described by k, and of the extent to which perturbations (the input) influences the intrasystem dynamics (the state), modeled in B. In this sense, P is associated with reachability: P relates to the way that a state is reached by the input, *i.e.*, how the intrasystem responds to perturbations. Similarly, in the same 1-dimensional case, the observability matrix Q becomes $C^2/2k$. Here, C

[2] A matrix exponential is a matrix function which for an arbitrary square matrix M is defined as

$$e^M = \sum_{i=0}^{\infty} \frac{M^i}{i!} = I + M + \frac{MM}{2!} + \frac{MMM}{3!} + \ldots,$$

where I is the identity matrix of the same dimension as M.

indicates how strongly the intrasystems dynamics influence the observation variable y, and in this sense Q is related to observability. The interpretation of P and Q is discussed in more detail in Section 2.2.5.

A transformation of the linear model (2.2) by an *arbitrary* transformation matrix K results in Grammians of the transformed model given by KPK^T and $K^{-T}QK^{-1}$, respectively. The balancing transformation matrix S is constructed such that the reachability and observability Grammians of the new, balanced model become equal and, furthermore, both become diagonal matrices with the non-negative eigenvalues on the diagonals arranged in decreasing order, *i.e.*,

$$SPS^T = S^{-T}QS^{-1} = \begin{pmatrix} \sigma_1 & & 0 \\ & \ddots & \\ 0 & & \sigma_n \end{pmatrix} \text{ where } \sigma_1 > \ldots > \sigma_n > 0. \tag{2.6}$$

The idea behind this particular arrangement of the Grammians is described in Section 2.2.5. There are several different algorithms to calculate a matrix S with the properties described above and the algorithm that we used for the calculations in this chapter is given in Appendix 2.A.

For a linear model of the form (2.2) and with Grammians P and Q given by (2.5), the *Hankel singular values* (HSVs) are defined as the square roots of the eigenvalues of the matrix product PQ. The values $\sigma_1, \ldots, \sigma_n$ are the eigenvalues of both the balanced Grammians—see (2.6)—and these values are hence also the HSVs of the balanced model. (Furthermore, from the definition of HSVs it follows that these are invariant under a linear transformation of the model and hence the HSVs of the linear unbalanced model are also $\sigma_1, \ldots, \sigma_n$.) The decreasing order of the HSVs in the balanced model ensures that its state variables are ordered according to their influence on the dynamics and the equalization of the two Grammians ensures that each state variable in the balanced model influences the input-to-state map to the same extent as it influences the state-to-output map; this is described in Section 2.2.5.

2.2.4 Truncation

Truncation is the elimination of the last $n - n_r$ state variables in the balanced model where n_r is the order of the resulting reduced model. The elimination consists in setting these variables to 0, *i.e.*, their steady state values. The reduced model is hence given by

$$\begin{aligned} \dot{x}_r(t) &= A_r x_r(t) + B_r u_l(t), \\ y_r(t) &= C_r x_r(t) + D_r u_l(t) \end{aligned} \tag{2.7}$$

where the state variables and the system matrices are given by

$$x_r = Rx_b,\ A_r = RA_bR^T,\ B_r = RB_b,\ C_r = C_bR^T,\ \text{ and } D_r = D_b.$$

and where $R = (I\ 0)$ is a truncation matrix being the association of an $n_r \times n_r$ identity matrix I and an $n_r \times (n - n_r)$ zero matrix 0.

The reduced model is an approximation of the linearized model (2.2), and the output variables of the linearized system (y_l) approximate the deviation from the steady output (y_s) in the original system (1.13); consequently, the output of the original model is approximated by $y(t) \approx y_s + y_r(t)$.

The number of state variables in the reduced model, which may be $1 \leq n_r < n$, is to be determined by the investigator. Guidance in this choice may be obtained from the HSVs of the linear model: the relative values of these represent the importance of the corresponding balanced state variables and hence a large difference between the m^{th} and $(m+1)^{st}$ HSVs suggests that $n_r = m$ may be a suitable choice. Often it is the case that the gap between several of the pairs of consecutive HSVs is large and hence that n_r may be chosen in several ways. In these cases the choice is based on a trade-off between the desired simplicity and accuracy of the reduced model.

2.2.5 The idea behind balancing

As described in Section 2.2.3, balancing amounts to diagonalization of the reachability and observability Grammians P and Q, respectively, and equalization and ordering of the HSVs. In this section we discuss the idea behind this procedure and the biochemical interpretation of it. The idea behind balancing is based on the so-called reachability and observability of the states and the related input and output energies and, therefore, we first define these concepts and, in the last subsection, we relate them to the properties of the state variables in the balanced model. We remark that the input and output energies are *not* related to energy in the physical or biochemical meaning of this term.

Because the concepts that we discuss below all pertain to linear models, we simplify our notation in this section by dropping the index l on the variables x_l, u_l, and y_l and, accordingly, write the linear model (2.2) as

$$\begin{aligned} \dot{x}(t) &= Ax(t) + Bu(t), \\ y(t) &= Cx(t) + Du(t). \end{aligned} \tag{2.8}$$

It is straight-forward from the equations above that if $x = 0$ and $u = 0$ then $\dot{x} = 0$ and $y = 0$ and hence $x = 0$ is a steady state of the linear model and $y = 0$ the steady output when u=0. For the interpretation outlined below, it is important to keep in mind that the variables in this model are approximations of the *deviations* from the steady state in the corresponding original, nonlinear model and hence the state $x = 0$ in this linear model corresponds to the steady state x_s in the nonlinear model, $y = 0$ corresponds to the steady output y_s, and $u = 0$ corresponds to the reference input value u_s—cf. Section 2.2.2.

Reachability and observability

Reachability refers to the extent to which the state variables of a system can be manipulated through the input variables and is related to the input-to-state map of the system. An input function which causes the state to assume a specific value $\bar{x}$ at a time τ ($x(\tau) = \bar{x}$), if starting at the zero state ($x(0) = 0$), is said to *reach* $\bar{x}$ *at time* τ. A *state* is called *reachable* if there exists an input function which reaches

that state in a finite time. A *system* is defined to be *reachable* if all states in its state space are reachable. To determine whether a linear system is reachable, one can make use of the fact that it is reachable if and only if the rank of the so-called reachability matrix—defined as

$$\text{Reach} = [B \; AB \; A^2B \; \ldots \; A^{n-1}B],$$

where A and B are the corresponding matrices of the linear system (2.8)—equals the number of state variables [1], *i.e.*, rank(Reach) $= n$.

In a control system, the state variables are in general unobservable while the output variables, which can be observed, provide information about the state variables. The concept of *observability* pertains to the extent to which information about the state variables can be obtained from observing the output variables and is related to the state-to-output map of the system. A *state* $\bar{x}$ (*i.e.*, an arbitrary vector in the n-dimensional state space) is defined to be *unobservable* if all the elements in the output vector y become identical to zero when starting in this state and no input is applied, *i.e.*, if

$$x(0) = \bar{x} \text{ and } u_l(t) = 0 \text{ for all } t \geq 0 \quad \Rightarrow \quad y(t) = 0 \text{ for all } t \geq 0.$$

A *system* is *observable* (through the output y) if no states in the state space are unobservable. Also observability is related to a rank condition, *i.e.*, a system is observable if and only if the rank of the so-called observability matrix—defined as

$$\text{Obs} = \begin{bmatrix} \text{C} \\ \text{CA} \\ \vdots \\ CA^{n-1} \end{bmatrix},$$

where A and C are the matrices of the linear system (2.8)—equals the number of state variables [1], *i.e.*, rank(Obs) $= n$.

Input and output energies

Related to the concepts of reachability and observability are the so-called *energies* of the input and output functions, E_r and E_o, respectively, defined as

$$E_r(\tau, u(t)) = \int_0^\tau u^T(t)u(t)dt \tag{2.9}$$

$$E_o(\tau, y(t)) = \int_0^\tau y^T(t)y(t)dt. \tag{2.10}$$

The minimum value of the input energy over the set of input functions which reaches a state $\bar{x}$ at a time τ is—if the system is reachable—given by

$$\min_{\{u(t)|x(\tau)=\bar{x}\}} E_r(\tau, u(t)) = \bar{x}^T P(\tau)^{-1}\bar{x}$$

where the matrix $P(\tau)$ is the *finite reachability Grammian* defined as

$$P(\tau) = \int_0^\tau e^{At} B B^T e^{A^T t} dt$$

and A and B are matrices of the linear model on the form (2.8) which is to be reduced. Further, from the definition of the Grammians it follows that these are symmetric and that $P(t_1) \leq P(t_2)$ for any $0 \leq t_1 \leq t_2$, meaning that $P(t_2) - P(t_1)$ is a positive semidefinite matrix (a real symmetric matrix M is positive semidefinite if $z^T M z \geq 0$ for all non-zero vectors z). Therefore, the minimal input energy required to steer the system from 0 to $\bar{x}$ is obtained as $\tau \to \infty$ and is given by

$$\epsilon_r(\bar{x}) = \bar{x}^T P^{-1} \bar{x} \tag{2.11}$$

where P is the *infinite reachability Grammian*, *i.e.*, $P = \lim_{\tau \to \infty} P(\tau)$.

Analogous to above, the output energy accumulated on the time interval from 0 to τ for an output function $\bar{y}(t)$—achieved for an initial state $x(0) = \bar{x}$ and an input function $u(t) = 0$ for $t \geq 0$—can be expressed as

$$E_o(\tau, \bar{y}(t)) = \bar{x}^T Q(\tau) \bar{x},$$

where $Q(\tau)$ is the *finite observability Grammian*,

$$Q(\tau) = \int_0^\tau e^{A^T t} C^T C e^{At} dt$$

where A and C pertain to the linear system (2.8). Further, for the observability Grammian it also holds that $Q(t_1) \leq Q(t_2)$ for any $0 \leq t_1 \leq t_2$ and hence the largest output energy produced by the state $\bar{x}$ is equal to

$$\epsilon_o(\bar{x}) = \bar{x}^T Q \bar{x} \tag{2.12}$$

where Q is the *infinite observability Grammian* $Q = \lim_{\tau \to \infty} Q(\tau)$.

A state with a high minimal input energy ϵ_r has little influence on the input-to-state map and *vice versa*, whilst correspondingly, a state with a high maximal output energy ϵ_o has large influence on the state-to-output map and *vice versa*. This is described in detail in the coming section where we describe a way to interpret the input and output energies and we relate these concepts to the idea behind balancing.

Balancing in terms of input and output energies

In this section we first express the input and output energies in terms of the eigenvalues of the corresponding Grammians and, subsequently, we discuss the interpretation of the energies and relate to the idea behind balancing.

Writing the state $\bar{x}$ as a linear combination of the scaled eigenvectors $e_1^p, \ldots, e_n^p$ of the infinite reachability Grammian P, *i.e.*,

$$\begin{aligned} \bar{x} &= k_1 e_1^p + \ldots + k_n e_n^p \text{ where} \\ (e_i^p)^T e_i^p &= 1 \text{ for } i = 1, \ldots, n \end{aligned}$$

and $k_1, \ldots, k_n$ are some real coefficients, the minimal input energy—given by (2.11)—to reach $\bar{x}$ becomes

$$\begin{aligned} \epsilon_r(\bar{x}) &= (k_1 e_1^p)^T P^{-1} k_1 e_1^p + \ldots + (k_n e_n^p)^T P^{-1} k_n e_n^p \\ &= \frac{k_1^2}{\lambda_1^p} + \ldots + \frac{k_n^2}{\lambda_n^p}. \end{aligned} \tag{2.13}$$

Here, $\lambda_1^p, \ldots, \lambda_n^p$ are the eigenvalues corresponding to the eigenvectors $e_1^p, \ldots, e_n^p$, respectively. The second equality is due to the fact that P is non-singular and hence the relation $Pe_i = \lambda_i^p e_i$ is equivalent with $P^{-1}e_i = (1/\lambda_i^p)e_i$ and, accordingly, the vector e_i is also an eigenvector of P^{-1} with eigenvalue $1/\lambda_i^p$. Furthermore, the fact that the eigenvalues are scaled is used in the same equality.

Analogous to the above, a state $\bar{x}$ can also be expressed as a linear combination of the scaled eigenvectors $e_1^q, \ldots, e_n^q$ of the infinite observability Grammian Q,

$$\bar{x} = k_1 e_1^q + \ldots + k_n e_n^q \text{ where } (e_i^q)^T e_i^q = 1 \text{ for } i = 1, \ldots, n.$$

The largest output energy—given by (2.12)—produced by the same state $\bar{x}$ can then be expressed as

$$\begin{aligned} \epsilon_o(\bar{x}) &= (k_1 e_1^q)^T Q k_1 e_1^q + \ldots + (k_n e_n^q)^T Q k_n e_n^q \\ &= k_1^2 \lambda_1^q + \ldots + k_n^2 \lambda_n^q, \end{aligned} \tag{2.14}$$

where $\lambda_1^q, \ldots, \lambda_n^q$ are the eigenvalues corresponding to the eigenvectors $e_1^q, \ldots, e_n^q$, respectively.

The expressions of the input and output energies (2.13) and (2.14), respectively, show that a state which is far from 0, *i.e.*, has large $|k_i|$ for all i, requires much input energy to reach and produces much output energy. In other words, such a state requires a large deviation of the input from 0 and causes the output to deviate much from 0—cf. the definition of input and output energies given by (2.9) and (2.10), respectively. Recall that the state, input, and output variables represent deviations from the corresponding variables in the nonlinear biochemical model—cf. Section 2.2.2; the conclusion above hence translates to, in the nonlinear biochemical model, that a state far from the biochemical steady state requires large deviations of the input from their reference values to be reached and that starting in a state far from the steady state will cause the output to deviate much from the steady output. In other words, a state far from steady state needs a 'wild' behavior of the input in order to be obtained and starting in such a state results in a 'wild' behavior of the output.

The degree that the energies are influenced by deviation from the steady state values of the various state variables depend on the eigenvalues of the Grammians. In a balanced system, these eigenvalues are equal, *i.e.*, $\lambda_i^p = \lambda_i^q = \sigma_i$ for all i—cf. (2.6)—where the σ_i's are the HSVs. A state $\bar{x}$ in a balanced model which only deviates from 0 in the i^{th} state variable, *i.e.*, $\bar{x} = (0, \ldots, 0, k_i, 0, \ldots, 0)$, hence requires the input energy

$$\epsilon_r(\bar{x}) = \frac{k_i^2}{\sigma_i}$$

to be reached and produces the output energy

$$\epsilon_o(\bar{x}) = k_i^2 \sigma_i.$$

Consequently, if σ_i is large, the state $\bar{x} = (0, \ldots, 0, k_i, 0, \ldots, 0)$ in the balanced model requires much energy to reach and produces little output energy and *vice versa*.

The state variables that are retained in the reduction by balancing and truncation are the first n_r ones which correspond to the highest HSVs. The states $\bar{x}$ which deviate from the steady state in only one of these first components, *i.e.*, the states on the form $\bar{x} = (0, \ldots, 0, k_i, 0, \ldots, 0)$ where $i = 1, \ldots, n_r$, require little input energy to be reached (need large deviation of the input from the reference input) and produce much output energy (causes large deviations of the output from the steady output). Consequently, the corresponding state variables react strongly, in terms of deviating from their steady states, to changes in the input variables away from its reference level and they also cause the output variables to react strongly. In this sense these states variables are important for the input-to-state map and the state-to-output map, respectively, and hence important for the dynamics. The less important variables, on the other hand, that are more difficult to reach and that have smaller effects on the output, are hence more suitable to approximate with their steady state values, which is done in the truncation step.

In a linear, unbalanced system, the eigenvalues of the reachability and observability Grammians are different and, therefore, ranking the state variables according to either of these sets of eigenvalues results in different rankings; reduction based on the ranking of the eigenvalues of the reachability matrix may result in throwing away variables which are important for the state-to-output dynamics, while reduction based on the observability matrix may result in a large loss of input-to-state dynamics. The balancing procedure ensures that the state variables in the balanced model have *equal* importance for the input-to-state and the state-to-output map and hence that the variables that are eliminated in the subsequent truncation are of little importance in *both* these respects.

2.2.6 Properties of the balancing transformation

Balancing and truncation has not been shown to be optimal in any norm, *i.e.*, no way has been found to express the difference (norm) between the input-to-output relations for the linear system (2.8) and truncated system (2.7) in such a way that this difference is minimized by the balancing transformation S. On the other hand, the balancing transformation S solves the minimization problem

$$\min_S \ \text{trace}\ [SPS^T + S^{-T}QS^{-1}].$$

(The *trace* of a matrix is the sum of its diagonal elements.) The terms SPS^T and $S^{-T}QS^{-1}$ in the expression above are the Grammians of the balanced system—cf. (2.6)—and hence minimization of the expression above relates to minimizing the minimal input energy (2.11) and maximizing the output energy (2.12) attributing equal importance to both. The minimum of this expression is twice the sum of the HSVs,

$2(\sigma_1, \ldots, \sigma_n)$, and the minimizing S is a balancing transformation. Further, the transformation S preserves stability: if the linear system (2.8) to be reduced is stable (*i.e.*, if all eigenvalues have negative real parts) then also the reduced system (2.7) will be stable. Moreover, the H_∞-norm of the system, *i.e.*, a norm of the input-to-output relation (or, more specifically, the maximum of the so-called frequency response function), is bounded by twice the sum of the *neglected* singular values, *i.e.*, $2(\sigma_{n_r+1}, \ldots, \sigma_n)$.

2.3 Application of linearization, balancing, and truncation to a model of glycolysis in yeast

In this section we use the method of linearization, balancing, and truncation to reduce a mathematical model of glycolysis in *Saccharomyces cerevisiae* (baker's yeast). (The model is available on JWS Online [142] and is an updated version of the model reported in [122].) As mentioned in the Introduction to this chapter, glycolysis is the well-known biochemical process that uses glucose to produce energy-rich compounds; for more details, see *e.g.* [122] and references therein. The mathematical model includes thirteen state variables; eleven of these represent concentrations and two represent linear combinations of concentrations, see Table 2.1. The 17 biochemical reactions included in the model are given in Table 2.2. The rates of twelve of these reactions are modeled as rational functions, *i.e.*, ratios of polynomials, two as simple polynomials, and three as constants. The rate expressions and further details about the model are provided in Appendix 2.B.

To prepare for the reduction of the glycolysis model, we brought it into the form of a control system (2.1). To this end, input and output functions had to be defined. As was described in Section 2.2.1, these should be chosen such that the behavior of the output is of interest to investigate as a function of different input behaviors. We considered a single-valued input function, being the maximum (limiting) rate of the transport of glucose through the cell membrane—this maximum rate was modeled by the parameter p_1 in the original model, see Appendix 2.B—and an output function being the vector of all thirteen state variables. The limiting rate of the glucose transporter (*i.e.*, the input) is subject to natural variations in the cell due to variations in *e.g.* the expression of this protein. The particular combination of input and output used here allows studying the time evolution of the entire state as a function of the time evolution of this maximum rate. We remark that, naturally, it is of interest to study the dynamics of the state as a function of most of the model parameters (given in Tables 2.3–2.4). However, the state variables of the model are highly robust to changes in many of these parameters (*e.g.* the concentration of extracellular glucose modeled by the parameter c_1 in Appendix 2.B), making these parameters less interesting as input variables; the parameter p_1 used here was one of the parameters to which the state variables were most sensitive.

Next, reference values for the input and state variables were defined. We set the reference of the input to the value of the corresponding parameter value ($u_s = 97.264$, cf. Table 2.3) and the reference of the state variables to the steady state of the model. The calculations of the steady state, as well as all further calculations in this chapter, were done in *Mathematica*.

State variable	Explanation	Short name
x_1	[intracellular glucose]	GLC
x_2	2[ATP]+[ADP], *i.e.* sum of high energy phosphates in adenine nucleotides	P
x_3	[glucose 6-phosphate]	G6P
x_4	[fructose 6-phosphate]	F6P
x_5	[fructose-1,6-bisphosphate]	F16BP
x_6	[glycerone phosphate] + [D-glyceraldehyde-3-phosphate]	GP DG3P
x_7	[Nicotinamide adenine dinucleotide] (reduced)	NADH
x_8	[1,3-bisphosphoglycerate]	BPG
x_9	[3-phosphoglycerate]	P3G
x_{10}	[2-phosphoglycerate]	P2G
x_{11}	[phosphoenolpyruvate]	PEP
x_{12}	[pyruvate]	PYR
x_{13}	[acetaldehyde]	ACE

Table 2.1: State variables in the nonlinear glycolysis model.

The model was then linearized at the reference point, following the procedure in Section 2.2.2, to obtain a model in the form (2.8). Subsequently, the linearized model was balanced as described in Section 2.2.3, using the algorithm described in Appendix 2.A. The HSVs of the system obtained in the balancing procedure, scaled by their sum, are shown in Figure 2.1. The ratios between several of the pairs of consecutive HSVs (reported in the legend to the same figure) are relatively large, indicating that several choices of the order of the reduced model may be possible. We therefore investigated the performance of reduced models of different orders, obtained as described in Section 2.2.4.

In Figure 2.2 we display the time courses of the fourth, fifth, and sixth order reduced models together with time courses of the original nonlinear glycolysis model and the 13^{th} order linear model. The time courses were calculated with the steady state as initial value for the state variables, and the constant input functions $u(t) = 0.9 \times u_s$ and $u(t) = 0.6 \times u_s$, respectively. In the case when the input function is $u(t) = 0.9 \times u_s$, the differences between the time courses of the original nonlinear model and the linear 13^{th} order model are relatively small for several of the output variables (*e.g.*, [intracellular glucose], 2[ATP]+[ADP], and [NADH]) while larger for others (e.g., [pyruvate]). In the case when $u(t) = 0.6 \times u_s$, the differences between the time courses of the same two models are relatively large for the entire set of output variables. The larger linearization errors in the latter case are to be expected since

Rate	Reaction
v_1	extracellular glucose $\rightarrow$ GLC_{in}
v_2	GLC_{in} + ATP $\rightarrow$ G6P + ADP
v_3	G6P $\rightarrow$ F6P
v_4	G6P $\rightarrow$ glycogen (side branch)
v_5	G6P $\rightarrow$ trehalose (side branch)
v_6	F6P + ATP $\rightarrow$ F16bP + ADP
v_7	ATP $\rightarrow \emptyset$ (lumped ATP consuming processes)
v_8	F16bP $\rightarrow$ DHAP + GAP
v_9	DHAP + NADH $\rightarrow$ glycerol + NAD
v_{10}	GAP + NAD $\rightarrow$ BPG + NADH
v_{11}	BPG + ADP $\rightarrow$ P3G + ATP
v_{12}	P3G $\rightarrow$ P2G
v_{13}	P2G $\rightarrow$ PEP
v_{14}	PEP + ADP $\rightarrow$ PYR + ATP
v_{15}	PYR $\rightarrow$ ACE
v_{16}	2 ACE + 3 NAD $\rightarrow$ succinate + 3 NADH
v_{17}	ACE + NADH $\rightarrow$ ethanol + NAD

Table 2.2: The reactions modeled in the nonlinear glycolysis model and the notation for the corresponding rates. Abbreviations: see Table 2.1.

linearizations typically become increasingly inaccurate with increasing distance to the reference values for the input and state variables.

In both the cases when $u(t) = 0.9 \times u_s$ and when $u(t) = 0.6 \times u_s$, the time courses of the sixth order reduced model are indistinguishable from those of the linear 13^{th} order model—this holds also for the time courses of the remaining nine output variables not displayed in the figure. Also the fifth order model exhibits dynamics very similar to the linear 13^{th} order model. The dynamics of the fourth order model, on the other hand, deviates substantially from that of the higher order models, particularly in the time course for intracellular glucose concentration. A model with five state variables thus seems to provide a good balance between simplicity and accuracy for the approximation of the linear 13^{th} order model. Indeed, the high value of the ratio $\sigma_5/\sigma_6 = 9.0$ confirms that a sixth order reduced model is expected to provide only a small improvement in accuracy as compared to the sixth order model while the lower value of $\sigma_4/\sigma_5 = 4.2$ indicates that a fourth order model may not be sufficiently accurate. However, the poor accuracy of the linearization step causes all three reduced models to only poorly approximate the dynamics of the nonlinear model.

The performance of the method of linearization, balancing, and truncation was also examined for several other sets of input and output variables and, in all cases, the errors due to the linearization were of the same order of magnitude as reported above

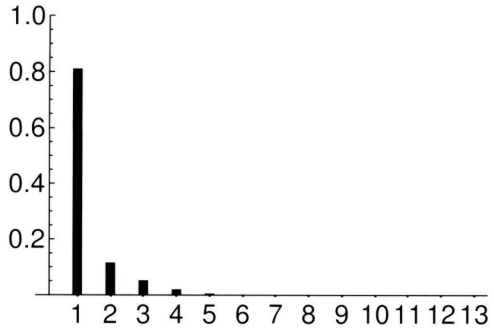

Figure 2.1: The thirteen scaled HSVs for the linearized glycolysis model with one input variable representing the rate of glucose transport into the cell and 13 output variables representing all the state variables. The ratios between the first pairs of consecutive HSVs are $\sigma_1/\sigma_2 = 7.1$, $\sigma_2/\sigma_3 = 2.2$, $\sigma_3/\sigma_4 = 2.7$, $\sigma_4/\sigma_5 = 4.2$, $\sigma_5/\sigma_6 = 9.0$, $\sigma_6/\sigma_7 = 5.1$, $\sigma_7/\sigma_8 = 5.3$, $\sigma_8/\sigma_9 = 9.5$, and $\sigma_8/\sigma_9 = 8.9$. (The remaining HSVs are so small that the calculation of their ratios becomes aberrated by numerical errors.)

while again, as expected, the balancing and truncation gave accurate approximations of the linearized models.

We also applied the reduction method to a model of the phosphotransferase system [99], also containing 13 state equations but in contrast to the glycolysis model the right hand sides of its state equations are simple expressions consisting of polynomials with only first and second order terms. However, also for this model the linearization caused approximation errors of the same order of magnitude as of those reported above for the glycolysis model.

In the next section, we demonstrate an alternative approach to reduce the glycolysis model, also based on balancing, which results in a nonlinear reduced model which succeeds in accurately approximating the dynamics of the original model.

2.4 Quantification of the influence of individual molecules on the dynamics of the yeast glycolysis model

In this section, we investigate the influence of the different state variables on the dynamics of the glycolysis model based on the coefficients in the balancing transformation matrix. Furthermore, we use this information to simplify the model in a straight-forward *ad hoc* manner.

As described in Section 2.2.3, the state variables in the balanced model (x_b) are linear combinations of those of the linearized model (x_l), given by $x_b = Sx_l$ where S is the balancing transformation matrix. Because the variables in x_b are ordered according to decreasing importance for the dynamics of the map from input to output, the values of the coefficients in the linear combinations defining the first (most important)

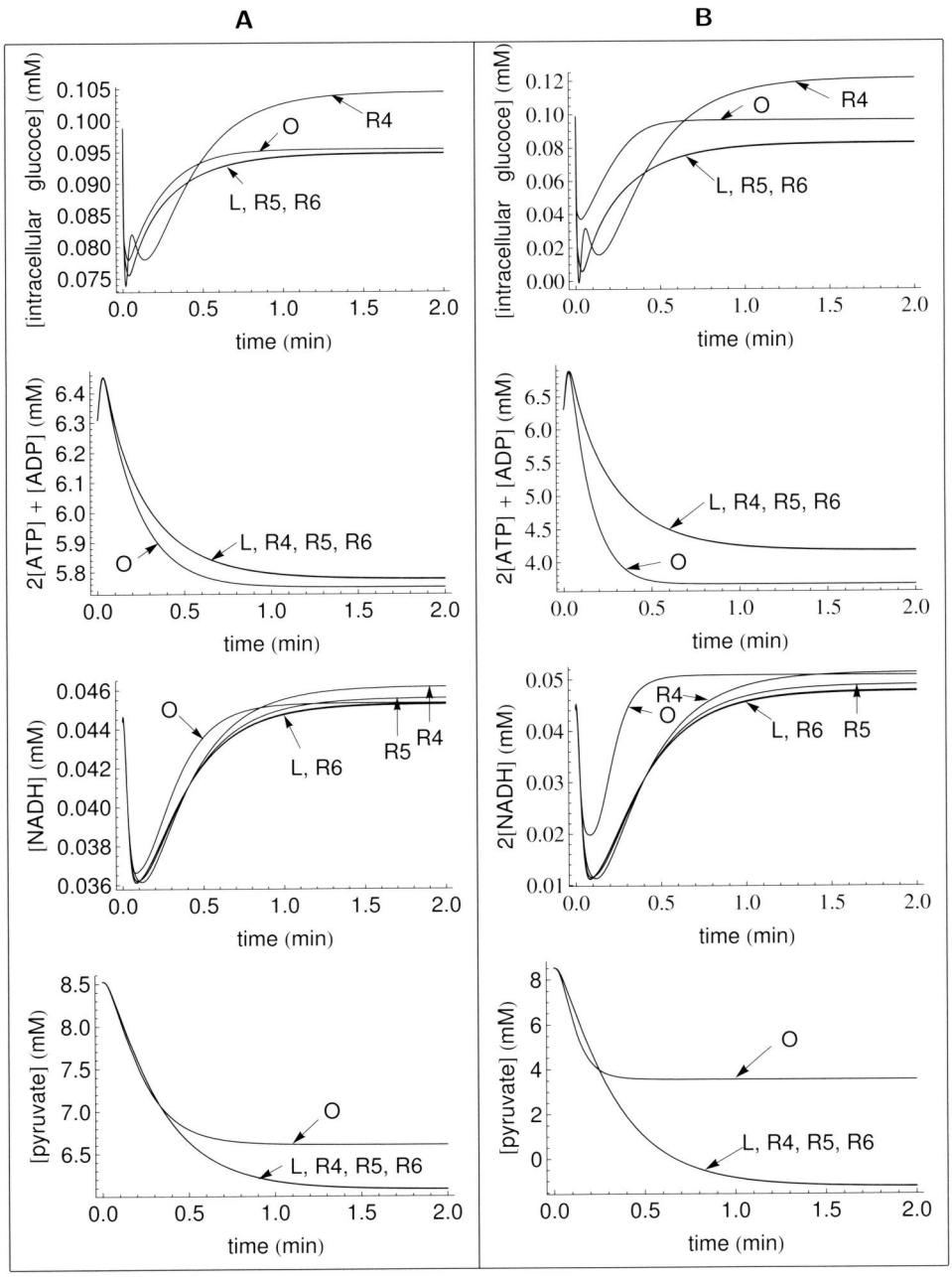

Figure 2.2: Time courses for the original (O), linear 13^{th} order (L), and reduced models of order 4, 5, and 6 (R4, R5, and R6) for four of the thirteen output variables. The input functions applied are the constant functions $u(t) = 0.9 \times u_s$ in (A) and $u(t) = 0.6 \times u_s$ in (B).

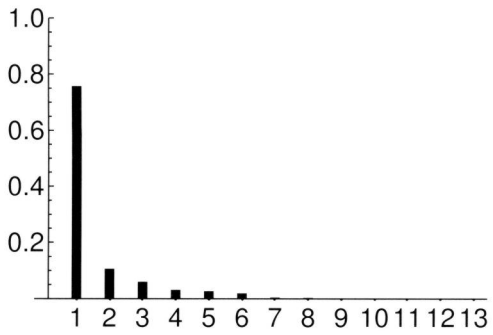

Figure 2.3: The scaled HSVs for the model obtained by linearizing the glycolysis model with as input variables all 92 parameters and as output variables all 13 state variables. The reference values of the input variables are the corresponding parameter values, and the reference state is the steady state. The numerical values are: 0.76, 0.11, 0.059, 0.030, 0.025, 0.018, 0.0035, 0.0024, 5.8×10^{-4}, 2.6×10^{-4}, 5.6×10^{-5}, 2.5×10^{-5}, 2.2×10^{-7}.

state variables in x_b provide information about the relative importance the different variables in x_l have on the model dynamics. To illustrate this, we consider a case when the HSVs show that the first of the variables in x_b has a dominant influence on the dynamics and this state variable is given by the linear combination

$$x_{b,1} = k_1 x_{l,1} + \ldots + k_i x_{l,i} + \ldots + k_n x_{l,n},$$

where k_i is the coefficient with the highest absolute value. Then, one could expect that the variable $x_{l,i}$ in the same term has a strong influence on $x_{b,1}$ and hence also on the dynamics of the system. The variables in x_l are approximations of the deviations of the original state variables from their reference values, *i.e.* $x_l \approx x - x_s$, and hence the coefficients in the linear combinations provide information about the influence of the *deviations* of the variables listed in Table 2.1 from their steady state values on the input to output map.

To investigate the importance of the state variables for a map which incorporates as much as possible of the dynamics of the glycolysis model, we studied a model with an input vector containing all the 92 parameters of the nonlinear model (88 kinetic parameters and 4 constant concentrations, see Appendix 2.B) and an output vector with all the thirteen state variables. We first performed the linearizations at the steady state of the model, calculated for the original set of parameter values. The HSVs of the model are shown in Figure 2.3. According to these values, the first balanced state variable influences 76% of the dynamics and, further, the second to sixth state variable also have certain influence although much smaller, while the last ones have a seemingly negligible impact. The three first of the balanced state

variables are given by

$$\begin{aligned} x_{b,1} \;=\; & -3.1\Delta[\text{GLC}] - 0.31\Delta[\text{P}] - 3.9\Delta[\text{G6P}] - 4.0\Delta[\text{F6P}] \\ & -4.4\Delta[\text{F16BP}] - 2.2\Delta([\text{GP}]+[\text{DG3P}]) - 0.91\Delta[\text{NADH}] \\ & -3.4\Delta[\text{BPG}] - 3.1\Delta[\text{P3G}] - 3.1\Delta[\text{P2G}] \\ & -3.2\Delta[\text{PEP}] - 2.9\Delta[\text{PYR}] - 0.87\Delta[\text{ACE}], \end{aligned}$$

$$\begin{aligned} x_{b,2} \;=\; & 2.2\Delta[\text{GLC}] - 3.1\Delta[\text{P}] - 0.24\Delta[\text{G6P}] + 0.45\Delta[\text{F6P}] \\ & -2.0\Delta[\text{F16BP}] - 1.3\Delta([\text{GP}]+[\text{DG3P}]) + 0.5\Delta[\text{NADH}] \\ & -3.4\Delta[\text{BPG}] - 0.42\Delta[\text{P3G}] - 0.52\Delta[\text{P2G}] \\ & -0.85\Delta[\text{PEP}] + 2.0\Delta[\text{PYR}] - 0.44\Delta[\text{ACE}], \qquad \text{and} \end{aligned}$$

$$\begin{aligned} x_{b,3} \;=\; & 5.9\Delta[\text{GLC}] + 0.47\Delta[\text{P}] + 7.3\Delta[\text{G6P}] + 6.0\Delta[\text{F6P}] \\ & +5.3\Delta[\text{F16BP}] + 2.1\Delta([\text{GP}]+[\text{DG3P}]) - 0.34\Delta[\text{NADH}] \\ & -0.13\Delta[\text{BPG}] - 0.69\Delta[\text{P3G}] - 0.84\Delta[\text{P2G}] \\ & -1.3\Delta[\text{PEP}] - 2.1\Delta[\text{PYR}] + 0.40\Delta[\text{ACE}]. \end{aligned}$$

The variables on the right hand sides of the equations above are the state variables in the linearized system $(x_{l,1}, \ldots, x_{l,13})$ that here are denoted by names that relate to the biochemical concentrations that they represent—cf. Table 2.1; the 'Δ' notation indicates that the variables represents the deviations from the steady state values.

In the linear combination for $x_{b,1}$—*i.e.*, the state variable with most impact on the dynamics—the three variables in x_l with lowest absolute values of their coefficients are $x_{l,2}$ (related to 2[ATP]+[ADP]), $x_{l,7}$ (related to [NADH]), and $x_{l,13}$ (related to [acetaldehyde]). In the expressions for $x_{b,2}$ and $x_{b,3}$, the two variables $x_{l,7}$ and $x_{l,13}$ again have low absolute values of their coefficients while $x_{l,2}$ has a high such value in the expression for $x_{b,2}$ and low in $x_{b,3}$. This suggests that $x_{l,7}$ and $x_{l,13}$ have a small impact on the dynamics in the glycolysis model while $x_{l,2}$ is likely to exert some influence in spite of its low coefficient in $x_{b,1}$. The variable in x_l with the highest absolute value of its coefficient in the expression for $x_{b,1}$ is $x_{l,5}$ (related to [fructose-1,6-bisphosphate]). This variable also has relatively large influence on the balanced variables $x_{b,2}$ and $x_{b,3}$, suggesting that it has strong influence on the dynamics.

As was demonstrated in the previous section, linearization is only accurate close to the reference point at which it is performed. Consequently, the conclusions above concerning the influence of state variables—which are based on a linearization at the steady state—only hold when the perturbations from the reference point are small. To investigate whether these conclusions also hold for states away from the steady state, we also performed the analysis of coefficients for other reference states. For the input, we used about a dozen of values for the maximum rate of glucose transporter on the range (44 mM, 125 mM) while the remaining input variables assumed the corresponding parameter values. As reference for the state we used a few points along each of the trajectories calculated using as initial condition the steady state of the original model and as input functions the constant functions assuming the different values of u_s. Again, the coefficients of $x_{l,7}$ and $x_{l,13}$ were small in all cases and those of $x_{l,5}$ were high in a majority of the cases, supporting the conclusions of the results above.

The small influences of $x_{l,7}$ and $x_{l,13}$ on the dynamics suggest that the corresponding state variables x_7=[NADH] and x_{13}=[acetaldehyde] may be eliminated from the nonlinear model without much impact on the dynamics. We therefore interchanged these variables for their steady state values and eliminated their state equations in the model in Appendix 2.B and compared the performance of this reduced 11^{th} order model with the original 13^{th} order nonlinear model. In Figure 2.4 we show the time courses for these two models upon a change in the parameter p_1 from its original value to 0.6 times this value. Indeed, the dynamics of the 11^{th} order model accurately approximates that of the original 13^{th} order model. We also investigated the performance of the 12^{th} order model obtained by eliminating x_5=[fructose-1,6-phosphate] in stead of x_7 and x_{13}; we show three of the time courses in Figure 2.5. As expected, the elimination of this variable results in highly inaccurate time courses; these results verify that the concentration of fructose-1,6-phosphate indeed has high influence on the dynamics.

2.5 Discussion

In this chapter we have explored the performance of balancing—one of the best-known techniques for model reduction within the area of control theory—for the reduction of a biochemical model of glycolysis in yeast with thirteen state variables. This technique has been extensively used in engineering contexts where the models to be reduced have been linear. However, the glycolysis model studied is, as most biochemical models are, nonlinear and therefore had to be linearized prior to application of balancing and truncation. Our results from linearization, balancing, and truncation of the nonlinear model of glycolysis in yeast (Section 2.3) show that, indeed, the accuracy of this reduction is limited by the error from the linearization step. When the input, *i.e.*, the maximum rate of the glucose transporter, was decreased by 10% from its reference value for the linearization, the time courses of certain of the output variables in the original nonlinear model were relatively accurately approximated by the time courses of the same variables in the linear model of the same order (Figure 2.2A). Nevertheless, already for this relatively small perturbation of the input value, the time courses of certain other output variables were only poorly approximated by the linear model (*e.g.* that of [pyruvate] in Figure 2.2A). When the input was decreased by 40% from its reference value (Figure 2.2B), the linearization step caused substantial approximation errors for the entire set of state variables.

Also other choices of the sets of input and output variables resulted in inaccuracy of the same order of magnitude as in the case described above. Moreover, also for a model of the phosphotransferase system with much less pronounced nonlinearities than in the glycolysis model—this model has relatively simple polynomial state equations in contrast to the more complex rational expressions in the glycolysis model—the linearization resulted in approximation errors of the same order of magnitude as for the glycolysis model. In biochemical contexts, perturbations of parameter values of 10 to 40% or more occur frequently and hence our results suggest that linearizations may in many situations not be sufficiently accurate approximations of biochemical models.

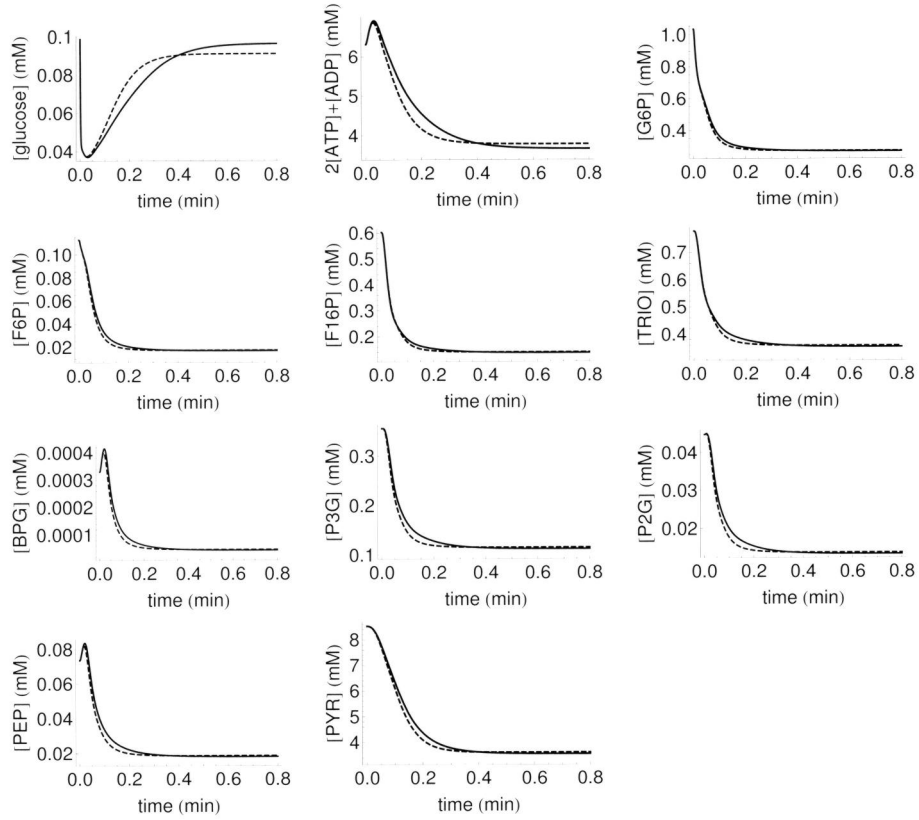

Figure 2.4: Time courses of the original 13^{th} order model (solid line) and the 11^{th} order model obtained by approximating the state variables representing [NADH] and [acetaldehyde] by their steady state values (dashed line). At time point 0 the parameter p_1 was decreased from its original value to 0.6 times this value.

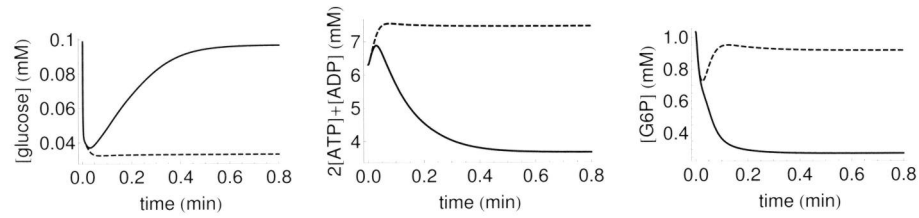

Figure 2.5: Time courses of the original 13^{th} order model (solid line) and the 12^{th} order model obtained by approximating the state variable representing [fructose-1,6-bisphosphate] by its steady state value (dashed line). At time point 0 the parameter p_1 was increased from its original value to 0.6 times this value.

We then also explored the information obtained from the balancing step in order to improve the understanding of the dynamics of the glycolysis model. By analyzing the coefficients in the linear combinations of the state variables in the balanced model we could estimate the importance of the original state variables for the dynamics of the glycolysis model. We performed this analysis for linear models obtained by linearizing the nonlinear model at a wide range of reference values for the input and state variables and similar results concerning the importance of the state variables was obtained. Hence, the conclusions do not hold only locally around one reference point but in relatively broad generality. We found that the concentration of fructose-1,6-phosphate has a crucial importance for the entire system dynamics. Further, the concentrations of NADH and acetaldehyde were found to have very small influence on the model dynamics. The small influence of [acetaldehyde] is not particularly surprising since this metabolite is the last one in a chain of reactions. The small influence of [NADH] as compared to that of 2[ATP]+[ADP], on the other hand, is less intuitive; based on the fact that these molecules play similar roles in the glycolysis one would expect that they instead would have similar importance. We remark that, naturally, our conclusions concerning the importance of the various state variables for glycolysis discussed above are based on the assumption that the glycolysis model that we study correctly models reality; however, the fact that the model that we studied is carefully validated proves the reliability of the results.

Another approach to investigate the influence of the parameters and state variables on the model dynamics is provided by metabolic control analysis (MCA) [17, 54]. In this framework for sensitivity analysis, the influence of changes of catalytic activities on the steady state concentrations or steady state flows is quantified by so-called control coefficients and the effect of small perturbations of state variables or parameters on the rates of individual, mostly enzyme-catalyzed, processes, is given by so-called elasticity coefficients. The balancing-based analysis performed here differs in scope from MCA; as has been outlined in this chapter, the *importance* of the state variables for the model dynamics refers to the influence that the deviations from their steady state values have on the map from input to output variables. Since the input and output variables are time-dependent variables, this map represents the entire dynamics of the model, *i.e.*, the behavior over the entire time span, in contrast to MCA which is a stationary approach, *i.e.*, it analyzes the behavior at a given point in time. In other words, the balancing-based analysis gives more general information about the dynamics which can be used to determine the importance of state variables for the over-all behavior of the model while MCA provides information about effects of specific changes at a given time point.

The information about the small importance of the concentrations of NADH and acetaldehyde for the dynamics of the glycolysis model was then used to construct a nonlinear reduced model with 11 state variables which accurately approximated the dynamics of the original model. The high accuracy of this model also confirms the small importance of the two eliminated variables. As a control, also a reduced model was constructed by elimination of the important state variable representing the concentration of fructose-1,6-bisphosphate; this indeed resulted in a poor approximation of the original model dynamics.

A reduction of the number of state variables from 13 to 11 is, however, relatively

modest and if further reduction of the simulation times is needed, other approaches have to be taken. In the coming chapters of this thesis we explore another simplification method which is nonlinear, *i.e.*, does not require linearization of the model, and which enables extensive reduction while retaining a high accuracy.

Appendices

2.A An algorithm for the construction of the balancing transformation matrix

For the calculations of the balancing transformation matrices in this chapter we have used the so-called *square root algorithm* [74], which we describe below. For details on efficient computation of this algorithm, see *e.g.* [3].

The input to the algorithm are the matrices A, B, and C of a linear model of the form (2.2).

Step 1. Determine the reachability and observability Grammians P and Q. These matrices can be obtained by solving the Lyapunov equations

$$AP + PA^T = -BB^T,\ QA + A^TQ = -C^TC.$$

Step 2. Perform Cholesky decompositions of the Grammians, *i.e.*, decompose them into

$$P = X^TX \text{ and } Q = Y^TY$$

where X and Y are upper triangular matrices.

Step 3. Perform the singular value decomposition

$$XY^T = UDV^T$$

where D is the diagonal matrix with the HSVs arranged in decreasing order on the diagonal.

Step 4. The transformation matrix is given by

$$S = D^{-1/2}V^TY$$

and its inverse is given by

$$S^{-1} = X^TUD^{-1/2}.$$

The output of the algorithm is the transformation matrix S which is used to construct the balanced model: the state variables in the balanced model, x_b, are given by $x_b = Sx_l$, where x_l are the state variables of the linear, unbalanced model, and the balanced model is given by (2.4).

2.B The model of glycolysis in yeast

Here we provide the model of glycolysis in *Saccharomyces cerevisiae* used in Section 2.3. The model is available on JWS Online [142] and is an updated version of the model presented in the original article [122]. The model contains thirteen state variables, $x = (x_1, \ldots, x_{13})$, representing concentrations or pools of concentrations as

shown in Table 2.1. The reactions included in the model are listed in Table 2.2 and we denote the rates of these reactions by $v_1, \ldots, v_{17}$ (with the ordering equivalent to that in Table 2.2). In the model, all concentrations are given in millimolar (mM), time is given in minutes (min) and the constants have units in conformance with these units. The dynamics of the model is given by the nonlinear ODE system

$$
\begin{aligned}
\dot{x}_1 &= v_1 - v_2,\\
\dot{x}_2 &= -v_2 - v_4 - v_5 - v_6 - v_7 + v_{11} + v_{14},\\
\dot{x}_3 &= v_2 - v_3 - v_4 - 2v_5,\\
\dot{x}_4 &= v_3 - v_6,\\
\dot{x}_5 &= v_6 - v_8,\\
\dot{x}_6 &= 2v_8 - v_9 - v_{10},\\
\dot{x}_7 &= -v_9 + v_{10} + 3v_{16} + v_{17},\\
\dot{x}_8 &= v_{10} - v_{11},\\
\dot{x}_9 &= v_{11} - v_{12},\\
\dot{x}_{10} &= v_{12} - v_{13},\\
\dot{x}_{11} &= v_{13} - v_{14},\\
\dot{x}_{12} &= v_{14} - v_{15},\\
\dot{x}_{13} &= v_{15} - 2v_{16} + v_{17},
\end{aligned}
$$

where the rates are given by the expresions

$$
\begin{aligned}
v_1 &= \frac{p_1\left(\frac{c_1}{p_2} - \frac{x_1(t)}{p_2 p_4}\right)}{1+\frac{c_1}{p_2}+\frac{x_1(t)}{p_3}+0.91\frac{c_1 x_1(t)}{p_2 p_3}},\\
v_2 &= \frac{p_5\left(\frac{x_1(t)}{p_6}\frac{h_1(t)}{p_8} - \frac{x_3(t)h_2(t)}{p_6 p_8 p_{10}}\right)}{\left(1+\frac{x_1(t)}{p_6}+\frac{x_3(t)}{p_7}\right)\left(1+\frac{h_1(t)}{p_8}+\frac{h_2(t)}{p_9}\right)},\\
v_3 &= \frac{p_{11}\left(\frac{x_3(t)}{p_{12}} - \frac{x_4(t)}{p_{12}p_{14}}\right)}{1+\frac{x_3(t)}{p_{12}}+\frac{x_4(t)}{p_{13}}},\ v_4 = p_{15},\ v_5 = p_{16},\\
v_6 &= \frac{p_{17}p_{18}x_4(t)h_1(t)h_7(t)}{p_{20}p_{21}(h_7(t)^2+h_9(t)h_8(t)^2)},\ v_7 = p_{84}h_1(t),\\
v_8 &= \frac{p_{31}\left(\frac{x_5(t)}{p_{32}} - \frac{h_{11}(t)h_{10}(t)}{p_{32}p_{36}}\right)}{1+\frac{x_5(t)}{p_{32}}+\frac{h_{11}(t)}{p_{33}}+\frac{h_{10}(t)}{p_{34}}+\frac{h_{11}(t)h_{10}(t)}{p_{33}p_{34}}+\frac{x_5(t)h_{11}(t)}{p_{35}p_{32}}},\\
v_9 &= \frac{p_{37}\left(\frac{h_{10}(t)x_7(t)}{p_{38}p_{39}} - \frac{c_4 h_{12}(t)}{p_{38}p_{39}p_{42}}\right)}{\left(1+\frac{h_{10}(t)}{p_{38}}+\frac{c_4}{p_{41}}\right)\left(1+\frac{x_7(t)}{p_{39}}+\frac{h_{12}(t)}{p_{40}}\right)},\\
v_{10} &= \frac{p_{49}\left(\frac{p_{43}h_{11}(t)h_{12}(t)}{p_{45}p_{47}} - \frac{p_{44}x_8(t)x_7(t)}{p_{46}p_{48}}\right)}{\left(1+\frac{h_{11}(t)}{p_{45}}+\frac{x_8(t)}{p_{46}}\right)\left(1+\frac{h_{12}(t)}{p_{47}}+\frac{x_7(t)}{p_{48}}\right)},\\
v_{11} &= \frac{p_{50}\left(\frac{p_{55}x_8(t)h_2(t)}{p_{52}p_{54}} - \frac{x_9(t)h_1(t)}{p_{52}p_{54}}\right)}{\left(1+\frac{x_8(t)}{p_{51}}+\frac{x_9(t)}{p_{52}}\right)\left(1+\frac{h_1(t)}{p_{54}}+\frac{h_2(t)}{p_{53}}\right)},\\
v_{12} &= \frac{p_{56}\left(\frac{x_9(t)}{p_{57}} - \frac{x_{10}(t)}{p_{57}p_{59}}\right)}{1+\frac{x_9(t)}{p_{57}}+\frac{x_{10}(t)}{p_{58}}},\\
v_{13} &= \frac{p_{60}\left(\frac{x_{10}(t)}{p_{61}} - \frac{x_{11}(t)}{p_{61}p_{63}}\right)}{1+\frac{x_{10}(t)}{p_{61}}+\frac{x_{11}(t)}{p_{62}}},
\end{aligned}
$$

$$v_{14} = \frac{p_{64}\left(\frac{x_{11}(t)h_2(t)}{p_{65}p_{67}} - \frac{x_{12}(t)h_1(t)}{p_{65}p_{67}p_{69}}\right)}{\left(1+\frac{x_{11}(t)}{p_{65}}+\frac{x_{12}(t)}{p_{66}}\right)\left(1+\frac{h_1(t)}{p_{68}}+\frac{h_2(t)}{p_{67}}\right)},$$

$$v_{15} = \frac{p_{70}x_{12}(t)^{p_{72}}}{p_{71}^{p_{72}}\left(1+\frac{x_{12}(t)^{p_{72}}}{p_{71}^{p_{72}}}\right)}, v_{16} = p_{73}x_{13}(t), \text{ and}$$

$$v_{17} = \frac{p_{74}\left(\frac{h_{12}(t)c_2}{p_{82}p_{76}} - \frac{x_7(t)x_{13}(t)}{p_{82}p_{76}p_{83}}\right)}{D(t)},$$

and the denominator of the last rate is given by

$$D(t) = 1 + \frac{h_{12}(t)}{p_{82}} + \frac{p_{78}c_2}{p_{82}p_{76}} + \frac{p_{77}x_{13}(t)}{p_{81}p_{75}} + \frac{x_7(t)}{p_{81}} + \frac{h_{12}(t)c_2}{p_{82}p_{76}}$$

$$+\frac{p_{77}h_{12}(t)x_{13}(t)}{p_{82}p_{81}p_{75}} + \frac{p_{78}c_2x_7(t)}{p_{82}p_{76}p_{81}} + \frac{x_7(t)x_{13}(t)}{p_{81}p_{75}} + \frac{h_{12}(t)c_2x_{13}(t)}{p_{82}p_{76}p_{79}} + \frac{c_2x_7(t)x_{13}(t)}{p_{80}p_{81}p_{75}}.$$

Above, the time-dependent variables which are not state variables are given by the substitution relations

$$h_1(t) = \frac{-h_5(t)+(h_5(t)^2-4h_4(t)h_6(t))^{0.5}}{2h_4(t)},$$

$$h_2(t) = -2\frac{-h_5(t)+(h_5(t)^2-4h_4(t)h_6(t))^{0.5}}{2h_4(t)} + x_2(t),$$

$$h_3(t) = \frac{\left(-2\frac{-h_5(t)+(h_5(t)^2-4h_4(t)h_6(t))^{0.5}}{2h_4(t)}+x_2(t)\right)^2 p_{87}}{\frac{-h_5(t)+(h_5(t)^2-4h_4(t)Pc)^{0.5}}{2h_4(t)}}$$

$$h_4(t) = 1 - 4p_{87},\ h_5(t) = p_{86} - x_2(t)(1 - 4p_{87}),\ h_6(t) = -p_{87}x_2(t)^2$$

$$h_7(t) = 1 + \frac{x_4(t)}{p_{20}} + \frac{h_1(t)}{p_{21}} + \frac{gRx_4(t)h_1(t)}{p_{20}p_{21}},\ \ h_8(t) = 1 + \frac{p_{22}h_1(t)}{p_{21}},$$

$$h_9(t) = \frac{p_{19}\left(1+\frac{p_{26}h_1(t)}{p_{25}}\right)^2\left(1+\frac{p_{24}h_3(t)}{p_{23}}\right)^2\left(1+\frac{p_{28}c_3}{p_{27}}+\frac{p_{30}x_5(t)}{p_{29}}\right)^2}{\left(1+\frac{h_1(t)}{p_{25}}\right)^2\left(1+\frac{h_3(t)}{p_{23}}\right)^2\left(1+\frac{c_3}{p_{27}}+\frac{x_5(t)}{p_{27}}\right)^2},$$

$$h_{10}(t) = \frac{1}{1+p_{85}}x_6(t),\ \ h_{11}(t) = \frac{p_{85}}{1+p_{85}}x_6(t),\ \ h_{12}(t) = p_{88} - x_7(t).$$

Here, $h_1(t)$, $h_2(t)$, $h_{10}(t)$, $h_{11}(t)$, and $h_{12}(t)$ represent the concentrations of ATP, ADP, DHAP, GAP, and NAD, respectively. The values of the kinetic parameters $(p_1, \ldots, p_{88})$ and the constant concentrations $(c_1, \ldots, c_4)$ in the model equations above are given in Table 2.3 and 2.4, respectively.

$p_1 = 97.264$	$p_2 = 1.1918$	$p_3 = 1.1918$	$p_4 = 1$
$p_5 = 182.903$	$p_6 = 0.08$	$p_7 = 30$	$p_8 = 0.15$
$p_9 = 0.23$	$p_{10} = 3800$	$p_{11} = 339.677$	$p_{12} = 1.4$
$p_{13} = 0.3$	$p_{14} = 0.314$	$p_{15} = 6$	$p_{16} = 2.4$
$p_{17} = 182.903$	$p_{18} = 5.12$	$p_{19} = 0.66$	$p_{20} = 0.1$
$p_{21} = 0.71$	$p_{22} = 3$	$p_{23} = 0.0995$	$p_{24} = 0.0845$
$p_{25} = 0.65$	$p_{26} = 100$	$p_{27} = 0.000682$	$p_{28} = 0.0174$
$p_{29} = 0.111$	$p_{30} = 0.397$	$p_{31} = 322.258$	$p_{32} = 0.3$
$p_{33} = 2$	$p_{34} = 2.4$	$p_{35} = 10$	$p_{36} = 0.069$
$p_{37} = 70.15$	$p_{38} = 0.4$	$p_{39} = 0.023$	$p_{40} = 0.93$
$p_{41} = 1$	$p_{42} = 4300$	$p_{43} = 1184.52$	$p_{44} = 6549.68$
$p_{45} = 0.21$	$p_{46} = 0.0098$	$p_{47} = 0.09$	$p_{48} = 0.06$
$p_{49} = 1$	$p_{50} = 1306.45$	$p_{51} = 0.003$	$p_{52} = 0.53$
$p_{53} = 0.2$	$p_{54} = 0.3$	$p_{55} = 3200$	$p_{56} = 2525.81$
$p_{57} = 1.2$	$p_{58} = 0.08$	$p_{59} = 0.19$	$p_{60} = 365.806$
$p_{61} = 0.04$	$p_{62} = 0.5$	$p_{63} = 6.7$	$p_{64} = 1088.71$
$p_{65} = 0.14$	$p_{66} = 21$	$p_{67} = 0.53$	$p_{68} = 1.5$
$p_{69} = 6500$	$p_{70} = 174.194$	$p_{71} = 4.33$	$p_{72} = 1.9$
$p_{73} = 21.4$	$p_{74} = 810$	$p_{75} = 1.11$	$p_{76} = 17$
$p_{77} = 0.11$	$p_{78} = 0.17$	$p_{79} = 1.1$	$p_{80} = 90$
$p_{81} = 0.031$	$p_{82} = 0.92$	$p_{83} = 6.9 \times 10^{-5}$	$p_{84} = 39.5$
$p_{85} = 0.045$	$p_{86} = 4.1$	$p_{87} = 0.45$	$p_{88} = 1.59$

Table 2.3: Kinetic parameters in the original model. Units are omitted.

Notation & value	Explanation
$c_1 = 50$	[extracellular glucose]
$c_2 = 50$	[ethanol]
$c_3 = 0.02$	[fructose-2,6-bisphosphate]
$c_4 = 0.15$	[glycerol]

Table 2.4: Constant concentrations in the yeast glycolysis model.

Chapter 3

Simplified yet highly accurate enzyme kinetics for cases of low substrate concentrations

Much of enzyme kinetics builds on simplifications enabled by the quasi-steady-state approximation (QSSA) and is highly useful when the concentration of the enzyme is much lower than that of its substrate. However, *in vivo*, this condition is often violated. Here we show that under conditions of realistic yet high enzyme concentrations, the QSSA approach may readily be off by more than a factor of 4 when predicting concentrations. We then present a novel extension of the QSSA based on the *zero-derivative principle* (ZDP) which requires considerably less theoretical work than did previous such extensions. We show that the first order ZDP, already, describes much more accurately the true enzyme dynamics at enzyme concentrations close to the concentration of their substrates. This should be particularly relevant for enzyme kinetics where the substrate is an enzyme, such as in phosphorelay and MAP kinase pathways. We illustrate this for the important example of the phosphotransferase system involved in glucose uptake, metabolism, and signalling. We find that this system with a potential complexity of nine dimensions can be understood accurately using first order ZDP in terms of the behavior of a single variable with all other concentrations constrained to follow that behavior.

3.1 Introduction

Approximations based on timescale separation have a long tradition in biochemistry, starting with the quasi-steady-state approximation (QSSA) dating back to the beginning of the previous century [6, 7, 12]—see the excellent review in [115]. The QSSA has been used to derive the tractable and abundantly used Michaelis–Menten kinetics from the more precise but more complex mass action kinetics, a clear indication of the important role it has played in biochemical modeling. A series of mathematical studies [115, 11, 124] have quantified its accuracy, proving it to be proportional to the timescale disparity present in the system to which it is applied. It follows that this approximation can be satisfactory in enzyme-catalyzed reactions where the concentration of enzyme is much smaller than that of its substrate since the timescale separation is large under this condition. In many other biochemical reactions such as those in signal transduction pathways, on the other hand, the timescale separation is often relatively small and for these reactions the quality of the approximation is much reduced.

Several approaches to extend the QSSA in order to obtain higher accuracy have been taken [32, 113, 110]. Common to many of these approaches is the *explicit identification* of a small parameter, typically denoted by ε, which measures the timescale disparity. This identification requires a host of theoretical considerations (see [115], for example), and it readily becomes prohibitively complicated for the realistically complex systems of biology. In this chapter, we propose a sequence of increasingly accurate refinements of the QSSA which are based on the zero-derivative principle (ZDP) [40, 139] and do not require the identification of such a parameter. The ZDP was pioneered by Kreiss and coworkers [13, 71, 72] in the applied mathematics/computational physics community. It has been employed previously in various fields to obtain accurate, yet simplified descriptions of complex models but not yet in the current biochemical context. We apply the ZDP to two systems: first, to a prototypical example with a reversible enzymatic reaction and, second, to the substantially more complex phosphotransferase system (PTS), a signal transduction pathway regulating and catalyzing glucose uptake in enteric bacteria. In both cases, we demonstrate that our results are more accurate than those obtained by the QSSA.

An alternative model reduction method which offers higher accuracy than QSSA and which also is based on timescale disparities although conceptually less similar to the QSSA than the methods discussed above, is the intrinsic low-dimensional manifold (ILDM) method [82]. This method has been used previously for the reduction of biochemical systems [121, 141]. As background research for the work presented in this chapter, we also implemented the ILDM method for the reduction of biochemical models; the main reason that we opted to work on ZDP instead was that we assessed the numerical issues associated with the implementation of this method easier to handle than those involved in the implementation of ILDM. Further, the ZDP approach is of interest since it offers a means to obtain *arbitrarily* high accuracy as opposed to ILDM.

In this chapter, we first revisit key ideas underlying the derivation of simplified models by exploiting the timescale separation present in biochemical systems and elucidate our discussion by working with the prototypical enzyme-catalyzed reaction

discussed above. Subsequently, we briefly review the QSSA and then motivate and present the ZDP. We apply both of these to our prototypical example and discuss the similarities and differences between the results yielded by each one of them. Finally, we apply the QSSA and ZDP to the large, realistic PTS model.

3.2 Timescale separation in biochemical systems

In this section, we briefly review how timescale separation leads to the emergence of constraining relations, and we demonstrate how these relations may be used to obtain simplified descriptions of dynamical systems. Our aim here is to provide a short, self-contained introduction to the subject of nonlinear multiscale reduction from a biochemical point of view. We refer to [45, 98, 63] for more detailed and broader introductions to this subject.

3.2.1 Timescale separation in an enzymatic reaction

For concreteness of presentation, we start with a specific mechanism, namely a reversible enzyme-catalyzed reaction. More specifically, we consider an enzyme E catalyzing the conversion of a substrate S to a product P by means of binding to S to form a complex C,

$$E + S \underset{k_{-1}}{\overset{k_1}{\rightleftharpoons}} C \underset{k_{-2}}{\overset{k_2}{\rightleftharpoons}} E + P. \tag{3.1}$$

We assume that both the binding of S to E and the release of P are reversible reactions, and hence the conversion of substrate to product is also an overall reversible reaction. This mechanism has been analyzed in detail, see [92, 112] and references therein. Our presentation here summarizes certain key facts which we shall need below.

In what follows, we denote the concentrations of S, P, E, and C by s, p, e, and c, respectively. We regard the total concentration of (free and bound) enzyme $e_{tot} = e + c$ as constant, based on the fact that changes on the genetic level are slow compared to those on the metabolic one. We further assume that p is also kept constant—for example, by introducing another enzyme-catalyzed reaction in which P is consumed and where the enzyme has very high elasticity with respect to P. (This second assumption serves to reduce the number of variables so as not to clutter our model. It by no means pertains to the nature of our analysis.)

Under these assumptions, the state of the system is fully described by two state variables, either s and c or s and e; for historical reasons, we choose to employ s and c. The evolution in time of the state variables is given by the ordinary differential equations (ODEs)

$$\dot{s} = -v_1 \quad \text{and} \quad \dot{c} = v_1 - v_2, \tag{3.2}$$

together with the initial conditions $s(0) = s_0$ and $c(0) = c_0$. The reaction rates v_1 and v_2 are given by mass action kinetics; since $e = e_{tot} - c$, we find that

$$v_1 = k_1 (e_{tot} - c)\, s - k_{-1}\, c \quad \text{and} \quad v_2 = k_2\, c - k_{-2} (e_{tot} - c)\, p, \tag{3.3}$$

where the rate constants $k_1, \ldots, k_{-2}$ are arbitrary but given.

The equilibrium of the enzymatic reaction (1), *i.e.* the state in which $v_1 = v_2 = 0$, is given by

$$(s^*, c^*) = \left(\frac{k_{-1}\, k_{-2}\, p}{k_1\, k_2}, \frac{k_{-2}\, p\, e_{tot}}{k_2 + k_{-2}\, p} \right). \tag{3.4}$$

The concentrations $s(t)$ and $c(t)$ approach the equilibrium at a decreasing rate. Plotting these concentrations in the (s, c)-plane yields a *trajectory* (a curve) which is parameterized by time—every point on the curve corresponds to a value $(s(t), c(t))$, for some time t, and *vice versa*, see Figure 3.1. It becomes evident from this figure that the evolution of s and c towards their equilibrium values runs through two distinct phases. In the first phase, c increases (or decreases) while s remains essentially constant, corresponding to an initial rapid binding of S to E (or dissociation of C). In the second phase, both variables evolve at similar rates towards their equilibrium values, corresponding to the consumption of substrate by the enzyme. The duration of the first phase is far shorter than that of the second one, a fact which has led researchers to label the dynamics driving the former *fast* (or *transient*) and those driving the latter *slow*. This fact also suggests that, except for a short initial period, the evolution of the system is described by the part of the trajectory corresponding to the second, slow phase.

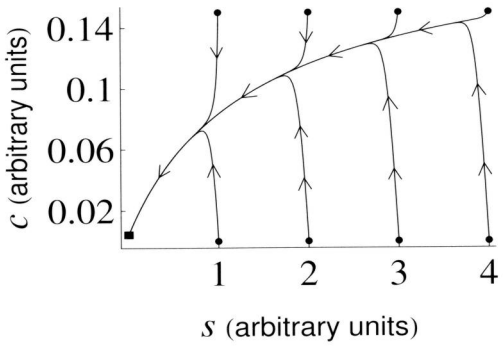

Figure 3.1: Graph of the $(s, c)-$plane for (3.2)–(3.3) with several trajectories corresponding to different initial conditions (round dots) and the steady state $(s^*, c^*) = (0.003, 0.0043)$ (square dot). The rate constants here are $k_1 = 1.833$, $k_{-1} = 0.25$, $k_2 = 2.5$, and $k_{-2} = 0.55$, while $e_{tot} = 0.2$ and $p = 0.1$.

A related feature of model (3.2–3.3) (and one of central importance to this study) becomes apparent upon plotting the trajectories corresponding to several initial conditions. In particular, Figure 3.1 shows that all trajectories approach a certain curve in the $(s, c)-$plane during the first phase and stay in a neighborhood of it during the second phase (see also [18] for the irreversible case). This curve is called a *normally attracting, slow invariant manifold (SIM)*. The SIM serves to link the full to the fully relaxed dynamics, as the system dynamics follows a cascade from *full* (approach to the SIM) to *partially relaxed* (close to the SIM) to, eventually, *fully relaxed* (close to

the equilibrium). In this sense, SIMs form the backbone on which the dynamics is organized at intermediate timescales.

The SIM is the graph of a *constraining relation*—that is, of a relation $c = c(s)$ dictating that, past the transient phase, the complex concentration is approximately a function of the substrate concentration. Knowledge of the constraining relation $c = c(s)$ allows one to *reduce* (3.2)–(3.3) to the single ODE

$$\dot{s} = -k_1 \left(e_{tot} - c(s)\right) s + k_{-1}\, c(s).$$

This ODE, together with the constraining relation $c = c(s)$ and the conservation laws $e(t) + c(t) = e_{tot}$ and $p(t) = p$, describes the dynamics of the system at the slow timescale.

3.2.2 General multiscale systems

Here, we generalize the notions introduced above to more general multiscale systems. In what follows, we use the term *state variables* to denote those time-dependent variables in a biochemical system which fully describe the system at any given moment. (State variables are, typically but not exclusively, molecular concentrations. In certain models, they can also be linear combinations of such concentrations or other time-dependent quantities such as pH or membrane potential.) First, we collect the values of all n state variables (where n is a natural number depending on the complexity of the system) at any time instant t in a column vector $z(t)$. The time evolution of the components of z is dictated by a set of *state equations* in the form of ODEs,

$$\dot{z}(t) = f(z(t)), \tag{3.5}$$

where f is a vector-valued function of n variables and with n components. In the case of the simple enzyme reaction model in the previous subsection, we have

$$n = 2, \quad z = \begin{pmatrix} s \\ c \end{pmatrix}, \quad \text{and} \quad f(s,c) = \begin{pmatrix} k_{-1}c - k_1(e_{tot} - c)s \\ (k_1 s + k_{-2}p)(e_{tot} - c) - (k_{-1} + k_2)c, \end{pmatrix},$$

see (3.2)–(3.3). The $n-$dimensional Euclidean space $\mathbb{R}^n$, which is where the state variables collected in z assume values, is called the *state space* (in the enzyme reaction example, this is the $(s,c)-$plane). A solution $z(t)$ of (3.5) corresponding to any given initial condition $z(0) = z_0$ and plotted in the state space for all t is a *trajectory*, whereas any value z^* satisfying $f(z^*) = 0$ is a *steady state*. (In the example above, the condition $f(s^*, c^*) = 0$ is fulfilled when $v_1 = v_2 = 0$, cf. (3.2), and therefore the unique steady state of that specific system is the equilibrium (3.4) of the enzymatic reaction.)

As we mentioned in the Introduction and demonstrated in the example above, the various processes in a biochemical system typically act at vastly disparate timescales, resulting in a separation of its dynamics into fast and slow. In this general case also, this behavior manifests itself in the state space by means of trajectories approaching a lower-dimensional SIM—that is, a manifold which is invariant under the dynamics,

attracts nearby orbits, and on which system evolution occurs on a slow timescale.[1] In what follows, we write $n_x < n$ for the dimension of this SIM and use the shorthand $n_y = n - n_x$ (in the case of the enzyme reaction model above, this SIM is a curve and thus $n_x = n_y = 1$). This approach occurs along specific directions *transversal* to the SIM (*normal attractivity*) and corresponding to n_y (possibly nonlinear) combinations of molecular concentrations remaining approximately constant during the fast transient. (In the case of the enzyme reaction in Figure 3.1, this approach is approximately vertical—$s \approx const.$—since s is approximately conserved in that phase.) Evolution on and near the SIM occurs on a *slower* timescale, while trajectories starting on the SIM remain on it for all times (*invariance*)—see [45, 63] for more technical definitions of these terms.

It is typically the case that the state variables collected in z can be partitioned into two groups,

$$z = \begin{pmatrix} x \\ y \end{pmatrix}, \text{ where } x \text{ is } n_x\text{–dimensional and } y \text{ is } n_y\text{–dimensional,}$$

so that the SIM is the graph of a constraining relation $y = g(x)$, for some function g of n_x variables and with n_y components. In that case, one may rewrite (3.5) as

$$\dot{x} = f_x(x, y) \quad \text{and} \quad \dot{y} = f_y(x, y), \tag{3.6}$$

where f_x and f_y collect the vector field components of f corresponding to x and y, respectively. Thus, one obtains the reduced system

$$\dot{x} = f_x(x, g(x)), \quad \text{together with the constraining relation } y = g(x), \tag{3.7}$$

which employs the n_x variables x and describes the slow dynamics. This ODE describes the dynamics of the partially relaxed phase and is typically easier to analyze and interpret than the full model (3.5) (or, equivalently, (3.6)). Thus, this reduced dynamics is also easier to relate to the investigator's intuitive understanding in order to reinforce or correct intuition, as the case may be.

Remark. It often occurs that a given system has *many* timescales instead of only two (fast and slow). In the course of each timescale, a number of processes approximately balance, and thus the number of approximately balanced processes increases from one phase to the next. This behavior is manifested in the state space through a *hierarchy of SIMs* of decreasing dimensions and embedded in one another. In this setting, there are no unique transient and partially relaxed phases, but rather a cascade of as many phases as timescales, with each consecutive phase exhibiting slower and lower dimensional dynamics than its predecessor. At the end of each phase, trajectories have been attracted to the next SIM in the hierarchy so that the system dimensionality decreases further. Hence, the dimension of the reduced model depends on the timescale that is of interest to the investigator.

[1] SIMs are typically not unique—instead, there is an entire continuous *family* of SIMs corresponding to trajectories with initial conditions in the slow region of the state space and each member of which may be used to reduce the system (see, *e.g.*, [63]).

3.3 Approximating the slow behavior

The explicit determination of the constraining relations $y = g(x)$ is impossible for most biochemical systems. Indeed, the timescale separation in realistic systems is always finite, and thus the transition from fast to slow dynamics described in the previous section is not instantaneous but gradual. As a result, the notions of fast and slow dynamics are not absolute but, rather, at an interplay with each other the assessment of which is a difficult task. To circumvent this difficulty, a collection of methods to *approximate* constraining relations has been developed. Among these, the QSSA is the best known and well-studied. It was developed to obtain an approximate reduced description of an enzymatic reaction valid over a slow timescale [12], and it is also the precursor to the ZDP. In the coming two sections, we review the QSSA and apply it to our enzyme reaction example. Then, we introduce the ZDP which extends the QSSA.

3.3.1 The quasi-steady-state approximation

In what follows, we assume the setting introduced in the previous section. In particular, we assume that the system under study is fully described by an n-dimensional vector z of state variables evolving under (3.5), for some function f, and also that it possesses a SIM of dimension $n_x < n$. The QSSA assumes that, during partial relaxation, certain of the variables (which we denote by $\bar{y}$, with $\dim(\bar{y}) = n_y = n - n_x$) are at quasi-steady-state with respect to the instantaneous values of the remaining state variables (which we denote by $\bar{x}$, with $\dim(\bar{x}) = n_x$). Mathematically, this assumption translates into the condition

$$f_{\bar{y}}(\bar{x}, \bar{y}) = 0. \tag{3.8}$$

Here, the dimensionality n_x and the decomposition of z into an n_x-dimensional component $\bar{x}$ and an n_y-dimensional component $\bar{y}$ is to be determined by the investigator, typically on the basis of experience stemming from experimental results and possibly also from simulation or analysis of the model. The system of n_y equations in n unknowns collected in (3.8) constitutes the *QSSA constraining relation* (an approximation to the exact constraining relation), and its set of solutions describes, under generic conditions, an n_x-dimensional manifold called the *QSSA manifold* (an approximation to a SIM). Typically, (3.8) can be solved for n_y of the state variables, which we denote by y (see also the previous section), to yield the explicit reformulation $y = g_{qssa}(x)$ of the QSSA constraining relation; here, g_{qssa} is a vector function of n_x variables and with n_y components. In geometric terms, the QSSA manifold is the graph of $y = g_{qssa}(x)$, and we say that the QSSA manifold is *parameterized* by x. (It is often the case that $\bar{y} = y$, *i.e.*, that (3.8) may be solved for the same variables $\bar{y}$ that are at quasi-steady-state—see also our treatment of the enzyme reaction example below.)

Whenever (3.8) can be written as $y = g_{qssa}(x)$, one can obtain an approximation to the slow dynamics by substituting this expression into the state equation for x,

$$\dot{x} = f_x\left(x, g_{qssa}(x)\right). \tag{3.9}$$

This system of n_x ODEs describes the slow dynamics *on* the QSSA manifold and, together with the constraining relation $y = g_{qssa}(x)$, also the approximate state of the system during the partially relaxed phase.

3.3.2 Enzyme kinetics based on QSSA

We now discuss the application of QSSA to the reversible enzyme reaction (3.1) and demonstrate that the reduced system corresponds to the enzyme kinetic expression for the rate of reversible reactions known as the *reversible Michaelis–Menten equation.* We also identify a parameter regime for which the QSSA produces an inaccurate description of the system dynamics.

Recall the network (3.1) and the corresponding ODE system (3.2)–(3.3),

$$\dot{s} = k_{-1}\, c - k_1\, (e_{tot} - c)\, s \quad \text{and} \quad \dot{c} = (e_{tot} - c)\, (k_1\, s + k_{-2}\, p) - (k_{-1} + k_2)\, c. \tag{3.10}$$

In living cells, there is often a huge excess of substrate with respect to the total enzyme, and we write $s_0 \gg e_{tot}$. As a result, the concentration c of complex may assume its quasi-steady-state with respect to the initial value of s rapidly, whereas the effect of this process on s is marginal. Following the discussion above, it is natural to set $\bar{x} = s$ and $\bar{y} = c$, so that $n_x = n_y = 1$ and

$$f_{\bar{x}} = f_s = k_{-1}\, c - k_1\, (e_{tot} - c)\, s \quad \text{and} \quad f_{\bar{y}} = f_c = (e_{tot} - c)\, (k_1\, s + k_{-2}\, p) - (k_{-1} + k_2)\, c.$$

The QSSA (3.8) $f_c = 0$ can be solved for either c (case $x = \bar{x}$, $y = \bar{y}$) or s (case $x = \bar{y}$, $y = \bar{x}$). Here, we follow the conventional, former option to obtain the explicit form

$$c = g_{qssa}(s) = \frac{(k_1\, s + k_{-2}\, p)\, e_{tot}}{k_1\, s + k_{-2}\, p + k_{-1} + k_2} \tag{3.11}$$

for the QSSA constraining relation. The graph of g_{qssa} in the state space constitutes the QSSA manifold. Substitution from (3.11) into the first ODE in (3.10), together with the definitions

$$V_s = k_2\, e_{tot}, \quad V_p = k_{-1}\, e_{tot}, \quad K_s = (k_{-1} + k_2)/k_1, \quad \text{and} \quad K_p = (k_{-1} + k_2)/k_{-2}, \tag{3.12}$$

yields the reversible Michaelis–Menten form

$$\dot{s} = -\frac{\frac{V_s}{K_s}\, s - \frac{V_p}{K_p}\, p}{1 + \frac{s}{K_s} + \frac{p}{K_p}}. \tag{3.13}$$

This is the QSSA-reduced system (3.9) for the model (3.1).

In Figure 3.2, we have plotted the QSSA manifolds given by (3.11) together with the time evolution of s and c, computed numerically using (3.10), for various initial conditions and for three different total enzyme concentrations. When the substrate concentration is much larger than the total enzyme concentration, as in Figure 3.2A, the trajectories approach a curve which is virtually indistinguishable from the QSSA manifold, as expected. When the total enzyme concentration is comparable to or even higher than that of the substrate, as in Figs. 3.2B and 3.2C, respectively, the

timescale separation is smaller but still sufficient to drive the trajectories onto a SIM. In those cases, the QSSA manifolds are poor approximations to the SIMs which are outlined by trajectories; this is to be expected, since the condition $s_0 \gg e_{tot}$ does not hold anymore. In what follows, we will see that the ZDP produces a more accurate approximation of the SIM than the QSSA manifold.

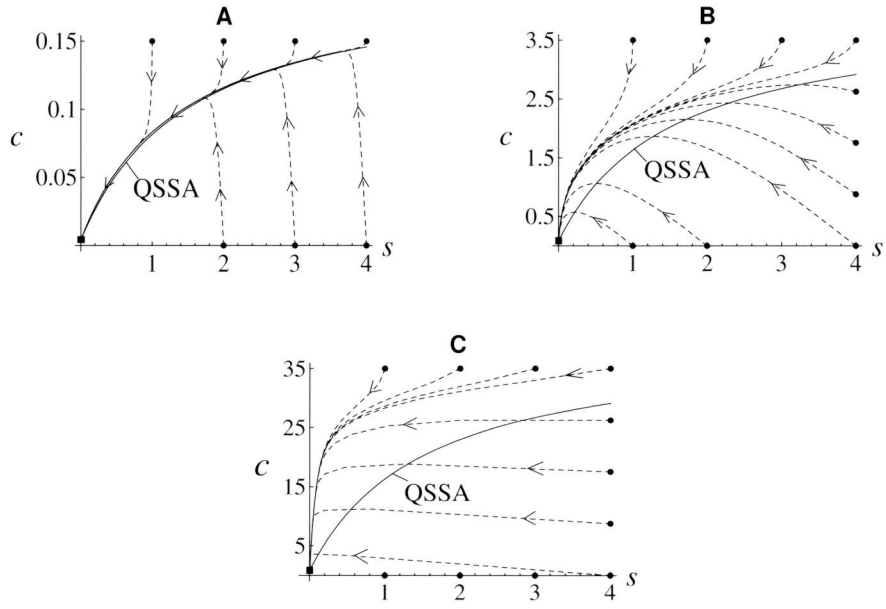

Figure 3.2: Trajectories of the system (3.10) together with QSSA manifolds (3.11). The parameter values of k_1, k_{-1}, k_2, k_{-2}, and p are the same as in Figure 3.1 and the total enzyme concentration is $e_{tot} = 0.2$ in panel A, $e_{tot} = 4$ in B, and $e_{tot} = 40$ in C.

3.3.3 The zero-derivative principle

Here, we introduce the ZDP as an accurate generalization of the QSSA. The ZDP manifold of order m—where m can take the values $0, 1, 2, \ldots$—is defined to be the set of points that satisfy the algebraic condition

$$\frac{d^{m+1}\bar{y}}{dt^{m+1}} = 0 \tag{3.14}$$

and denoted by ZDP_m. As was the case with the QSSA, $\bar{y}$ denotes variables that can be assumed to be in partial relaxation, that is, variables which evolve in a fast timescale. The time derivative in the ZDP condition (3.14) is calculated using (3.5),

so that this condition becomes

$$0 = \frac{d\bar{y}}{dt} = f_{\bar{y}} \quad \text{for} \quad m = 0, \tag{3.15}$$

$$0 = \frac{d^2\bar{y}}{dt^2} = \frac{\partial f_{\bar{y}}}{\partial \bar{x}} f_{\bar{x}} + \frac{\partial f_{\bar{y}}}{\partial \bar{y}} f_{\bar{y}} \quad \text{for} \quad m = 1, \tag{3.16}$$

and similarly for higher values of m, see also Chapter 4 of this thesis.

Plainly, the QSSA manifold and ZDP_0 coincide, as the conditions (3.8) and (3.14)–(3.15) defining them are identical: the QSSA and the zeroth order ZDP yield the same approximate constraining relation. The ZDP manifolds of higher orders, in turn, do not coincide with the QSSA manifold in general—for example, ZDP_1 generally differs from the QSSA manifold because of the presence of the first term in the right-hand side of (3.16). Instead, the ZDP conditions of higher orders are natural *extensions* of the QSSA: they, also, yield a system (3.14) of algebraic equations, and the ZDP_m is the locus of points satisfying them. The sole difference between the two approaches is that the ZDP replaces the first order time derivative employed by the QSSA with *higher order* time derivatives, see (3.14).

Although technically more involved, this approach has proven to perform well; in fact, the sequence of manifolds ZDP_0, ZDP_1, ... limits to a SIM and hence serves to approximate an exact constraining relation with *arbitrary* accuracy [138]. To gain insight into this result, we recall that a SIM is the locus of points where system evolution is slow: the time derivatives of *all* orders of the state variables are small. On the QSSA manifold, $d\bar{y}/dt = 0$—nevertheless, the higher order time derivatives remain large on it. On ZDP_1, in turn, $d^2\bar{y}/dt^2 = 0$ and, additionally, $d\bar{y}/dt$ is small—higher order derivatives are, here also, large. More generally, $d^{m+1}\bar{y}/dt^{m+1}$ is identically zero on ZDP_m and $d\bar{y}/dt, \ldots, d^m\bar{y}/dt^m$ are small on it, as long as the variables $\bar{y}$ evolve on a fast timescale and the matrix $\partial f_{\bar{y}}/\partial \bar{y}$ appearing in (3.16) is non-singular [40, 138]. Since the ZDP_m with $m > 1$ achieves to bound more time derivatives than the QSSA manifold, it is also typically closer to a SIM. Alternatively, each time differentiation of a solution to (3.5) amplifies its fast component, and hence higher order ZDP conditions filter out this fast dynamics to successively higher orders: points satisfying these conditions yield solutions with fast components of smaller magnitude, *i.e.*, these points lie closer to a SIM.

In biochemical terms, and focusing on our enzyme kinetics example to add concreteness to our exposition, if substrate is injected into an enzyme assay at time zero, one observes a rapid binding of substrate to enzyme; accordingly, the concentration c of complex increases rapidly. Subsequently, both c and the concentration s of the injected substrate decreases very slowly in time: it is this second phase that our simplified enzyme kinetics should describe accurately. As the change in c is slow compared to that during the initial transient, the most straightforward approach would be to neglect it—the SIM is then approximated by requiring c to be constant, $dc/dt = 0$. This approach corresponds to the zeroth order ZDP approach, which is identical to the well-known QSSA approach, and it cannot be exact as c *does* change—albeit slowly. The first order ZDP assumption is similar to that underlying QSSA: here, c is allowed to change in time, albeit at a constant rate of change—*i.e.*, it is the time derivative of $v_1 - v_2$ that is set to zero, $d(v_1 - v_2)/dt = d^2c/dt^2 = 0$. This assumption

is also inexact, since it leads to linear temporal decay; nevertheless, it is more realistic than the QSSA, since the temporal evolution of $v_1 - v_2$ is slower (compared to its evolution over the initial transient) than that of c. This is precisely the amplification effect mentioned above, and it is plain to see in Figure 3.3: as e_{tot} increases, the change in $v_1 - v_2$ during the fast transient becomes larger than that during the slow phase by whole orders of magnitude. A similar reasoning applies to higher order ZDP conditions.

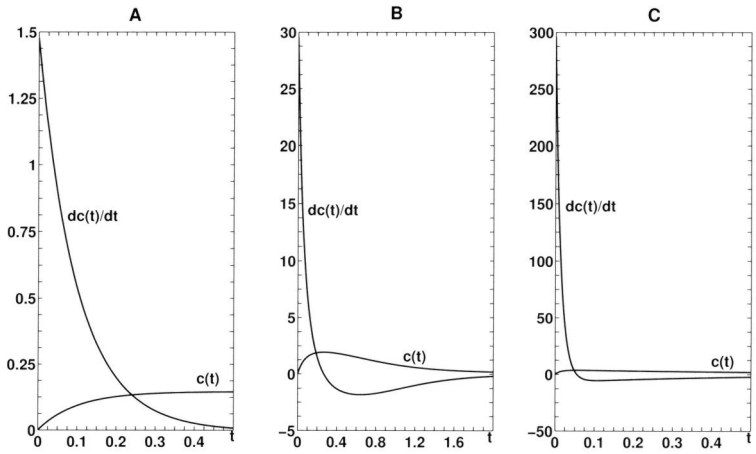

Figure 3.3: The time evolution of c and $\dot{c}$ for the system (3.10). The parameter values of k_1, k_{-1}, k_2, k_{-2}, and p and the total enzyme concentrations in each panel are the same as in Figure 3.2.

When enzyme kinetics is analyzed in intact systems, the dynamic scenario will be more complex. Still higher order ZDP approaches can be expected to be closer to the true behavior than lower order ZDPs.

3.4 Accurate enzyme kinetics based on ZDP

In this section, we apply the first order ZDP to our enzyme reaction example (3.1) and derive the corresponding rate law which is comparable to the reversible Michaelis–Menten (3.13) albeit more accurate. Then, we demonstrate that the ZDP-reduced model remains accurate even when the QSSA-reduced model fails.

Recalling (3.10) and (3.16), we find that the condition defining ZDP_1 becomes

$$\frac{d^2c}{dt^2} = -v_1\frac{\partial(v_1 - v_2)}{\partial s} + (v_1 - v_2)\frac{\partial(v_1 - v_2)}{\partial c} = 0, \tag{3.17}$$

where v_1 and v_2 are given in (3.3). This equation can be solved for either s or c; we choose the latter so as to express c as a function of s (here again, then, $x = \bar{x}$ and

$y = \bar{y}$, see also (3.11)). A tedious but direct calculation using (3.3) shows that (3.17) can be written in the quadratic form $\alpha(s)\,c^2 - \beta(s)\,c + \gamma(s) = 0$ where

$$\begin{aligned}\alpha(s) &= k_1(k_1 s + k_{-1}),\\ \beta(s) &= (k_1 s + k_{-1} + k_2 + k_{-2}p)^2 + k_1 e_{tot}(2k_1 s + k_{-1}),\\ \gamma(s) &= k_1^2 e_{tot}^2 s + e_{tot}(k_1 s + k_{-2}p)(k_1 s + k_{-1} + k_2 + k_{-2}p).\end{aligned}$$

The solutions to $\alpha(s)\,c^2 - \beta(s)\,c + \gamma(s) = 0$ are given by the standard formula $c_\pm(s) = [\beta(s) \pm \sqrt{[\beta(s)]^2 - 4\alpha(s)\gamma(s)}]/(2\alpha(s))$. The solution c_+, associated with the plus sign, is an artifact of the method and it must be discarded as it does not admit physical interpretation. Indeed, the steady state (s^*, c^*) does not belong to this solution. Also, for large s, one can show that $c_+(s) \approx s$ and thus also $c > e_{tot}$; plainly, this is impossible since the concentration of enzyme bound in substrate cannot exceed that of the total enzyme. The solution c_- associated with the minus sign, on the other hand, can be recast in the form

$$c_- = g_{zdp_1}(s) = R_1(s)\,\frac{e_{tot}\,(k_1\,s + k_{-2}\,p)}{k_1\,s + k_{-1} + k_2 + k_{-2}\,p}, \tag{3.18}$$

where

$$R_1(s) = \frac{1 + \frac{k_1^2 e_{tot}\, s}{(k_1 s + k_{-2}p)\,(k_1 s + k_{-1} + k_2 + k_{-2}p)}}{1 + \frac{k_1 e_{tot}\,(2k_1 s + k_{-1})}{(k_1 s + k_{-1} + k_2 + k_{-2}p)^2}}\;\frac{2}{\left[1 + \sqrt{1 - 4\,\alpha(s)\,\gamma(s)/[\beta(s)]^2}\right]}.$$

The rightmost factor on the right-hand side of (3.18) is precisely the expression for the QSSA manifold, see (3.11). The coefficient $R_1(s)$, on the other hand, assumes moderate values and is close to 1 at large values of s, so that ZDP_1 lies close to the QSSA manifold for large s—this is plainly visible in Figure 3.4. This figure also shows that, in the region where the two manifolds differ significantly, the former better approximates a SIM than the latter, as evidenced by the trajectories approaching it. When the enzyme concentration exceeds that of the substrate, the two manifolds differ by a factor as large as 4.1, see lower panel of Figure 3.4B.

To obtain the reduced model corresponding to ZDP_1, we substitute from (3.18) into the first ODE in (3.10) and obtain

$$\dot{s} = -\frac{\frac{V_s}{K_s}s - \frac{V_p}{K_p}p + (R_1(s) - 1)\left[\left(\frac{s}{K_s} + \frac{p}{K_p} + \frac{V_p}{V_s}\left(1 + \frac{s}{K_s} + \frac{p}{K_p}\right)\right)\frac{V_s}{K_s}s - \frac{V_p}{K_p}p\right]}{1 + \frac{s}{K_s} + \frac{p}{K_p}}, \tag{3.19}$$

with $V_s, \ldots, K_p$ expressed in terms of $k_1, \ldots, k_{-2}$ via the parameter change (3.12). This is the precise analogue of (3.13). In Figure 3.5, we have plotted the curves $(s, -\dot{s})$ corresponding to these two reduced equations against that corresponding to a simulation of the full mass action kinetic model (3.10). Plainly, the ZDP-derived reduced model performs better than the QSSA-derived one. In particular, the latter *overestimates* the decay rate $-\dot{s}$, an artifact which we now proceed to explain. First, in reality, c decreases ($\dot{c} < 0$) during the slow timescale; contrast this to the QSSA, $\dot{c} = 0$. Now, (3.10) reads

$$\dot{c} = e_{tot}\,(k_1\,s + k_{-2}\,p) - (k_1\,s + k_{-1} + k_2 + k_{-2}\,p)\,c,$$

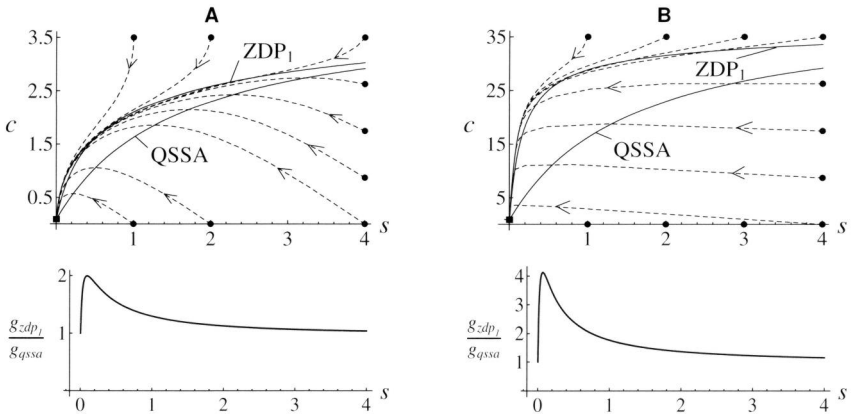

Figure 3.4: Upper panels: trajectories of the system (3.10) together with the ZDP_1 (3.18) and the QSSA (3.11) manifolds; parameter values in A and B are as in Figure 3.2B and 3.2C, respectively. Lower panels: the ratio $g_{zdp_1}(s)/g_{qssa}(s)$ for the corresponding parameter sets.

and thus $\dot{c}$ decreases with c. Hence, to sustain the inequality $\dot{c} < 0$ during the partially relaxed phase, the *actual* partially equilibrated value $c = g(s)$ must be *higher* than the value $c = g_{qssa}(s)$ predicted by the QSSA and satisfying $\dot{c} = 0$. (Recall that g corresponds to the exact constraining relation.) In other words, the QSSA underestimates c, see also Figure 3.4. Now, the ODE for s in (3.10) reads

$$-\dot{s} = k_1\, e_{tot}\, s - (k_{-1} + k_1\, s)\, c,$$

and hence $-\dot{s}$ decreases with c. Therefore, $-\dot{s}$ assumes a higher value if $c = g_{qssa}(s)$ is used instead of the exact $c = g(s)$, as Figure 3.5 also shows. Naturally, the first order ZDP, $d^2c/dt^2 = 0$, is also inexact; nevertheless, Figure 3.5 shows that it remains valid for modest timescale separations.

It became evident from this example that the analytic expressions for the approximate constraining relations provided by ZDP become increasingly complex as m increases. Additionally, since the number of equations in (3.14) equals $n_y < n$, and since n is much larger than 2 for most biochemical systems, one might wish to set $n_y > 1$, *i.e.*, eliminate *several* state variables. Such an elimination yields a *system* of nonlinear algebraic equations; analytic solutions of such systems are typically unattainable. Hence, high values of m and/or n_y imply that analytical solutions of (3.14) may be prohibitively complex or even unavailable. The obvious alternative to an analytical solution is a numerically computed approximation of it. In the next section, we demonstrate a method to calculate ZDP manifolds numerically.

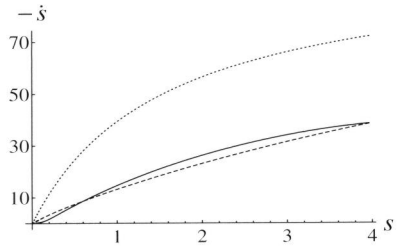

Figure 3.5: The curves $(s(t), -\dot{s}(t))$ given by the mass action kinetic model (3.10) (solid line), the QSSA-reduced model (3.13) (dotted line), and the ZDP_1-reduced model (3.19) (dashed line); the initial condition used was $s(0) = 4$ for the latter two systems and for the former system the additional initial condition used was $c(0) = 33.6$ (*i.e.*, the initial point is close to the SIM). The parameter values are the same as in Figure 3.4B.

3.5 ZDP for the phosphotransferase system in bacteria

In this section, we calculate numerically the one-dimensional ZDP_0 and ZDP_1 manifolds for the phosphotransferase system (PTS) as modeled in [99]. The PTS is a signal transduction pathway in enteric bacteria regulating the uptake of carbon sources and, in addition, it catalyzes the uptake of glucose. The model in [99] has thirteen state variables and all reaction rates are described by mass action kinetics. The reaction network is depicted in Figure 3.6, with further details given in Materials and methods.

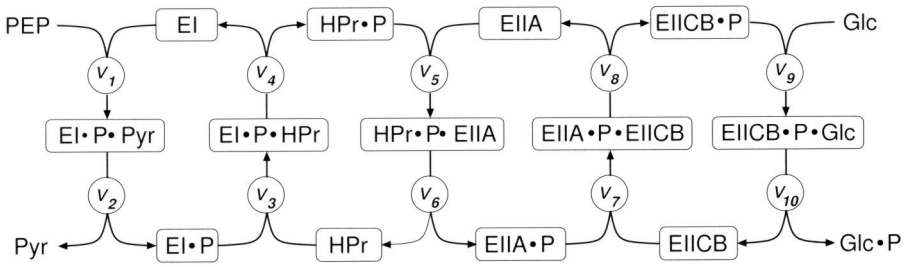

Figure 3.6: Reaction scheme for the PTS. The concentrations of the molecules depicted in boxes are the state variables in the model [99] while the concentrations of the remaining molecules are modeled as constants. Molecular names containing dots correspond to molecular complexes and P's denote phosphate groups. For explanations of the molecules involved, see Materials and methods.

3.5.1 Calculation of ZDP manifolds for the PTS model

As preparation for the application of ZDP, we first identify all four conservation relations for our model corresponding to the conserved total concentrations of the four proteins involved. This allows us to eliminate four state variables without any trade-off and in this way reduce the dimensionality of the state space to nine ($n = 9$), see Materials and methods.

As we remarked earlier, multiscale systems often possess a hierarchy of SIMs of decreasing dimension, embedded in one another, and corresponding to increasingly longer timescales. Since we aim to demonstrate ZDP, we restrict ourselves to one- and two-dimensional ZDP manifolds so as to be able to plot them. A simple timescale analysis using the eigenvalues of the Jacobian at the steady state shows that there is a considerable timescale difference between the least negative eigenvalue λ_1 and the second least negative eigenvalue λ_2 (in particular, $\lambda_2/\lambda_1 \approx 5.1$, see Materials and methods). By contrast, $\lambda_3/\lambda_2 \approx 1.5$ for the second and third least negative eigenvalues, and thus the corresponding timescale difference is relatively small. These calculations suggest, first, the existence of a one-dimensional SIM corresponding to the slowest timescale and, second, that the next manifold in the hierarchy is at least three-dimensional and thus not depictable. For these reasons, we focus on one-dimensional manifolds—that is, $n_x = 1$, and $n_y = 8$. We remark here that, first, more reliable methods to assess timescale disparities do exist and should be employed as needed (see also Chapter 4); second, this timescale analysis is only valid locally. To address this latter issue, the timescale disparity could be monitored as the SIM is being tabulated.

Having settled on the dimensionality of the SIMs to be investigated, the investigator must select the single state variable x parameterizing these SIMs as well as the eight state variables constituting $\bar{y}$ which reach a partial equilibrium on a fast timescale and are used to formulate the ZDP conditions (3.14). Where biochemical intuition is present, it should guide this choice of $\bar{y}$ along the same lines as in the QSSA case; in this example, we identified the choices of $\bar{y}$ yielding manifolds which attract nearby trajectories (and which, then, are good candidates for SIMs). Having investigated also which choices of x lead to a fast tabulation of the SIMs, we settled on $x = \bar{x} = [\mathrm{EIIA} \cdot \mathrm{P}]$ for both ZDP_0 and ZDP_1; hence, $y = \bar{y}$ contains the remaining eight state variables.

Using this choice of x, we tabulate ZDP_0 (equivalently, the QSSA manifold) and ZDP_1 over a grid consisting of 3901 equidistant points on the interval $[0.4, 39.4]$, *i.e.* almost the entire possible range of [EIIA·P] as $[\mathrm{EIIA}]_{tot}$=40 (the steady state value of [EIIA·P] is 15.4 μM). For each point x_j on the grid, we solved the eight-dimensional, nonlinear system (3.14) using the Newton–Raphson method. This calculation over the entire grid takes less than 5 sec in MATLAB on an Intel Pentium 4 CPU at 2.80 GHz and with 512 MB of RAM. The algorithm is described in detail in Chapter 4 of this thesis in which also a *Mathematica* version of the algorithm is given; the MATLAB code is provided in the Supporting information of [52]. Our results are shown in Figure 3.7. Plainly, all trajectories approach a SIM and subsequently move along it towards the steady state. Further, the trajectories remain closer to the ZDP_1 than to the QSSA manifold on their way to the steady state—an indication that the former is closer to a SIM than the latter. Using these plots and having measured

the concentration of EIIA·P, the investigator can read the values of the remaining 8 concentrations off the y-axes. For example, a concentration of 25 μM for EIIA·P yields a concentration of approximately 40 μM for HPr·P.

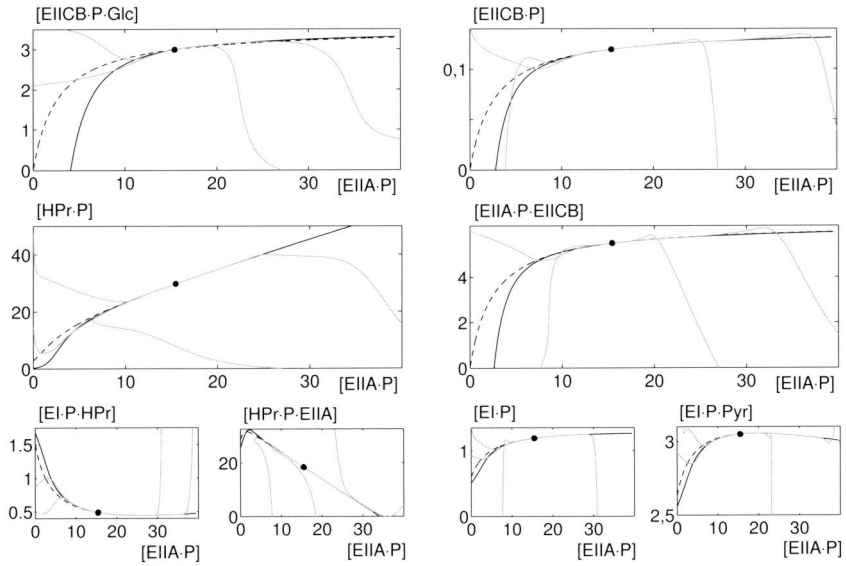

Figure 3.7: QSSA manifold (dashed), ZDP_1 (solid black), and trajectories (solid gray) for the PTS model. The one-dimensional manifolds are embedded in the nine-dimensional state space and are therefore depicted in eight plots: in each one of these, one of the state variables collected in y is plotted against the parameterizing variable x =[EIIA·P]. Four of the plots are enlarged to show more detail. The steady state is indicated, in each plot, by a black dot.

As we remarked earlier, an important assumption underlying both the QSSA and the ZDP_1 is that all variables collected in $\bar{y}$ evolve on a timescale which is fast relative to that of the behavior on the SIM. If this assumption is violated, then both methods yield erroneous results. For example, taking $\bar{x} = x$ = [EIICB·P·Glc], we obtain QSSA and ZDP manifolds which are very bad approximations of a SIM, see Figure 3.8. The reason for this is that the concentration of EIIA·P, which is now part of $\bar{y}$, evolves on a slow timescale compared to that of EIICB·P·Glc.

3.5.2 Using the tabulated ZDP_1 manifold to reduce the PTS model

As we saw, an explicit expression for a ZDP manifold—such as (3.18)—can be used to obtain a lower-dimensional model—such as (3.19). When a ZDP manifold is only available in tabulated form, though, such a reduced equation cannot be written out

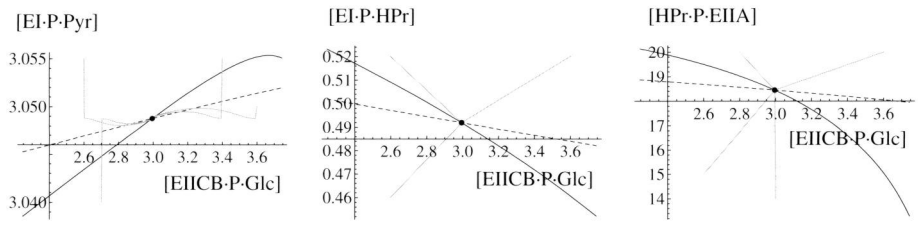

Figure 3.8: The analogue of Figure 3.7 for $x = \bar{x} =$[EIICB·P·Glc]. Three of the eight plots are shown.

explicitly. Nevertheless, one can still employ it in a computational setting, as we now proceed to show.

In the case of the PTS, the reduction to a one-dimensional ZDP_1 effectuates a description of the long-term dynamics by an (analytically unavailable) ODE of the form (3.7), with g_1 replacing g and with $x = [\mathrm{EIIA} \cdot \mathrm{P}]$. The unknown quantity $g_1(x)$ may be approximated, at any point x in the domain, either by explicitly solving (3.14) (with $m = 1$) at that point in the way described above or, instead, by first tabulating g_1 over a fine grid and then using this tabulation and an interpolation technique to approximate g_1 at *any* point x. The two major advantages of this reduced ODE over the full ODE system are, first, that its dynamics are one-dimensional and thus transparent and, second, that only the slow timescale is present in it and thus it is both easier and faster to integrate numerically.

To demonstrate the validity of this last statement, we compared the performance of a simple integrator for the ZDP_1-reduced PTS system against that of a state-of-the-art integrator for the full PTS system. Our simple integrator was coded up in MATLAB and is the standard, explicit, fourth-order Runge–Kutta method RK4 [49] coupled with a fine grid of 1001 points on the computational domain for x (which took 5sec to generate in MATLAB) and linear interpolation. The state-of-the-art integrator is MATLAB's implicit, stiff, fully automated integrator `ode23s` [116]. Normally speaking, explicit integrators are *prohibitively* costly when applied to stiff (*i.e.*, multiscale) problems [50]. In this case, though, and depending on the proximity of the initial condition to the steady state, our explicit integrator for the reduced system was between 5 and 25 times faster than the implicit integrator for the full model—a tangible indication of the degree to which the ZDP_1-reduced PTS system indeed describes the slow, non-stiff dynamics of the PTS model.

The behavior of the ZDP_1-reduced integrator is depicted in Figure 3.9. To produce it, we have set the initial value of each state variable to one-half of its steady state value (thus obtaining a point off the SIM) and then used MATLAB's aforementioned stiff integrator to obtain numerically the corresponding trajectory over a time horizon of 50msec. At the same time, we projected this initial condition on ZDP_1 and used it to initialize the reduced integrator and obtain the corresponding trajectory for the reduced system. It becomes evident that, following a short transient during which the two solutions differ, the solutions enter a phase where they converge to each

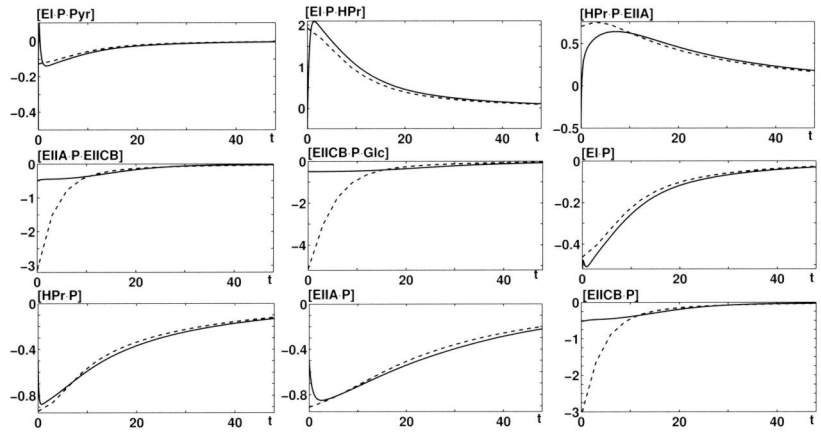

Figure 3.9: Time courses of the scaled state variables $(z_i - z_i^*)/z_i^*$, with $i = 1, \ldots, 9$, obtained by integrating the nine-dimensional PTS model with MATLAB's `ode23s` ODE suite (solid curves) and with the time measured in msec. The dashed curves are the corresponding solutions to the one-dimensional, ZDP_1-reduced model. The initial condition for all scaled variables was set to 0.5 (one half of the steady state, in terms of the unscaled variables z_i) and all time trajectories approach zero (as the unscaled variables tend to the steady state).

other and progress in unison towards the steady state: the reduced model matches the full one once the fast dynamics has been filtered out.

3.6 Discussion

The development of biochemical modeling for use in experimental design, drug development, and decipherment of cellular processes has accelerated in the last decade. Due to this, systems biology faces substantial challenges—most notably that of combining a large number of models of cellular processes to produce comprehensive quantitative descriptions of cellular function. Since these models—and hence also the resulting comprehensive descriptions—tend to be complex, the exploration of reduction methods designed to extract the core dynamics pertaining to cellular function is of great interest.

In this article, we have focused on the idea that biochemical systems may be reduced by exploiting the wide range of timescales typically present in them. In biochemistry, the most prominent reduction result is the Michaelis–Menten kinetics derived by employing QSSA to the mass action kinetic description of single enzymatic reactions. The Michaelis–Menten rate laws have proven extremely useful in describing the kinetics of reactions in which the enzyme concentrations are much lower than those of the substrate.

Such conditions are often encountered in *in vitro* assays and in the many processes *in vivo* in which the substrates are low-molecular weight molecules, as is the

case in *e.g.* metabolic pathways. However, as cell biology has developed, attention has shifted away from major metabolic pathways to pathways of gene expression and signal transduction. Hence, the substrates of enzymatic activity are no longer exclusively low-molecular weight substances but, instead, are often macromolecules (such as other enzymes). In certain cases, such as in the autokinase activity of growth factor receptors, the difference between substrate and enzyme is blurred. By consequence, the vast separation in the concentrations of enzymes and substrates disappears. This is also the case with enzymes acting on polynucleotides (such as DNA gyrase and ribosomes), where the concentrations of enzymes and binding sites are often of the same order of magnitude. In all of these cases, the accuracy of Michaelis–Menten kinetics is unsatisfactory due to the small timescale separation. Particular examples where the QSSA fails include the signal transduction routes such as the MAP kinase cascade, the EGF receptor transphosphorylation upon dimerization, and the regulation of processes through sequestration [5].

For mechanisms such as those mentioned above, where enzyme and substrate concentrations are comparable, modeling approaches offering higher accuracy are called for. Several approaches to develop rate laws for such cases have been taken. Specifically, for the example of phosphorylation cycles, the rapid-equilibrium approximation has been employed to derive such laws [101]. As discussed in the Introduction to this chapter, several methods extending the QSSA for general biochemical systems have been explored. In this article, we have introduced a novel generalization of the QSSA for general biochemical systems which is based on the zero-derivative principle (ZDP) and, contrary to these previous attempts, requires little theoretical work.

We derived the rate expression based on the (first order) ZDP for a reversible enzyme-catalyzed reaction, and we compared it to the corresponding Michaelis–Menten rate law. We showed that these two expressions match except for an additional multiplicative factor present in the ZDP description and absent from the QSSA one. This factor compensates, to a very large extent, for the fact that the concentration of the enzyme–substrate complex changes with time instead of remaining constant as the QSSA dictates. In cases of vast timescale separation, this factor is close to one and thus inconsequential. For modest timescale separations, however, this factor comes into play and renders the first order ZDP approximation considerably more accurate than the QSSA. We therefore expect that the novel kinetic description developed here will be useful in the many cases discussed above, *i.e.*, when the concentration levels of enzymes and their substrates are comparable.

To illustrate the usefulness of ZDP in cases where analytic expressions cannot be derived (as is typically the case already for systems of any complexity), we used it to perform the same task in a numerical setting and for the PTS model (which has a total of nine state variables). Using a standard numerical procedure, we computed the first order ZDP approximation for this model and demonstrated its superior accuracy. This study shows that the nine-dimensional PTS model behaves as a one-dimensional system in the slowest and most relevant timescale: tracing the evolution of [EIIA·P] suffices for understanding the behavior of the system as a whole over that timescale. We then also showed that calculation of time courses by numerical integration based on the ZDP_1 manifold is between 5 and 25 times faster than using a standard stiff

integrator in MATLAB to integrate the nine-dimensional PTS model, depending on the initial condition used.

An important reason for the ubiquitous use of enzyme kinetics of QSSA type has been its mathematical simplicity. In contrast, the ZDP methodology is quite complex and often defies analytical solutions, as is the case for the PTS model above, for example. In the past, this analytic intractability would have detracted greatly from the use of the method. Presently, however, the utilization of numerical mathematics in biochemistry has become so much more frequent that this limitation is retreating while the importance of accurate modeling and analysis approaches aiming at understanding the complex interactions in living cells is increasing.

Appendix

3.A The PTS model

Here we present the PTS model [99] in detail, list the linear conservation relations associated with it, and report numerical data related to the dimensionality and the choice of a parameterizing variable x for the ZDP manifolds.

The PTS is a mixed signal transduction, metabolic, and transport pathway involved in transporting various sugars into enteric bacteria, and the model we consider here deals particularly with glucose uptake. The source of free energy in this pathway is the phosphate group on phosphoenolpyruvate (PEP) which can be translocated by successive phosphorylations of pyruvate (Pyr), enzyme I (EI), histidine protein (HPr), enzyme IIA (EIIA), enzyme IICB (EIICB), and finally glucose (Glc), see Figure 3.6. The last phosphorylation prevents the glucose transporter from recognizing it and in this manner enables further glucose import into the cell. Consequently, the PTS enables the cell to maintain a glucose concentration gradient through the membrane. The PTS also regulates the uptake of various carbon sources depending on their availability, a phenomenon known as *carbon catabolite repression*. The model we consider, however, focuses on the uptake of the most common carbon source, *i.e.* glucose, and hence does not deal with this particular regulation.

The model in [99] (*original model*) has 13 state variables representing concentrations of macromolecules; these are listed in Table 3.1. The dynamics of the model is determined by the ODE system $\dot{\tilde{z}} = \tilde{N} v(\tilde{z})$, where the 13×10 stoichiometric matrix $\tilde{N}$, the 10 reaction rates collected in $v(\tilde{z})$, and the values of the kinetic parameters and of the constant concentrations are given in Table 3.2. We remark that, for the constant concentrations we used the values determined *in vivo* from the original article. All concentrations are measured in micromolar (μM) and time is measured in minutes. Since $\tilde{N}$ is of rank 9, there are 4 linear conservation relations. These can be determined as in [97], and they express mathematically the fact that the total concentration of each one of the four proteins is conserved. In particular, they are

$$\begin{array}{rclrcl} [\mathrm{EI}]_{tot} &=& \tilde{z}_1 + \tilde{z}_2 + \tilde{z}_6 + \tilde{z}_7, & [\mathrm{HPr}]_{tot} &=& \tilde{z}_2 + \tilde{z}_3 + \tilde{z}_8 + \tilde{z}_9, \\ [\mathrm{EIIA}]_{tot} &=& \tilde{z}_3 + \tilde{z}_4 + \tilde{z}_{10} + \tilde{z}_{11}, & [\mathrm{EIICB}]_{tot} &=& \tilde{z}_4 + \tilde{z}_5 + \tilde{z}_{12} + \tilde{z}_{13}. \end{array} \tag{3.20}$$

Using these, we can express $\tilde{z}_6$, $\tilde{z}_8$, $\tilde{z}_{10}$, and $\tilde{z}_{12}$ in terms of the remaining state variables, substitute these expressions in the original model, and obtain the nine-dimensional ODE system $\dot{z} = N v(z)$ (*final model*). Here, z is the vector of the new state variables (see Table 3.1) and the 9×10 stoichiometric matrix N is obtained from $\tilde{N}$ by deleting its sixth, eighth, tenth, and twelfth rows. We also note that we used the *in vivo* values from [99] for the conserved moieties collected in (3.20).

To select the dimension of the SIM and apply ZDP to the PTS system, we used the eigenvalues of the Jacobian $N \partial v(z)/\partial z|_{z^*}$, where $z^* = (3.05,\ 0.49,\ 18.45,\ 5.47,\ 2.99,\ 1.19,\ 29.78,\ 15.44,\ 0.12)$ is the steady state. Here, we report these eigenvalues: $\lambda_1 = -1732$, $\lambda_2 = -8851$, $\lambda_3 = -14109$, $\lambda_4 = -68060$, $\lambda_5 = -115750$, $\lambda_6 = -131042$, $\lambda_7 = -379063$, $\lambda_8 = -690343$, and $\lambda_9 = -6070420$.

Compound	O	F	Compound	O	F
EI·P·Pyr	$\tilde{z}_1$	z_1	HPr	$\tilde{z}_8$	–
EI·P·HPr	$\tilde{z}_2$	z_2	HPr·P	$\tilde{z}_9$	z_7
HPr·P·EIIA	$\tilde{z}_3$	z_3	EIIA	$\tilde{z}_{10}$	–
EIIA·P·EIICB	$\tilde{z}_4$	z_4	EIIA·P	$\tilde{z}_{11}$	z_8
EIICB·P·Glc	$\tilde{z}_5$	z_5	EIICB	$\tilde{z}_{12}$	–
EI	$\tilde{z}_6$	–	EIICB·P	$\tilde{z}_{13}$	z_9
EI·P	$\tilde{z}_7$	z_6			

Table 3.1: The state variables of the original (O) and the final (F) model represent the concentrations of the listed compounds.

$v_1 = k_{1f}\tilde{z}_6[\text{PEP}] - k_{1r}\tilde{z}_1$	$v_6 = k_{6f}\tilde{z}_3 - k_{6r}\tilde{z}_8\tilde{z}_{11}$
$v_2 = k_{2f}\tilde{z}_1 - k_{2r}\tilde{z}_7[\text{Pyr}]$	$v_7 = k_{7f}\tilde{z}_{11}\tilde{z}_{12} - k_{7r}\tilde{z}_4$
$v_3 = k_{3f}\tilde{z}_7\tilde{z}_8 - k_{3r}\tilde{z}_2$	$v_8 = k_{8f}\tilde{z}_4 - k_{8r}\tilde{z}_{10}\tilde{z}_{13}$
$v_4 = k_{4f}\tilde{z}_2 - k_{4r}\tilde{z}_6\tilde{z}_9$	$v_9 = k_{9f}\tilde{z}_{13}[\text{Glc}] - k_{9r}\tilde{z}_5$
$v_5 = k_{5f}\tilde{z}_9\tilde{z}_{10} - k_{5r}\tilde{z}_3$	$v_{10} = k_{10f}\tilde{z}_5 - k_{10r}\tilde{z}_{12}[\text{Glc·P}]$
$1 = \tilde{N}[1,1] = \tilde{N}[2,3] = \tilde{N}[3,5] = \tilde{N}[4,7] =$ $= \tilde{N}[5,9] = \tilde{N}[6,4] = \tilde{N}[7,2] = \tilde{N}[8,6] = \tilde{N}[9,4] =$ $= \tilde{N}[10,8] = \tilde{N}[11,6] = \tilde{N}[12,10] = \tilde{N}[13,8],$ $-1 = \tilde{N}[1,2] = \tilde{N}[2,4] = \tilde{N}[3,6] = \tilde{N}[4,8] =$ $= \tilde{N}[5,10] = \tilde{N}[6,1] = \tilde{N}[7,3] = \tilde{N}[8,3] = \tilde{N}[9,5] =$ $= \tilde{N}[10,5] = \tilde{N}[11,7] = \tilde{N}[12,7] = \tilde{N}[13,9]$	
$[\text{Glc}] = 500, [\text{Glc·P}] = 50, [\text{Pyr}] = 900, [\text{PEP}] = 2800,$ $k_{1f} = 1960, k_{1r} = 480000, k_{2f} = 108000, k_{2r} = 294,$ $k_{3f} = 14000, k_{3r} = 14000, k_{4f} = 84000, k_{4r} = 3360,$ $k_{5f} = 21960, k_{5r} = 21960, k_{6f} = 4392, k_{6r} = 3384,$ $k_{7f} = 880, k_{7r} = 880, k_{8f} = 2640, k_{8r} = 960,$ $k_{9f} = 260, k_{9r} = 389, k_{10f} = 4800, k_{10r} = 0.0054,$ $[\text{EI}]_{tot} = 5, [\text{HPr}]_{tot} = 50,$ $[\text{EIIA}]_{tot} = 40, [\text{EIICB}]_{tot} = 10$	

Table 3.2: Reaction rates (top), nonzero entries of the matrix $\tilde{N}$ (middle), and the values of the four boundary metabolite concentrations, the twenty kinetic parameter values, and the four total protein concentrations (bottom).

Chapter 4

An algorithm for the calculation of slow invariant manifolds based on the zero-derivative principle

In this chapter we present an algorithm for the numerical calculation of approximations to one- and two-dimensional slow invariant manifolds. The algorithm is based on the zero-derivative principle, which provides algebraic equations defining approximations to these manifolds, and it uses Newton's method to solve for points on the manifolds over a grid. We also provide the *Mathematica* code.

4.1 Introduction

The differences between the timescales on which the various processes in biochemical systems take place causes the dynamics of these systems to be organized around slow invariant manifolds (SIMs), which the trajectories in the system are attracted towards. In the previous chapter, we described how these SIMs can be used to construct reduced models and to obtain simplified views of the dynamics of the system. We also introduced the zero-derivative principle (ZDP) which defines manifolds that are approximations of SIMs, denoted ZDP manifolds, and we calculated such manifolds analytically and numerically for biochemical models and demonstrated their use for reduction of these models. In this chapter, we provide the numerical algorithm for the tabulation of ZDP manifolds that was employed in that chapter.

In the next section, we briefly review the dynamical setting that we will need here and we present the tabulation algorithm for the cases of one- and two-dimensional SIMs. Subsequently, we discuss in more detail certain technical issues pertaining to the algorithm. The *Mathematica* code is provided in Appendix 4.A. (A MATLAB code is provided in the supplementary information to our article [52].)

4.2 An algorithm for the tabulation of SIMs

4.2.1 Preliminaries

We assume the setting introduced in the previous chapter. In particular, the state of our biochemical system at any time instant t is fully determined by the values of n *state variables* (where n is a natural number depending on the complexity of the system), and we collect these in a column vector $z(t)$. The time evolution of z is determined by a model in the form of a system of ODEs (*state equations*),

$$\dot{z} = f(z(t)). \tag{4.1}$$

Here, $f : \mathbb{R}^n \to \mathbb{R}^n$ is an $n-$dimensional vector field of n variables, and the $n-$dimensional vector z takes values in the $n-$dimensional Euclidean space $\mathbb{R}^n$ (*state space*). We assume that the trajectories $z(t)$ of (4.1) approach a SIM, write $n_x < n$ for its dimension, and use the shorthand $n_y = n - n_x$. It is typically the case that the state variables collected in z can be partitioned into two groups,

$$z = \begin{pmatrix} x \\ y \end{pmatrix}, \text{ where } x \text{ is } n_x\text{–dimensional and } y \text{ is } n_y\text{–dimensional,}$$

so that the SIM is the graph of a *constraining relation* $y = g(x)$, for some function $g : \mathbb{R}^{n_x} \to \mathbb{R}^{n_y}$. In that case, we rewrite (4.1) as

$$\dot{x} = f_x(x, y) \quad \text{and} \quad \dot{y} = f_y(x, y), \tag{4.2}$$

where $f_x : \mathbb{R}^n \to \mathbb{R}^{n_x}$ and $f_y : \mathbb{R}^n \to \mathbb{R}^{n_y}$ are the vector field components corresponding to x and y, respectively. As explained in Chapter 3, our aim is to approximate the function g.

As we mentioned in Chapter 3, it is often the case that there are more than two timescales present in the dynamics of (4.1). In these cases, the dimension n_x of the SIM is dictated by the timescale of interest to the investigator. The simplest way to identify the timescales of the system is through a timescale analysis based on the eigenvalues of the Jacobian $\partial f/\partial z$. For the nine-dimensional phosphoenolpyruvate:glycose phosphotransferase system (PTS) considered in Chapter 3, in particular, we used this method to select $n_x = 1$. A more powerful (but substantially more involved) method to perform the same task is to use the finite-time Lyapunov exponents of the system [83, 84].

Once n_x has been selected, one has to investigate *which* $n_y = n - n_x$ state variables evolve on a fast timescale. These n_y variables, which we denote collectively by $\bar{y}$, are used to formulate the ZDP conditions

$$\frac{d^{m+1}\bar{y}}{dt^{m+1}} = 0. \tag{4.3}$$

The guiding principle behind this choice is that *all* n_y state variables collected in $\bar{y}$ must evolve on a fast timescale (compared to that of the dynamics on the SIM), so that the ZDP yields relevant results (see also Chapter 3). To the best of the author's knowledge, no universal method to determine fast variables has been developed; $\bar{y}$ is chosen, instead, based on experiments and simulations around the steady state z^*. Such a trial and error method has traditionally been used with success to determine $\bar{y}$ for the calculation of QSSA. The same considerations apply when employing a (higher order) ZDP, so that a choice of $\bar{y}$ which is suitable for QSSA may also be expected to be suitable for ZDP.

Once n_x and, subsequently, $\bar{y}$ have been selected, the $m-$th order ZDP condition (4.3) can be immediately formulated. This condition constitutes a system of n_y nonlinear, algebraic equations,

$$G_m(z) = \left.\frac{d^{m+1}\bar{y}}{dt^{m+1}}\right|_z = 0. \tag{4.4}$$

Here, the $(m+1)^{st}$ time derivative is calculated using the state equations (4.2), that is,

$$\begin{aligned} \frac{d\bar{y}}{dt} &= f_{\bar{y}}, \\ \frac{d^2\bar{y}}{dt^2} &= \frac{d}{dt}\left(\frac{d\bar{y}}{dt}\right) = \frac{df_{\bar{y}}}{dt} = \frac{\partial f_{\bar{y}}}{\partial \bar{x}}\frac{d\bar{x}}{dt} + \frac{\partial f_{\bar{y}}}{\partial \bar{y}}\frac{d\bar{y}}{dt} = \frac{\partial f_{\bar{y}}}{\partial \bar{x}} f_{\bar{x}} + \frac{\partial f_{\bar{y}}}{\partial \bar{y}} f_{\bar{y}}, \end{aligned} \tag{4.5}$$

and similarly for higher values of m.

Our aim is to identify the zero level set of the function G_m defined above, that is, the points z satisfying $G_m(z) = 0$. Identification of this type is typically done *parametrically*, that is, the investigator selects n_x variables (denoted by x) among the n variables z and, for each x, attempts to find values for the rest of the variables (denoted by y) such that $G_m(x, y) = 0$. In other words, one seeks a function $y = g_m(x)$ such that $G_m(x, g_m(x)) = 0$, for each x. (As explained in Chapter 3, there is no universal method to select x; often $x = \bar{x}$ is selected.) Unfortunately, an analytic

solution g_m for *nonlinear* systems $G_m(x, g_m(x)) = 0$ can only rarely be found. In this section, we present a numerical alternative to analytic solutions which is based on Newton's method [65]: for each fixed value of x (drawn from a discrete grid), one starts from an initial guess $y^{(0)}$ (typically depending on the value of x) and forms the sequence $\{y^{(0)}, y^{(1)}, y^{(2)}, \ldots\}$ by means of the explicit iteration rule

$$y^{(k+1)} = y^{(k)} - \left(\frac{\partial G_m\left(x, y^{(k)}\right)}{\partial y} \right)^{-1} G_m\left(x, y^{(k)}\right), \quad \text{for } k = 0, 1, \ldots. \tag{4.6}$$

(See [65, Chapter 5] for more details.) Provided that $y^{(0)}$ is close enough to $y = g_m(x)$, the sequence $\{y^{(k)}\}_k$ converges to $g_m(x)$ [65, Theorem 5.1.1].

In principle, an algorithm based on Newton iteration may be developed for any values of n and of $n_x < n$. Here, we limit ourselves to the cases of an arbitrary n and of $n_x = 1, 2$. The reasons behind this choice are, first, to retain the simplicity of presentation and, second, the fact that numerically tabulated manifolds of dimension three or more are often of limited applicability due to the computational cost associated with their tabulation.

4.2.2 The algorithm for the calculation of one-dimensional manifolds

Here, we provide the algorithm for the tabulation of approximations to one-dimensional SIMs, *i.e.*, for the case $n_x = 1$. The inputs to the algorithm are m (an arbitrary but fixed nonnegative integer) and an ODE model of the form (4.2). It follows implicitly that the partition of the state variables into $\bar{x}$ and $\bar{y}$ and then also into x and y has been achieved.

Step 1. Identify z^*. This identification can be done in a variety of ways, *e.g.*, by direct simulation of the system until it fully equilibrates or by solving the equation $f(z) = 0$ numerically or analytically.
Step 2. Construct a grid: Select the step size $dx > 0$, that is, the distance between neighboring points in the grid. (For simplicity of presentation, we will focus on a *uniform* grid.) Then, using x^*, the $x-$coordinate of z^*, and dx, construct the grid over which ZDP_m will be tabulated,

$$D = \{x_i = x^* + i\,dx \,|\, i_{min} \leq i \leq i_{max}\}.$$

Here, i takes all integer values between the integers $i_{min} \leq 0$ and $i_{max} \geq 0$. The values of i_{min} and i_{max}, together with the value of dx, determine the size of the interval around x^* over which the ZDP_m is tabulated. Plainly, $x_0 = x^*$.
Step 3a. Set $y_0 = y^*$; this is the desired value $g_m(x^*)$ of y, since it may be shown that $G_m(z^*) = 0$ for all values of m. (In other words, the steady state belongs to the ZDP manifolds of all orders.)
Step 3b. If $i_{max} = 0$, go to the next step. Otherwise, tabulate the manifold at the grid point x_1 using Newton iteration (4.6) with $x = x_1$ and with $y_1^{(0)} = y^*$. Declare the iteration procedure converged when the value of the quantity $\|y_1^{(k+1)} - y_1^{(k)}\|$ drops below a prescribed tolerance `tol`, since $y_1^{(k+1)} \approx g_m(x_1)$ for values of `tol` small

enough. (Other convergence criteria may also be used, see [65, Section 5.2].) Call the converged value y_1.

Step 3c. If $i_{min} = 0$, go to the next step. Otherwise, tabulate the manifold at the grid point x_{-1} using the procedure in Step 3b with x_{-1} replacing x_1 and with $y_{-1}^{(0)} = y^*$. Call the converged value y_{-1}.

Step 4a. If $i_{max} \leq 1$, go to the next step. Otherwise, tabulate the manifold at the grid points $x_2, \ldots, x_{i_{max}}$ (in this order) using the Newton iteration (4.6). For each $2 \leq i \leq i_{max}$, set $x = x_i$ and $y_i^{(0)} = 2y_{i-1} - y_{i-2}$ (this is the linear extrapolant from the tabulated values (x_{i-2}, y_{i-2}) and (x_{i-1}, y_{i-1}) to (x_i, y_i)). Call the converged value y_i.

Step 4b. If $i_{min} \geq -1$, go to the next step. Otherwise, tabulate the manifold at the grid points $x_{-2}, \ldots, x_{i_{min}}$ (in this order) as in Step 2c. The linear extrapolant in this case reads $y_i^{(0)} = 2y_{i+1} - y_{i+2}$. Call the converged value y_i.

The outcome of the algorithm are the pairs $\{(x_i, y_i)\}$ tabulating the ZDP_m over D. Further details on certain technical issues are provided in the next section.

4.2.3 The algorithm for the calculation of two-dimensional manifolds

Here, the algorithm for the tabulation of approximations to two-dimensional SIMs is given, *i.e.*, for the case when $n_x = 2$. The algorithm in this case follows closely the algorithm presented in the previous subsection, the sole major difference being the initialization of the Newton iteration. The inputs to the algorithm are the same as in the case $n_x = 1$.

Step 1. Same as Step 1 for the algorithm in the case $n_x = 1$.

Step 2. Select the step sizes $dx_1 > 0$ and $dx_2 > 0$ for the variables x_1 and x_2, respectively, and then construct the rectangular grid

$$D = \left\{ x_{i,j} = x^* + \begin{pmatrix} i\,dx_1 \\ j\,dx_2 \end{pmatrix} \;\middle|\; i_{min} \leq i \leq i_{max} \text{ and } j_{min} \leq j \leq j_{max} \right\}.$$

Here, i takes all integer values between the integers $i_{min} \leq 0$ and $i_{max} \geq 0$; similarly, j takes all integer values between the integers $j_{min} \leq 0$ and $j_{max} \geq 0$. Plainly, $x_{0,0} = x^*$.

Step 3a. Set $y_{0,0} = y^*$ as in Step 3a in the algorithm for $n_x = 1$.

Step 3b. If $i_{max} = 0$, go to the next step. Otherwise, tabulate the manifold at the grid point $x_{1,0}$ using Newton iteration (4.6) and with $y_{1,0}^{(0)} = y^*$. Declare the iteration procedure converged when the value of the quantity $\|y_{1,0}^{(k+1)} - y_{1,0}^{(k)}\|$ drops below a prescribed tolerance `tol`.

Step 3c. If $i_{min} = 0$, go to the next step. Otherwise, tabulate the manifold at the grid point $x_{-1,0}$ using the procedure in Step 3b and with $y_{-1,0}^{(0)} = y^*$.

Step 3d. If $j_{max} = 0$, go to the next step. Otherwise, tabulate the manifold at the grid point $x_{0,1}$ using the procedure in Step 3b and with $y_{0,1}^{(0)} = y^*$.

Step 3e. If $j_{min} = 0$, go to the next step. Otherwise, tabulate the manifold at the grid point $x_{0,-1}$ using the procedure in Step 3b and with $y^{(0)}_{0,-1} = y^*$.
Step 4a. If $i_{max} \leq 1$, go to the next step. Otherwise, tabulate the manifold at the grid points $x_{2,0}, \ldots, x_{i_{max},0}$ (in this order) using the Newton iteration (4.6). For each $2 \leq i \leq i_{max}$, set $y^{(0)}_{i,0} = 2y_{i-1,0} - y_{i-2,0}$ (see also Step 4a in the algorithm for $n_x = 1$).
Step 4b. If $i_{min} \geq -1$, go to the next step. Otherwise, tabulate the manifold at the grid points $x_{-2,0}, \ldots, x_{i_{min},0}$ (in this order) as in Step 4a with $y^{(0)}_{i,0} = 2y_{i+1,0} - y_{i+2,0}$.
Step 4c. If $j_{max} \leq 1$, go to the next step. Otherwise, tabulate the manifold at the grid points $x_{0,2}, \ldots, x_{0,j_{max}}$ (in this order) as in Step 4a with $y^{(0)}_{0,i} = 2y_{0,i-1} - y_{0,i-2}$.
Step 4d. If $j_{min} \geq -1$, go to the next step. Otherwise, tabulate the manifold at the grid points $x_{0,-2}, \ldots, x_{0,j_{min}}$ (in this order) as in Step 4a with $y^{(0)}_{0,i} = 2y_{0,i+1} - y_{0,i+2}$.
Step 5a. If $i_{max} = 0$ or $j_{max} = 0$, go to the next step. Otherwise, tabulate the manifold at the grid points $x_{1,1}, \ldots, x_{i_{max},1}, \ldots, x_{1,j_{max}}, \ldots, x_{i_{max},j_{max}}$ (in this order) using the Newton iteration (4.6). For each $1 \leq i \leq i_{max}$ and $1 \leq j \leq j_{max}$, set $y^{(0)}_{i,j} = y_{i-1,j} + y_{i,j-1} - y_{i-1,j-1}$; this is the linear extrapolant from $z_{i-1,j}$, $z_{i,j-1}$, and $z_{i-1,j-1}$ (the already tabulated three nearest neighbors to the left and below) to $z_{i,j}$.
Step 5b. If $i_{min} = 0$ or $j_{max} = 0$, go to the next step. Otherwise, tabulate the manifold at the grid points $x_{-1,1}, \ldots, x_{i_{min},1}, \ldots, x_{-1,j_{max}}, \ldots, x_{i_{min},j_{max}}$ (in this order) as in Step 5a with $y^{(0)}_{i,j} = y_{i+1,j} + y_{i,j-1} - y_{i+1,j-1}$.
Step 5c. If $i_{min} = 0$ or $j_{min} = 0$, go to the next step. Otherwise, tabulate the manifold at the grid points $x_{-1,-1}, \ldots, x_{i_{min},-1}, \ldots, x_{-1,j_{min}}, \ldots, x_{i_{min},j_{min}}$ (in this order) as in Step 5a with $y^{(0)}_{i,j} = y_{i+1,j} + y_{i,j+1} - y_{i+1,j+1}$.
Step 5d. If $i_{max} = 0$ or $j_{min} = 0$, go to the next step. Otherwise, tabulate the manifold at the grid points $x_{1,-1}, \ldots, x_{i_{max},-1}, \ldots, x_{1,j_{min}}, \ldots, x_{i_{max},j_{min}}$ (in this order) as in Step 5a with $y^{(0)}_{i,j} = y_{i-1,j} + y_{i,j+1} - y_{i-1,j+1}$.

Here also, technical details are given in next section.

4.3 Technical issues

In this section, we discuss a number of technical issues pertaining to the algorithms presented in the previous section. In particular, we discuss efficient ways to calculate the $(m+1)^{st}$ time derivative G_m, the Jacobian block $\partial G_m/\partial y$, and the application of its inverse to G_m as required by Newton's method (4.6).

4.3.1 Calculation of G_m

The function G_m can be calculated, at any point z, in at least two manners. The first of these corresponds to using the recursive formulas

$$\begin{aligned} G_0(z) &= f_{\bar{y}}(z), \\ G_{m+1}(z) &= \left(\frac{\partial G_m(z)}{\partial \bar{x}}\right) f_{\bar{x}}(z) + \left(\frac{\partial G_m(z)}{\partial \bar{y}}\right) f_{\bar{y}}(z), \quad \text{for } m = 0, 1, \ldots, \end{aligned} \tag{4.7}$$

to obtain analytic formulas for G_m. The first of these formulas is precisely (4.5), while the second one is derived through the elementary calculation

$$G_{m+1} = \frac{d^{m+2}\bar{y}}{dt^{m+2}} = \frac{d}{dt}\left(\frac{d^{m+1}\bar{y}}{dt^{m+1}}\right) = \frac{dG_m}{dt} = \frac{\partial G_m}{\partial \bar{x}}\frac{d\bar{x}}{dt} + \frac{\partial G_m}{\partial \bar{y}}\frac{d\bar{y}}{dt}$$

and (4.2). In this manner, one can iteratively calculate analytic expressions for the functions $G_0, G_1, \ldots$ using a symbolic manipulation package to carry out the differentiations.

The second manner in which $G_m(z)$ may be calculated (or, rather, approximated) is through the *forward difference scheme* described in [40]. To approximate $G_m(z)$, one needs first to generate a numerical solution $z(t)$ of (4.1) with initial condition $z(0) = z$; this can be achieved by using a stiff integrator such as, for example, the routine `ode25s` in MATLAB. Then, one approximates G_m by means of the formula

$$G_m(z) = \frac{d^{m+1}\bar{y}}{dt^{m+1}}(z) \approx \frac{1}{H^{m+1}} \sum_{k=0}^{m+1} (-1)^{m+1-k} \begin{pmatrix} m+1 \\ k \end{pmatrix} \bar{y}(kH) = G_{m,H}(z). \quad (4.8)$$

Here, $H > 0$ is a small parameter and $\{\bar{y}(0), \bar{y}(H), \ldots, \bar{y}((m+1)H)\}$ is the $\bar{y}-$component of the (numerically obtained) solution $\{z(0), z(H), \ldots, z((m+1)H)\}$ of (4.1) (with initial condition at $t = 0$ equal to z, the point at which we wish to approximate G_m) and sampled at times $t = 0, \ldots, t = (m+1)H$. It can be shown that $G_{m,H}(z)$ converges to $G_m(z)$, as $H \downarrow 0$, and thus $G_{m,H}(z) \approx G_m(z)$ for small values of H.

4.3.2 Calculation of $\partial G_m(z)/\partial y$

Similarly to G_m, its Jacobian block $\partial G_m(z)/\partial y$ can be evaluated in a variety of ways. First, if an analytic formula for G_m has been obtained through (4.7), then $\partial G_m(z)/\partial y$ can be obtained through symbolic differentiation (using a symbolic manipulation package), through automatic differentiation (see http://www.autodiff.org), or through a finite difference scheme (see below). If such an analytic formula is unavailable, then $\partial G_m(z)/\partial y$ may be approximated by using either automatic differentiation or a finite difference scheme.

Both symbolic and automatic differentiation are rather involved and thus carried out by commercially available packages. Finite difference schemes, on the other hand, are easy to implement by means of the approximation formula

$$\frac{\partial (G_m)_i(z)}{\partial y_j} \approx \frac{(G_m)_i(z + h\mathrm{e}_j) - (G_m)_i(z)}{h} \quad (4.9)$$

yielding an approximation to the $(i,j)-$th entry $\partial (G_m)_i/\partial y_j$ of the Jacobian block $\partial G_m/\partial y$. Here, $1 \leq i, j \leq n$, $(G_m)_i$ is the $i-$th component of the vector-valued function G_m, e_j is the $j-$th standard basis vector in $\mathbf{R}^n$ (that is, the unit vector along the $j-$th coordinate axis), and $h > 0$ is a small parameter. If an analytic expression for G_m is unavailable, the approximation $G_{m,H}$ defined in (4.8) can be used instead in formula (4.9).

4.3.3 Calculation of $(\partial G_m(z)/\partial y)^{-1} G_m(z)$

It is well-established that matrix inversion is numerically unstable. The alternative used in practice to calculate matrix–vector products of the form $A^{-1}b$ (where A is a given square matrix and b is a given vector) is solving the linear equation $Ax = b$ numerically for x to obtain $x = A^{-1}b$. What differentiates one method from another in this framework is the approach taken to solving $Ax = b$. The easiest and simplest to implement way is *Gaussian elimination*—see also [65] for a list of methods (in particular, Krylov subspace methods) which are computationally more efficient for large systems.

In this setting, an iteration with Newton's method (cf. Eq. (4.6)) reads

$$y^{(k+1)} = y^{(k)} - \Delta y, \quad \text{where } \Delta y \text{ solves } \left(\frac{\partial G_m\left(x, y^{(k)}\right)}{\partial y} \right) \Delta y = G_m\left(x, y^{(k)}\right).$$

Appendices

4.A *Mathematica* code for the calculation of a one-dimensional ZDP manifold

This code calculates a one-dimensional ZDP manifold for a model of the phosphotransferase system given in Appendix 3.A. To calculate the one-dimensional manifold of another model, that model should be specified in Section 4.A.1 and its steady state calculated in Section 4.A.2. The order of the manifold may be set to 0, 1, or 2 in Section 4.A.6.

4.A.1 State equations of the model

Reaction rates.

```
rates = {v1 ->  k1f (EItot - z1 - z2 - z6) PEP - k1r z1,
   v2 -> k2f z1 - k2r z6 Pyr,
   v3 -> k3f z6 (HPrtot - z2 - z3 - z7) - k3r z2,
   v4 -> k4f z2 - k4r (EItot - z1 - z2 - z6) z7,
   v5 -> k5f z7 (EIIAtot - z3 - z4 - z8) - k5r z3,
   v6 -> k6f z3 - k6r (HPrtot - z2 - z3 - z7) z8,
   v7 -> k7f z8 (EIICBtot - z4 - z5 - z9) - k7r z4,
   v8 -> k8f z4 - k8r (EIIAtot - z3 - z4 - z8) z9,
   v9 -> k9f z9 Glc - k9r z5,
   v10 -> k10f z5 - k10r (EIICBtot - z4 - z5 - z9) GlcP
   };
v = {v1, v2, v3, v4, v5, v6, v7, v8, v9, v10};
```

Parameter values.

```
param =  {Glc -> 500, GlcP -> 50, Pyr -> 900, PEP -> 2800,
   k1f -> 1960, k1r -> 480000, k2f -> 108000, k2r -> 294,
   k3f -> 14000, k3r -> 14000, k4f -> 84000, k4r -> 3360,
   k5f ->  21960, k5r ->  21960, k6f ->  4392, k6r -> 3384,
   k7f -> 880, k7r -> 880, k8f -> 2640, k8r -> 960,
   k9f -> 260, k9r -> 389, k10f -> 4800, k10r -> 0.0054,
   EItot -> 5, HPrtot -> 50, EIIAtot -> 40, EIICBtot -> 10};
```

Stoichiometric matrix N.

```
Stoich = {{1, -1, 0, 0, 0, 0, 0, 0, 0, 0 },
   {0, 0, 1, -1, 0, 0, 0, 0, 0, 0},
   {0, 0, 0, 0, 1, -1, 0, 0, 0, 0 },
   {0, 0, 0, 0, 0, 0, 1, -1, 0, 0 },
   {0, 0, 0, 0, 0, 0, 0, 0, 1, -1},
   {0, 1, -1, 0, 0, 0, 0, 0, 0, 0},
   {0, 0, 0, 1, -1, 0, 0, 0, 0, 0},
```

```
   {0, 0, 0, 0, 0, 1, -1, 0, 0, 0},
   {0, 0, 0, 0, 0, 0, 0, 1, -1, 0}};
```

Vector field $f(z(t))$.

```
Forig = Stoich.v /. rates /. param;
```

4.A.2 Steady state

Definition of lists that will be needed later in the code.

```
z = {z1, z2, z3, z4, z5, z6, z7, z8, z9};
z'[t] = Table[(z[[i]])'[t], {i, 1, 9}];
subst = Table[z[[i]] -> z[[i]][t], {i, 9}];
backsubst = Table[z[[i]][t] -> z[[i]], {i, 9}];
```

List of the 9 state equations.

```
ode = Table[z'[t][[i]] == (Forig[[i]] /. subst), {i, 1, 9}];
```

Initial conditions (from JWS online [142]).

```
Init = {z1[0] == 0, z2[0] == 0, z3[0] == 0, z4[0] == 0,
z5[0] == 0, z6[0] == 2, z7[0] == 25, z8[0] == 20, z9[0] == 5};
```

Integration of the system with the given initial conditions.

```
sol = NDSolve[Join[ode, Init], z, {t, 0, 400}];
```

Numerical calculation of a steady state, 'zSS', initializing with the last point of the trajectory calculated above.

```
guesses = Table[{z[[i]][t], z[[i]][400] /. sol[[1]]}, {i, 1, 9}];
zSS = FindRoot[Forig == 0, guesses /. backsubst];
```

4.A.3 Parameterizing variable and one-dimensional grid

The variable 'x' defined below is used both to parameterize the manifold and to formulate the ZDP condtion, *i.e.*, it represents both x and $\bar{x}$.

```
x = {z8};
```

Variables specifying the grid:

'Hub'	The hub of the grid, assigned the steady state values of the parameterizing variable.
'Delta'	The distance between the grid points.
'nL'	The number of grid points to the left of the steady state value.
'nR'	The number of grid points to the right of the steady state value.

The total number of grid points thus becomes nL+nR+1.

```
Hub = x /. zSS;
Delta = (x[[1]] /. zSS)/200;
nL = 50;
nR = 50;
```

Check of the end points of the grid.

```
EndPoints = {Hub[[1]] - nL Delta, Hub[[1]] + nR Delta}
```

Definition of the one-dimensional grid.

```
grid = Table[(i - nL) Delta + x[[1]] /. zSS, {i, 0, nL + nR}];
```

4.A.4 Rearrangement of state equations

In this section a permutation is applied to the state vector in order to make the parameterizing variable the first element in the list.

'y'	List of the fast variables in alphabetical order.
'zTot'	List with all state variables, parameterizing variable first.
'nOrig'	Total number of state variables.
'nManif'	Number of parameterizing variables.

```
y = Complement[z, x];
zTot = Join[x, y];
nOrig = Dimensions[z][[1]];
nManif = Dimensions[x][[1]];
```

Definition of the permutation matrix 'PermMat', fulfilling
zTot = PermMat $\times$ z.

```
perm = Table[0, {i, nOrig}];
For[i = 1, i <= nOrig, i++,
  For[j = 1, j <= nOrig, j++,
    If[zTot[[j]] == z[[i]], perm[[j]] = i];
    ];
  ];
PermMat = IdentityMatrix[nOrig][[perm]];
```

Rearrangement of the state equations according to their order in 'zTot'.

```
Subst[w_] := Table[zTot[[i]] -> w[[i]], {i, nOrig}];
F[w_] := PermMat.Forig /. Subst[w];
```

4.A.5 The Jacobian and its eigenvalues and eigenvectors

Calculation of the Jacobian $df(z(t))/dz$, evaluated at the steady state, and its eigenvalues and eigenvectors. (This section is not necessary for the calculations of the manifold.)

```
JacA = D[Forig, {z}] /. rates /. param;
Amatrix = JacA /. zSS;
MatrixForm[Amatrix];
Eigenvalues[Amatrix];
Eigenvectors[Amatrix] // MatrixForm;
```

4.A.6 Settings for the ZDP manifold tabulation

'm' The order of the derivative in the ZDP condition. Can be set to 0 (yielding QSSA/ZDP_0), 1 (ZDP_1), or 2 (ZDP_2).

'TOL' Tolerance level for the error in Newton's method.

```
m = 1;
TOL = 10^-11;
```

4.A.7 Calculation of A and b symbolically

'bb' $G_m(z)$—cf. (4.4)

'AA' $dG_m(z)/dz$

```
If[m == 0,
  bb = Take[F[z], {nManif + 1, nOrig}];
  AA = D[bb, {Take[z, {nManif + 1, nOrig}]}];
  ];
If[m == 1,
  bb = D[Take[F[z], {nManif + 1, nOrig}], {z}].F[z];
  AA = D[bb, {Take[z, {nManif + 1, nOrig}]}];
  ];
If[m == 2,
  bb = D[D[Take[F[z], {nManif + 1, nOrig}], {z}], {z}].F[z].F[z] +
    D[Take[F[z], {nManif + 1, nOrig}], {z}].D[F[z], {z}].F[z];
  AA = D[bb, {Take[z, {nManif + 1, nOrig}]}];
  ];
```

4.A.8 Calculation of one point on the manifold

In the module below, Newton's method is implemented for the calculation of one point on the ZDP manifold, given a value of the slow variable x on the grid. The input 'z0' is a list with n elements, the first of which is the value of x at the current grid point and the remaining ones are guesses of the values of y on the manifold at this grid point. In the while-loop below, this guess is iteratively updated (according

to Newton's method). In every iteration, the symbolic expressions 'AA' and 'bb' are evaluated at the current values of the state vector. The loop continues until the difference between two consecutive guesses is less than 'TOL'.

```
ManifoldPoint[z0_] := Module[{zz = z0},
   err = 2 TOL; (*Setting err > TOL,
   enabling entrance to the loop*)
   While[ err > TOL,
    rules = Table[z[[i]] -> zz[[i]], {i, nOrig}];
    A = AA /. rules;
    b = bb /. rules;
    w = LinearSolve[A, b];
    err = Max[Abs[w]];
    For[k = nManif + 1, k <= nOrig, k++,
     zz[[k]] = zz[[k]] - w[[k - nManif]]
     ]
    ];
   Return[zz];
   ];
```

4.A.9 Tabulation of the manifold over the one-dimensional grid

Below, the list 'zPP' is assigned the steady state values of the state variables, with that of the parameterizing variable first. The variable 'ZDPmanifold' is allocated.

```
zPP = zTot /. zSS (*PP = previous previous*);
ZDPmanifold = Table[0, {i, nL + 1 + nR}];
```

The steady state value of the state variables is filled in at the hub position of 'ZDP-manifold'.

```
ZDPmanifold[[nL + 1]] = Take[zPP, {nManif + 1, nOrig}];
```

Tabulation of the right arm. First, the first point to the right of the hub is calculated with the hub value as initial guess. Next, in the for-loop, the points on the right arm are calculated using initial values by linear extrapolation from the two previous values.

```
If[nR != 0,
  zPP[[1]] = grid[[nL + 2]];
  zP = ManifoldPoint[zPP];
  ZDPmanifold[[nL + 2]] = Take[zP, {nManif + 1, nOrig}];
  For[i = 3, i <= 1 + nR, i++,
   z0 = 2 zP - zPP;
   z0[[1]] = grid[[nL + i]];
   z0 = ManifoldPoint[z0];
   ZDPmanifold[[nL + i]] = Take[z0, {nManif + 1, nOrig}];
   ];
  ];
```

Tabulation of the left arm (analogous to the calculations above).

```
If[nL != 0,
  zPP[[1]] = grid[[nL]];
  zP = ManifoldPoint[zPP];
  ZDPmanifold[[nL]] = Take[zP, {nManif + 1, nOrig}];
  For[i = 1, i <= nL - 1, i++,
   z0 = 2 zP - zPP;
   z0[[1]] = grid[[nL - i]];
   z0 = ManifoldPoint[z0];
   ZDPmanifold[[nL - i]] = Take[z0, {nManif + 1, nOrig}];
   ];
  ];
```

4.A.10 Representations of the one-dimensional manifold

The variable 'ZDPmanifold' contains the tabulated manifold with the columns corresponding to the variables y (in the order that they appear in the last part of 'zTot') and the rows corresponding to the grid points (as they are ordered in 'grid'). The variable 'plot' contains a simple plot of the manifold.

```
ZDPmanifold // MatrixForm;

For[k = 1, k <= nOrig - nManif, k++,
 t[k] = Table[{grid[[i]], ZDPmanifold[[i]][[k]]},
 {i, 1, nR + nL + 1}];
 ]
table = Array[t, nOrig - nManif];

For[k = 1, k <= nOrig - nManif, k++,
 p[k] = ListPlot[t[k]]
 ]
plot = Array[p, nOrig - nManif];
```

4.B *Mathematica* code for the calculation of a two-dimensional ZDP manifold

For the calculation of a two-dimensional manifold, most of the code for the calculation of a one-dimensional one can be reused; only Sections 4.A.3, 4.A.9, and 4.A.10 should be replaced by the coming three sections.

4.B.1 Parameterizing variables and two-dimensional grid

The variables $x = \bar{x}$ are now two-dimensional.

```
x = {z6, z8};
```

2D grid settings:

'Hub'	The hub of the grid, assigned the steady state values of the parameterizing variables.
'DeltaH'	Distance between the grid points in the horizontal direction.
'nL'	# grid points on one row, to the left of the hub.
'nR'	# grid points on one row, to the right of the hub.
'DeltaV'	Distance between the grid points in the vertical direction.
'nD'	# grid points in one column, below the hub.
'nU'	# grid points in one column, above the hub.

```
Hub = x /. zSS;
DeltaH = (x[[1]] /. zSS)/101;
nL = 10;
nR = 10;
DeltaV = (x[[2]] /. zSS)/101;
nD = 10;
nU = 10;
```

Checking the borders of the grid.

```
HorizontalBorders = {Hub[[1]] - nL DeltaH, Hub[[1]] + nR DeltaH}
VerticalBorders = {Hub[[2]] - nD DeltaV, Hub[[2]] + nU DeltaV}
```

Definition of the grid.

```
grid = Table[{(i - nL) DeltaH + x[[1]] /. zSS, (j - nU) DeltaV
        + x[[2]] /.zSS}, {j, 0, nD + nU}, {i, 0, nL + nR}];
grid // MatrixForm;
```

4.B.2 Tabulation of the manifold over the two-dimensional grid

The four backbones are tabulated analogously to the right and left arms on the one-dimensional manifold. The four quadrants are tabulated using initialization by 3-point linear extrapolation.

```
zPP = zTot /. zSS; (*PP = previous previous*)
ZDPmanifold = Table[0, {j, nU + 1 + nD}, {i, nL + 1 + nR}];
ZDPmanifold[[nU + 1, nL + 1]] = Take[zPP, {3, nOrig}];

If[nR != 0,
  zPP[[1]] = grid[[nU + 1]][[nL + 2]][[1]];
  zP = ManifoldPoint[zPP];
  ZDPmanifold[[nU + 1, nL + 2]] = Take[zP, {3, nOrig}];
  For[i = 3, i <= 1 + nR, i++,
   z0 = 2 zP - zPP;
   z0[[1]] = grid[[nU + 1]][[nL + i]][[1]];
```

```
   (*Print["z, zP, zPP",z,zP,zPP];*)
   z0 = ManifoldPoint[z0];
   (*Print["Final z",z0];*)
   ZDPmanifold[[nU + 1, nL + i]] = Take[z0, {3, nOrig}];
   ];
  Print["Manifold at right backbone is calculated."]
  ];

If[nL != 0,
  zPP[[1]] = grid[[nU + 1]][[nL]][[1]];
  zP = ManifoldPoint[zPP];
  ZDPmanifold[[nU + 1, nL]] = Take[zP, {3, nOrig}];
  For[i = 1, i <= nL - 1, i++,
   z0 = 2 zP - zPP;
   z0[[1]] = grid[[nU + 1]][[nL - i]][[1]];
   z0 = ManifoldPoint[z0];
   ZDPmanifold[[nU + 1, nL - i]] = Take[z0, {3, nOrig}];
   ];
  Print["Manifold at left backbone is calculated."]
  ];

If[nU != 0,
  zPP[[1]] = grid[[nU]][[nL + 1]][[1]];
  zPP[[2]] = grid[[nU]][[nL + 1]][[2]];
  zP = ManifoldPoint[zPP];
  ZDPmanifold[[nU, nL + 1]] = Take[zP, {3, nOrig}];
  For[i = 1, i <= nU - 1, i++,
   z0 = 2 zP - zPP;
   z0[[2]] = grid[[nU - i]][[nL + 1]][[2]];
   z0 = ManifoldPoint[z0];
   ZDPmanifold[[nU - i, nL + 1]] = Take[z0, {3, nOrig}];
   ];
  Print["Manifold at upper backbone is calculated."]
  ];

If[nD != 0,
  zPP[[2]] = grid[[nU + 2]][[nL + 1]][[2]];
  zP = ManifoldPoint[zPP];
  ZDPmanifold[[nU + 2, nL + 1]] = Take[zP, {3, nOrig}];
  For[i = 3, i <= nD + 1, i++,
   z0 = 2 zP - zPP;
   z0[[2]] = grid[[nU + i]][[nL + 1]][[2]];
   z0 = ManifoldPoint[z0];
   ZDPmanifold[[nU + i, nL + 1]] = Take[z0, {3, nOrig}];
   ];
  Print["Manifold at lower backbone is calculated."]
```

```
  ];

If[nR != 0 && nU != 0,
  For[j = 1, j <= nU, j++,
   For[i = 1, i <= nR , i++,
     zH =
      ZDPmanifold[[nU + 1 - j, nL + i]];
                    (*Point on the same horizontal height*)
     zD = ZDPmanifold[[nU + 2 - j, nL + i]];      (*Diagonal*)
     zV = ZDPmanifold[[nU + 2 - j, nL + 1 + i]]; (*Vertical*)
     zG =
      Join[grid[[nU + 1 - j]][[nL + 1 + i]], zH + zV - zD];
                              (*Guess at present grid point*)
     ZDPmanifold[[nU + 1 - j, nL + 1 + i]] =
      Take[ManifoldPoint[zG], {nManif + 1, nOrig}];
     ];
   ];
  Print["Manifold at first quadrant is calculated."];
  ];

If[nL != 0 && nU != 0,
  For[j = 1, j <= nU, j++,
   For[i = 1, i <= nL , i++,
     zH =
      ZDPmanifold[[nU + 1 - j, nL + 2 - i]];
     zD = ZDPmanifold[[nU + 2 - j, nL + 2 - i]];
     zV = ZDPmanifold[[nU + 2 - j, nL + 1 - i]];
     zG =
      Join[grid[[nU + 1 - j]][[nL + 1 - i]],
       zH + zV - zD];
     ZDPmanifold[[nU + 1 - j, nL + 1 - i]] =
      Take[ManifoldPoint[zG], {nManif + 1, nOrig}];
     ];
   ];
  Print["Manifold at second quadrant is calculated."];
  ];

If[nL != 0 && nD != 0,
  For[j = 1, j <= nD, j++,
   For[i = 1, i <= nL , i++,
     zH =
      ZDPmanifold[[nU + 1 + j, nL + 2 - i]];
     zD = ZDPmanifold[[nU + j, nL + 2 - i]];
     zV = ZDPmanifold[[nU + j, nL + 1 - i]];
     zG =
      Join[grid[[nU + 1 + j]][[nL + 1 - i]], zH + zV - zD];
```

```
      ZDPmanifold[[nU + 1 + j, nL + 1 - i]] =
       Take[ManifoldPoint[zG], {nManif + 1, nOrig}];
      ];
   ];
  Print["Manifold at third quadrant is calculated."];
  ];

If[nR != 0 && nD != 0,
  For[j = 1, j <= nD, j++,
   For[i = 1, i <= nR , i++,
      zH = ZDPmanifold[[nU + 1 + j, nL + i]];
      zD = ZDPmanifold[[nU + j, nL + i]];
      zV = ZDPmanifold[[nU + j, nL + 1 + i]];
      zG =
       Join[grid[[nU + 1 + j]][[nL + 1 + i]],
        zH + zV - zD];
      ZDPmanifold[[nU + 1 + j, nL + 1 + i]] =
       Take[ManifoldPoint[zG], {nManif + 1, nOrig}];
      ];
   ];
  Print["Manifold at fourth quadrant is calculated."];
  ];
```

4.B.3 Representations of the two-dimensional manifold

The variable "ZDPmanifold" contains the tabulated manifold. The variable "plot" contains a simple plot of it.

```
ZDPmanifold // MatrixForm;

For[k = 1, k <= nOrig - nManif, k++,
  t[k] = Table[
     Join[grid[[i, j]], {ZDPmanifold[[i]][[j]][[k]]}], {j, 1,
      nR + nL + 1}, {i, 1, nU + nD + 1}];
  ];
table = Array[t, nOrig - nManif];

For[k = 1, k <= nOrig - nManif, k++,
 p[k] = ListPointPlot3D[t[k], PlotRange -> All]
 ]
plot = Array[p, nOrig - nManif];
```

Chapter 5

Relaxation behavior of rates in the phosphotransferase system

To understand the functioning of living cells, simplified views of the underlying biochemical networks are often of assistance. In this chapter we develop an approach that makes use of inherent timescale separation based on the zero-derivative principle, to construct simplified pictures of the behavior of the reaction rates in the phosphotransferase system during the slow, partially relaxed phase of its dynamics. We show that the rates in this network are partitioned into collectives; within each of these collectives, all rates assume the same magnitude during the slow phase, while rates belonging to different collectives assume different magnitudes. This relaxation behavior of the rates was observed upon a large variety of perturbations of the parameter set. These results suggest that this behavior is likely to be encountered for various environmental conditions as well as in other signal transduction pathways possessing structures similar to that of the phosphotransferase system.

5.1 Introduction

For systems biology, understanding of complex networks is essential. Understanding often requires simplification, but simplification without removing the essence [27]. Many simplification approaches that exist at the moment however tend to throw away information about the biological functionality that emerges in the nonlinear biochemical interactions in the cell. Here we report on the discovery that a new method based on the zero-derivative principle (ZDP) is able to provide simplified views of biochemical systems, while retaining essential information about their nonlinear behavior.

In the previous chapters we treated reduction of biochemical models with the primary aims of reducing the simulation times and of developing simple yet accurate kinetic expressions for reaction rates in terms of the concentrations of the reactants and the enzymes. In this chapter we shall focus on the interpretation and analysis of the simplified models and demonstrate how the simplified views of systems may provide additional insight in their biochemical behavior. In particular, we shall focus on the kinetic model of the phosphotransferase system (PTS) developed in [99] (and revamped in Appendix 3.A of this thesis) and on the simplified descriptions of this system based on the zero-derivative principle (ZDP) which were derived numerically in Chapter 3.

As described in Appendix 3.A, the PTS is a mixed signal transduction, metabolic, and transport pathway involved in transporting various sugars into enteric bacteria, in phosphorylating those sugars, and in signalling to the transport and gene-expression machinery that the sugar is available [26, 96]. The PTS model in [99] exhibits nonlinear dynamics and it contains 13 state variables that represent the concentrations of the molecular components in the pathway. Consequently, its dynamics could be enormously complex. To elucidate this, we make the thought experiment that each of these state variables could assume only 10 different values each; then, the number of states that the full system could assume is 10^{13}, *i.e.*, its dynamics would be tremendously complex. In reality, each component can take any of a continuum of values, *i.e.* the state can be any point in a 13-dimensional state space, in which the axes represent the concentrations of the 13 components. On the other hand, the interactions necessary for the biological function of the PTS, though possibly complex, might not need to be that complex: the PTS should transport, phosphorylate, and signal. The question we address in this chapter is whether the PTS exhibits maximal possible complexity, *i.e.*, makes use of the entire 13-dimensional state space, or whether its behavior might be much less complex than that.

The approach we take here is based on simplified descriptions of PTS dynamics through the ZDP. In Chapter 3 we introduced the reduction of biochemical systems by implementing the ZDP, a method which may be seen as a more accurate extension of the quasi-steady-state approximation (QSSA). In the same chapter, we also employed the ZDP to calculate approximations to curves or manifolds towards which the trajectories of the model are attracted and on which the dynamics is slow, *i.e.*, slow invariant manifolds (SIMs). We used such to reduce the computation times required for integration over the PTS.

A second potential asset of these approximations of the SIM is that they eluci-

date the essence of the dynamics of the PTS. In this chapter, we shall examine this potential. We shall analyze the dynamics of the reaction rates in the PTS during the partially relaxed phase, *i.e.*, during the phase following the initial transient phase, by evaluating the rate expressions on the numerical approximations of the SIM. We find that along the SIM, the reactions have adapted their rates to each other.

In the next section we recapitulate the aspects of the calculation of the ZDP manifolds for the PTS that are essential for the presentation here. In the subsequent section, we describe the relaxation behavior of the rates in the PTS. Thereafter, we describe the behavior of the rates for a variety of parameter sets. Finally, we discuss our results.

5.2 One-dimensional ZDP manifolds for the PTS model with 13 state variables

In Chapter 3 we determined approximations to a SIM for a PTS model with 9 state variables; this model was obtained by eliminating the 4 state variables representing unphosphorylated proteins from the model in [99] with 13 state variables, using the 4 conservation relations, as described in Appendix 3.A. The reduction by these conservation relations demonstrates that there is a first constraint on the complexity of the behavior of the PTS: for as long as gene expression variation is absent, *i.e.*, the total protein concentrations are constant (as was assumed also in the original model), the PTS does not move in a 13-dimensional space but in a 9-dimensional one.

In the same chapter, we also examined whether the behavior of the PTS might be further confined to a subspace of the 9-dimensional space. To this end, we analyzed the eigenvalues of the Jacobian at the steady state. These eigenvalues represent the timescales present in the system close to the steady state: largely negative values correspond to fast dynamics, negative values close to 0 correspond to slow dynamics, while positive values correspond to unstable dynamics, *i.e.*, a movement that is not approaching the steady state. (In biological systems, all eigenvalues are typically negative, *i.e.*, the system is stable.) The information about the timescales at steady state gives an indication of whether there exists a SIM and, in that case, which dimension it has. If all eigenvalues are of the same order of magnitude, there is no timescale separation and no SIM exists. If a few, say n_r, of the eigenvalues are of one order of magnitude while the rest of another—where the latter are more negative than the former ones and hence correspond to the fast dynamics—then there exists an n_r-dimensional SIM. As described in the remark in Section 3.2.2, there may also exist several SIMs of different dimensions, those of lower dimension embedded in those of higher dimension—in this case there are eigenvalues of more than two different orders of magnitude. The comparison of the eigenvalues of the PTS model at steady state in Section 3.5.1 showed a large gap between the two slowest eigenvalues. This hence indicated that there exists a 1-dimensional SIM, *i.e.*, a curve towards which trajectories of the state of the system rapidly move. In other words, the behavior of the PTS may be much simpler than a fairly arbitrary movement through its 9-dimensional state space.

To compute an approximation to the 1-dimensional SIM, in order to investigate

the behavior on it, we then partitioned the state variables in the PTS model into a 1-dimensional slow component $\bar{x}$, chosen to be the state variable [EIIA·P], and an 8-dimensional fast component $\bar{y}$, containing the remaining variables. For the formulation of the ZDP_0 (which is equivalent to the QSSA) and ZDP_1 conditions we put

$$\frac{d\bar{y}}{dt} = 0 \text{ or } \frac{d^2\bar{y}}{dt^2} = 0, \tag{5.1}$$

respectively. These two conditions hence lead to two different algebraic equation systems consisting of 8 equations and 9 unknowns (*i.e.*, the state variables). They define the 1-dimensional slow ZDP_0 and ZDP_1 manifolds, respectively, both of which approximations of the SIM. We employed the numerical algorithm presented in Chapter 4 to tabulate the ZDP_0 and ZDP_1 manifolds. This algorithm performs the tabulation over a grid consisting of a set of equidistant values of a parameterizing variable x which we chose as x=[EIIA·P], as this choice led to fast computations. In other words, the algorithm substituted each value of [EIIA·P] on the grid into one of the equation systems in (5.1)—reducing the number of unknown variables to 8, *i.e.*, the same as the number of equations—and for each grid point it computed values of the remaining 8 state variables that together solved the equation system (for the original parameter set given in Appendix 3.A) and the results were tabulated. In Figure 5.1 we display these manifolds together with the four free protein concentrations tabulated over the same manifolds using the conservation relations (3.20). For details on the computation of these two manifolds, see Section 3.5.1.

Due to physical constraints, the values of all state variables are bounded from below by 0 (since they represent concentrations) and from above by one of the total concentrations of the four proteins: [EI·P·Pyr], [EI·P·HPr], [EI], and [EI·P] have to be lower than $[EI]_{tot} = 5$ μM; [HPr] and [HPr·P] lower than $[HPr]_{tot} = 50$ μM; [HPr·P·EIIA], [EIIA], and [EIIA·P] lower than $[EIIA]_{tot} = 40$ μM; and [EIIA·P·EIICB], [EIICB·P·Glc], [EIICB], and [EIICB·P] lower than $[EIICB]_{tot} = 10$ μM. On the part of the ZDP_1 manifold where [EIIA·P] is low—*i.e.*, less than approximately 3 μM—[EIICB·P], [EIICB·P·Glc], and [EIIA·P·EIICB] assume negative values while [EIICB] assumes values above its upper bound $[EIICB]_{tot} = 10$ μM—cf. Figure 5.1. Similarly, for large values of [EIIA·P], *i.e.*, where it is larger than approximately 35 μM, [HPr], [HPr·P·EIIA], and [EIIA] assume values below 0 while [HPr·P] assumes values above its upper bound $[HPr]_{tot} = 50$ μM. These parts of the manifold have no biochemical interpretation; only trajectories with initial conditions outside the physically feasible domain are attracted to this part of the manifold while trajectories starting inside this domain will stay inside of it. Note, however, that [EIIA·P] may well assume values lower than approximately 3 μM and higher than 35 μM *before* the trajectory reaches the SIM: it is constrained to values above between these bounds only during the slow phase.

5.3 Relaxation behavior of rates

To explore the behavior of the reaction rates in the PTS during the partially relaxed phase—*i.e.*, the slow phase in which the dynamics evolves along the SIM—we

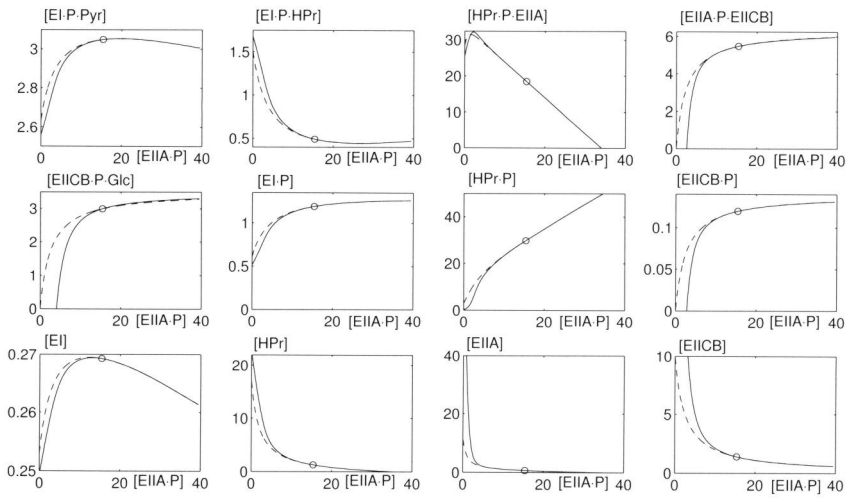

Figure 5.1: One-dimensional ZDP_0 and ZDP_1 manifolds (dashed and solid lines, respectively) for the 9-dimensional PTS model plotted against the parameterizing variable x=[EIIA·P] (eight upper panels) and the four total protein concentrations tabulated over the same manifolds and plotted against the same parameterizing variable (four bottom panels). In each plot, the steady state is indicated by a circle. Together, these 12 plots represent a SIM in the full model with 13 state variables. All concentrations are given in μM.

tabulated the values of all ten rates, using the rate expressions in Table 3.2, over numerically calculated ZDP_0 and ZDP_1 manifolds obtained using $x = \bar{x}$ =[EIIA·P]. In Figure 5.2 we show these rates plotted against the corresponding points on the ZDP_0 and ZDP_1 manifolds—these points are represented by the parameterizing variable [EIIA·P]—and we denote the resulting curves the ZDP_0 and ZDP_1 *rate profiles*, respectively. Evidently, the ZDP_0 rate profiles suggest that the values of v_1 through v_6 are identical to each other during the slow phase, as are v_7 through v_{10}. This is to be expected, as ZDP_0 sets the right-hand sides of all state equations except the one for the parameterizing variable equal to 0, and thus $v_1 = \ldots = v_6$ and $v_7 = \ldots = v_{10}$—cf. (3.8) and the state equations of the PTS model given in Appendix 3.A. The ZDP_1 rate profiles suggest a similar grouping on a major part of the calculated manifold with the important difference that v_5 is now grouped in the latter rate collective on the major part of the manifold, including the vicinity of the steady state.

The difference in the results obtained by the ZDP_0 and ZDP_1 approaches raises the question whether any of them correctly describes the rate behavior in the partially relaxed phase. To investigate this issue, we calculated the rates along some trajectories and compared with the rate profiles; the rates along the trajectories were visualized through the curves $(v_\cdot(t), [\mathrm{EIIA{\cdot}P}](t))$ parameterized by time, which we de-

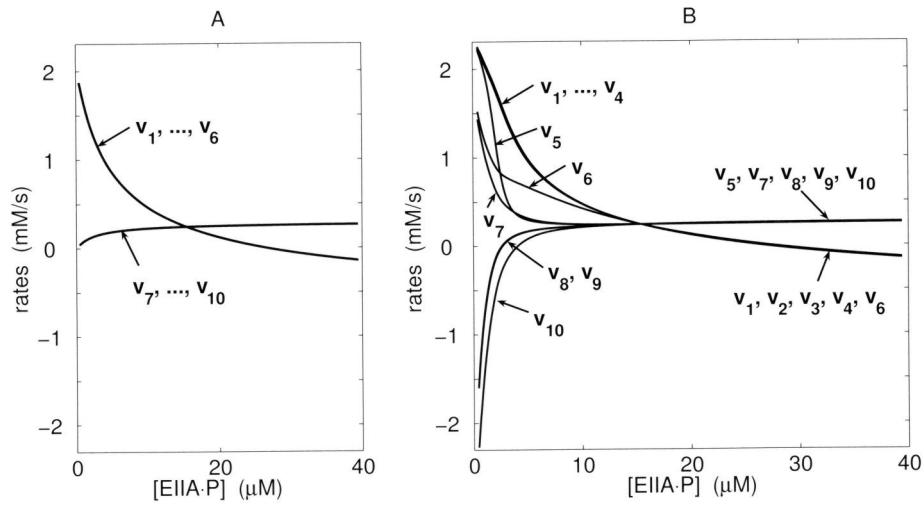

Figure 5.2: The ten reaction rates of the PTS model evaluated on (A) the ZDP_0 manifold and (B) the ZDP_1 manifold. On the x-axes, the value of the parameterizing variable [EIIA·P] represents the point of the manifold at which the rates were evaluated.

note *rate trajectories*. In Figure 5.3, we display these rate trajectories together with the corresponding ZDP_0 and ZDP_1 rate profiles for two out of the ten rates. The rate trajectories approach the ZDP_1 rather than the ZDP_0 rate profiles, showing that ZDP_1 more accurately captures the behavior of the rates in the slow phase than ZDP_0 does. In particular, the fact that the slow dynamics of v_5 is more accurately approximated by ZDP_1 than by ZDP_0 (Figure 5.3A) verifies the validity of grouping this rate in the latter collective, *i.e.*, the constitution of the collectives of rates suggested by ZDP_1 was correct while that of ZDP_0 was wrong. Because of the better performance of ZDP_1 as compared to ZDP_0, we will only use ZDP_1 for further analysis in this chapter.

The ZDP_1 results point to the following interesting phenomenon: starting at any initial condition in the state space, and following a short transient, the rates v_1, v_2, v_3, v_4, and v_6 assume very similar magnitudes; the same holds for v_5, v_7, v_8, v_9, and v_{10}; the magnitudes of the latter differ significantly from those of the former. In other words, the behavior of the rates in the PTS is much less complex than it could have been: their slow dynamics in the partially relaxed phase is restricted to approximately two main curves, *i.e.*, a small part of the 'rate space', instead of being spread out on ten widely separated profiles, one for each rate.

Interestingly, the two collectives of reactions correspond to two different parts of the PTS network as seen from Figure 5.4. This suggests that the grouping pertains to partial equilibration between adjacent reactions and lack of such equilibration across the substances HPr·P, HPr·P·EIIA, and EIIA·P, *i.e.*, the substances located on the boundary between the two network parts.

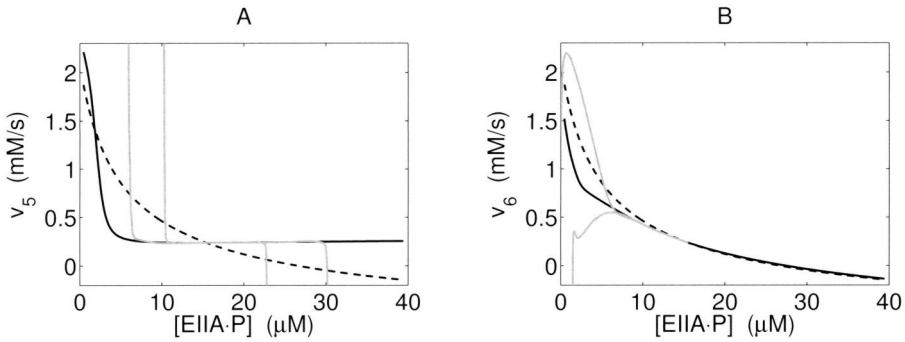

Figure 5.3: Rate trajectories for (A) v_5 and (B) v_6 (gray solid lines) and the rate profiles based on ZDP_0 (black dashed lines) and ZDP_1 manifold (black solid lines) for the corresponding rates.

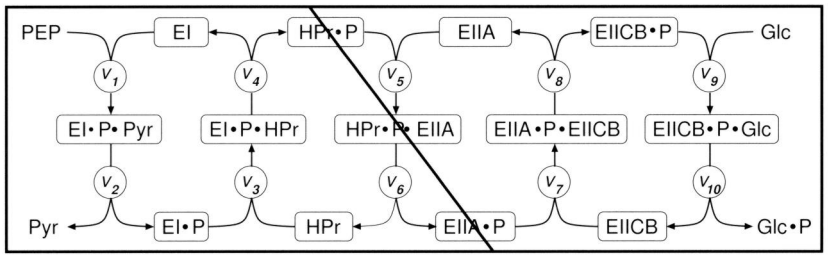

Figure 5.4: Reaction network for the PTS with its partitioning according to the grouping of the rates.

As a result of the behavior outlined above, only the concentrations of HPr·P, HPr·P·EIIA, and EIIA·P change significantly during the partially relaxed phase, as their production and consumption are governed by rates belonging to *different* collectives. The remaining state variables, instead, are produced and consumed by reactions with rates belonging to the same of the two collectives. Consequently, the latter variables change only to a minor extent during the partially relaxed phase and hence assume values close to their steady state levels already by the end of the fast transient.

The difference in the rates of change in the slow phase between the state variables on the boundary and the remaining ones is also reflected on the ZDP_1 manifolds. The boundary concentrations [HPr·P], [HPr·P·EIIA], and [EIIA·P] assume values on a wider range on the biochemically interpretable part of the ZDP_1 manifold than the remaining variables do: [EIIA·P], which is the parameterizing variable, assumes values between approximately 3 and 35 μM as discussed in the end of Section 5.2; further, as seen from Figure 5.1, [HPr·P] assumes values between approximately 15 and 50 μM on this domain and [HPr·P·EIIA] between approximately 30 and 0 μM

(recall that [EIIA·P] is the parameterizing variable); [EI·P], on the other hand, which is not on the boundary, assumes values on the small range between 0.8 and 1.3 μM and similarly holds for all the remaining state variables, *i.e.*, they are confined to relatively small intervals. Accordingly, the boundary variables change more extensively during the slow phase, as was also the conclusion from the difference in consumption and production rates discussed above.

5.4 Dependence on parameter values

We next asked whether there might be reduced complexity in the sense of minor dependence of the behavior on parameter values. In the (unlikely) simplest situation, the system's behavior would be parameter independent. In the maximally complex case, every new parameter set would lead to an entirely different behavior.

5.4.1 Limited parameter dependence of the relaxation behavior

We first tabulated the values of the rates on the ZDP_1 manifolds calculated for parameter sets that only differed from the original one in *one* of the four boundary concentrations [PEP], [Pyr], [Glc], and [Glc·P], by a multiplicative factor of 10 or 0.1, respectively. In all these eight cases we again used $x = \bar{x}$ =[EIIA·P] for the formulation of the ZDP_1 condition and for parametrization of the manifold; we verified the suitability of this choice by comparing the rate trajectories with the ZDP_1 rate profiles (cf. the analogous analysis in the previous section) and in all cases the ZDP_1 rate profiles proved to be highly accurate approximations (data not shown). The rate profiles obtained for the parameter set in which the concentration of external pyruvate was multiplied by a factor of ten (*i.e.*, [Pyr]=9000 μM) are shown in Figure 5.5A–B. In a neighborhood of the steady state, the rates $v_1, \ldots v_4$ appear to fall into one collective, v_8 and v_9 into another, while the profiles of the remaining rates are distinct from the other profiles (Figure 5.5A). However, on the part of the manifold where [EIIA·P] is high, the grouping of the rates resembles the grouping obtained for the original parameter set in the sense that two main rate collectives are formed (*i.e.*, v_1, v_2, v_3, v_4, and v_6 constitute one collective and v_5, v_7, v_8, v_9, and v_{10} another one, see Figure 5.5B). In the remaining seven cases the original grouping into two parts was reproduced on a major part of the physically feasible range of [EIIA·P], including the neighborhood of the steady state—one of these cases (*i.e.*, when [Glc] is increased by a factor 10) is shown in Figure 5.5C.

We also calculated the ZDP_1 rate profiles using parameter sets which differed from the original one in only one of the four total protein concentrations, also by a factor of 10 or 0.1. In the two parameter sets with $[EI]_{tot}$=50 μM (original value was 5 μM) and $[EIICB]_{tot}$=1 μM (original value was 10 μM), the same grouping as that for the original parameter set was achieved. The two cases with $[HPr]_{tot}$=500 μM (original value was 50 μM) and $[EI]_{tot}$=0.5 μM resulted in a grouping similar to that achieved above for Pyr=9000 μM (shown in Figure 5.5A-B): in a neighborhood of the steady state some of the rates were forming groups, in both cases of a constitution similar to that in Figure 5.5A), while on a large part of the manifold the two original collectives prevailed. For the parameter set with $[HPr]_{tot}$=5 μM a different pattern

was observed: on one part of the manifold which included the steady state, the two collectives $v_1, \ldots v_6$ and $v_7, \ldots v_{10}$ were formed, while on the part of the manifold where [EIIA·P] is high, the rate v_5 joined the opposite collective and hence again the original grouping was achieved—this is shown in figure Figure 5.5D. The same pattern was observed for $[\text{EIIA}]_{tot}$=400 μM (with original value 40 μM). For the six parameter sets mentioned we used $x = \bar{x}$ =[EIIA·P] and again we verified this choice by comparing rate trajectories with the corresponding rate profiles. For the case when [EIICB]=100 μM, the two slowest eigenvalues of the Jacobian at steady state were complex conjugates of each other and, effectively, no one-dimensional SIM existed. When $[\text{EIIA}]_{tot}$=4 μM, the ratio between the two slowest eigenvalues was only 1.4 and hence the one-dimensional SIM only weakly attracted the trajectories. We also investigated the rates for the two parameter sets in which all four total enzyme concentrations were either multiplied or divided by a factor of two. Both these cases resulted in the original grouping. Here, again $x = \bar{x}$ =[EIIA·P] was used and the choice was verified.

For all the eighteen parameter sets investigated above, the resulting collectives comprised connected parts of the network—the groupings obtained on the part of the manifolds near the steady state for the parameter sets with [Pyr]=9000 μM and with $[\text{HPr}]_{tot}$=5 μM are shown in Figure 5.6.

The fact that collectivization was observed for almost all parameter sets that were investigated above suggests that the PTS may exhibit grouping of the rates under a variety of environmental conditions, corresponding to changes in the parameter values. The differences in the constitution of the rate collectives obtained for different parameter sets—however with many similarities between the constitutions—show that the collectivization of the PTS rates is not maximally simple, but relatively simple with respect to the dependence of the parameters.

5.4.2 Relaxation behavior in signal transduction pathways in general

Signal transduction pathways consisting of coupled cycles of phosphorylation, acetylation, or ubiquitination all exhibit network structures that are similar to that of the PTS and hence they can be described by models with structures equivalent to that of the PTS model (given in Appendix 3.A) but with other values of the parameters. Therefore, analysis of the type outlined above for the same model structure but for arbitrarily chosen parameter sets, which hence may differ vastly from those in the PTS, gives information about whether the grouping behavior may be expected in other signal transduction pathways. Two examples of the rates calculated on the ZDP_1 manifold for two arbitrarily chosen parameter sets (A and B, reported in Appendix 5.A) substantially different from that of the original model are shown in Figure 5.7. Here we used $x = \bar{x} = z_8$ and $x = \bar{x} = z_7$ for the parameter sets A and B, respectively (in the PTS z_8=[EIIA·P] and z_7=[HPr·P], see Appendix 3.A) and we verified that the rate trajectories indeed approach the ZDP_1 rate profiles. In Figure 5.8 we display the corresponding partitioning of the network for the same two cases. The same type of analysis was also performed for several other parameter sets and in all cases grouping of the rates was observed—but with different constitution of the collectives—and the collectives constituted connected parts of the network (data not shown).

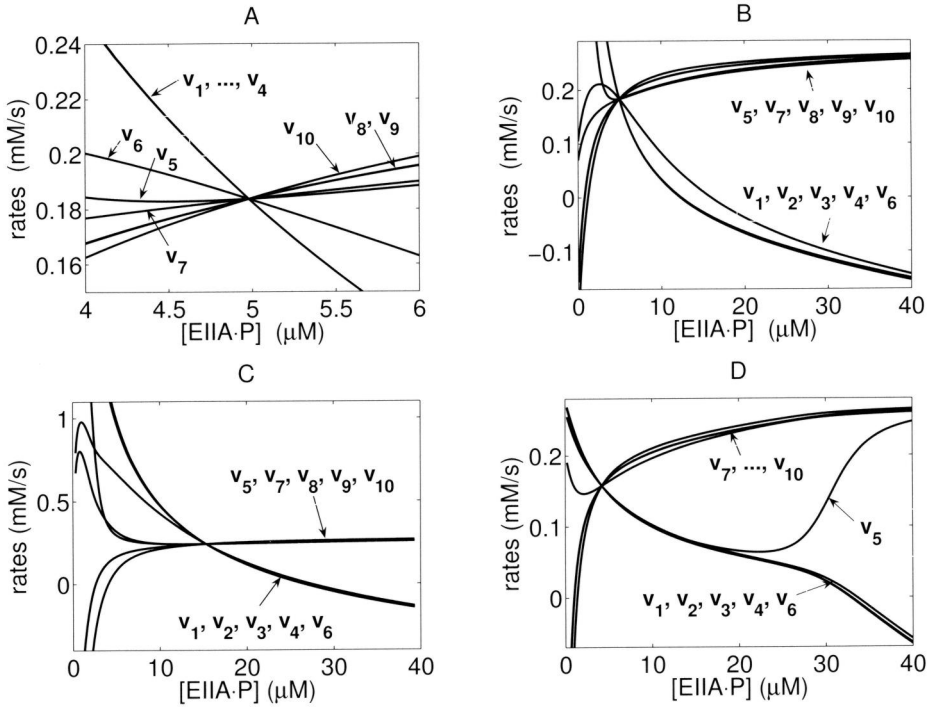

Figure 5.5: The ZDP_1 rate profiles for the PTS model with parameter sets differing from the original one in only one parameter value: in (A–B) [Pyr]=9000 μM, in (C) [Glc]=5000 μM, and in (D) $[HPr]_{tot}$=5 μM. Panels (A) and (B) differ in their range for [EIIA·P]: in panel (A), only small parts of the profiles in a close vicinity to the steady state are displayed, while in panel (B) the profiles are displayed over the entire interval for [EIIA·P].

5.5 Discussion

The complexity of biochemical systems in living cells renders their dynamics unintuitive and their function difficult to fathom. It is therefore of interest to explore methods to construct simplified views of their dynamics—but importantly—without throwing away their essential complexity [27]. The PTS serves as a prime example of a model with complicated dynamics as it involves a large number of molecular components exhibiting nonlinear dynamics. This system is of great interest to study since it participates in advanced regulatory functions of many prokaryotic cells and it has the unique property that it integrates three major types of molecular processes, *i.e.* metabolism, transport and signalling. It is hence of interest to achieve a reduced—though not oversimplified—overall view of its dynamics. In this chapter we developed an approach based on the ZDP which provides such an overall view of the dynamics of the reaction rates in a model of the PTS [99].

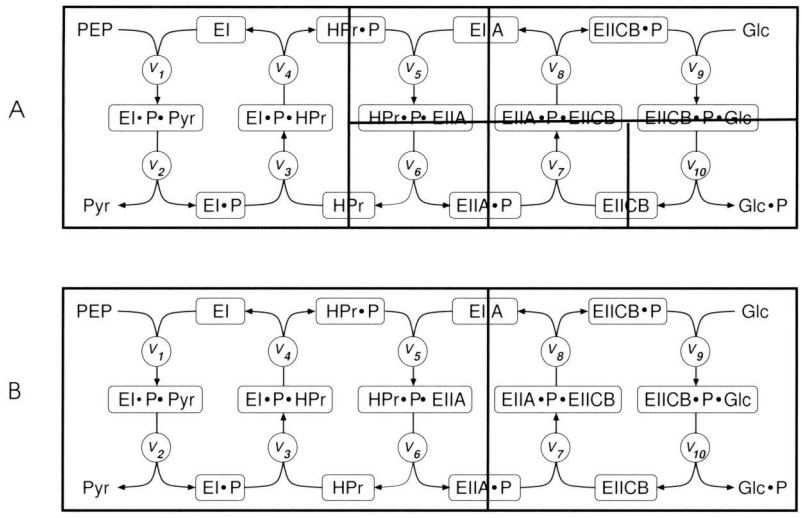

Figure 5.6: The partitioning of the PTS network fluxes into 6 (A) and 2 (B) collectives in a neighborhood of the steady state for the parameter sets differing from the original one only by [Pyr]=9000 μM in (A) and by $[\mathrm{HPr}]_{tot}$=5 μM in (B).

We first employed both the zeroth and the first order ZDP, the former being equivalent to the QSSA, to determine the behavior of the rates in the slow, partially relaxed phase. These two approximation methods both yielded rate profiles partitioned into two groups, within which the levels of the rates were identical. The constitutions of the rate collectives were similar for the QSSA and ZDP_1 cases but differed in the classification of one of the rates which was assigned to opposite collectives by the two methods. By comparing the rate profiles with the rates calculated along trajectories we showed that the ZDP_1 yielded considerably more accurate results than the QSSA and hence only ZDP_1 succeeded to reproduce the correct grouping of all rates. These results illustrate the limitations with QSSA, which oversimplifies the model and hence throws away important dynamic features. The ZDP_1 approach, on the other hand, yields a correct simplified view of the behavior.

The reactions in the two collectives yielded by ZDP_1 were clearly divided into two different parts of the PTS network (see Figure 5.4). This fact suggests that the grouping pertains to the communication between adjacent reactions; seemingly, the reactions within each collective communicate well on the fast timescale and, accordingly, the rates internally adjust already during the transient, *i.e.*, they reach levels resembling steady state levels in view of the fast timescale. During the partially relaxed phase, then, the two network parts operate at these separate, internally adjusted levels while the communication *between* the two collectives, which occurs on the slow timescale, slowly brings the system towards the steady state in which all rates are equal.

Our analysis of the rates naturally describes the behavior of the *model* under

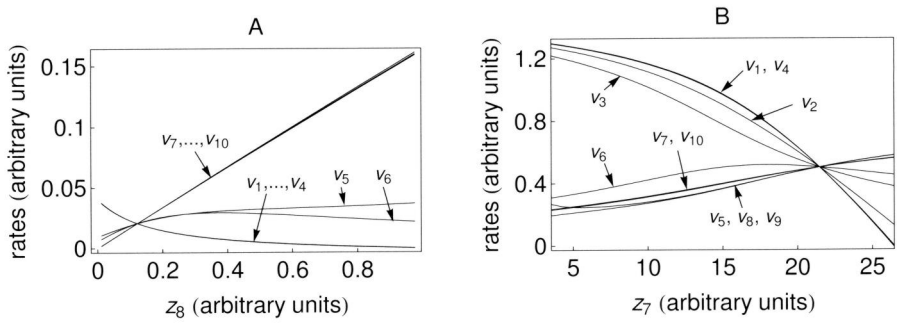

Figure 5.7: A–B: The ten reaction rates evaluated on the ZDP_1 manifold for the two parameter sets A and B, respectively.

consideration and, due to the possibility of uncertainties in the model resulting from *e.g.* measurement errors or lacking information, the dynamics we observed may differ from the actual behavior *in vivo*. To investigate this issue further we analyzed the robustness of the collectivization to changes in parameter values by determining the rate profiles also for a variety of different parameter sets. Small alterations of the parameter set (*i.e.*, changing one of the parameter values by a factor of ten, or four of the parameters by a factor two) all resulted in some variation in the grouping; the constitution of the collectives varied slightly. These results suggest that the grouping phenomenon is rather robust to errors in the parameter values and hence strengthens the probability of finding the phenomenon *in vivo*.

The sensitivity analysis above also indicates how the grouping may depend on natural environmental variations such as changes in the gene expression pattern, in metabolism, or in the availability of extracellular glucose. Interestingly, the constitution of the rate collectives seems to be rather robust to changes in the external metabolite concentrations [PEP], [Pyr], [Glc], and [Glc·P] but more sensitive to changes in total protein concentrations $[\mathrm{EI}]_{tot}$, $[\mathrm{HPr}]_{tot}$, $[\mathrm{EIIA}]_{tot}$, and $[\mathrm{EIICB}]_{tot}$. In particular, when $[\mathrm{EIIA}]_{tot}$ was increased by a factor of ten or when $[\mathrm{HPr}]_{tot}$ was decreased by a factor of 0.1 (which may result *e.g.* from a differential expression of the corresponding genes), the rate of the fifth reaction (in which HPr·P and EIIA are forming a complex) was assigned to the opposite collective as compared to the original grouping (see Figure 5.5D) on a large part of the manifold including the steady state. The difference in constitution of the collectives upon variation of certain parameter values suggests that the PTS exhibits different operational modes and that the mode which it temporarily resides in depends on the environmental conditions; this differential behavior might play a role in the regulatory functions of the PTS.

We also altered the original parameter set to larger extents in order to investigate the likelihood of finding the grouping phenomenon also in other signal transduction pathways with the same structure as that of PTS, *i.e.*, consisting of coupled cycles of phosphorylation, ubiquitination, or acetylation. In these cases we also observed grouping in all the cases that we analyzed, which affirms that the grouping might

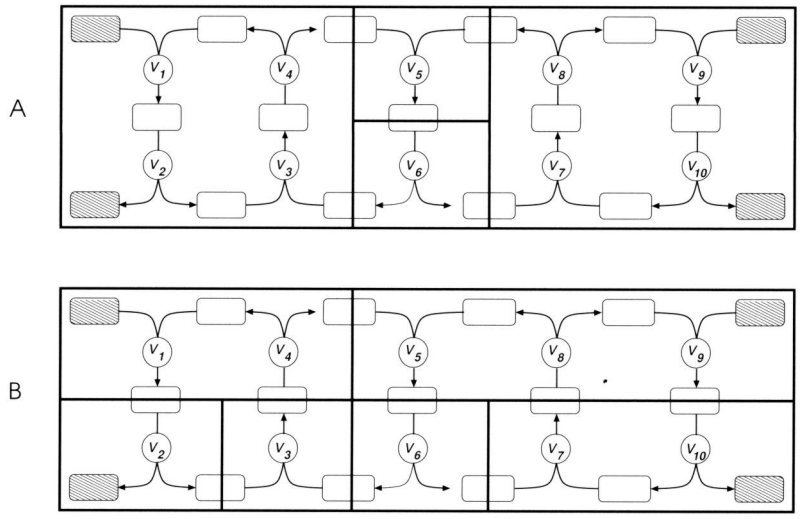

Figure 5.8: A–B: Partitioning of signal transduction networks with parameter sets A and B, respectively. The empty boxes represent time-dependent concentrations (being state variables in the model) and the filled boxes represent constant concentrations (*i.e.*, model parameters).

be a more general phenomenon recurring in a variety of pathways. It would also be interesting to perform the rate analysis described in this chapter for models with similar network structures, such as models containing fewer or more coupled cycles, or for models with entirely different network structures in order to investigate whether the grouping phenomenon may appear also in such systems.

The behavior of the rates in the PTS that we have reported on in this chapter could have been partially unmasked also without the determination of a SIM; simple simulations of the model show that after an initial transient phase, certain rates assume the same magnitudes and subsequently they coherently approach their steady state values. Simulating the model for a large number of initial conditions would hence enable a characterization of the collectivization behavior. The power of the approach that we used, based on analysis of the SIM, is that it provides a *general* overview of the slow dynamics, and this without delving into details about the behavior of particular trajectories: any initial condition in the entire state space will result in a trajectory that initially approaches the SIM before approaching the steady state. An approach based on investigating time courses would become cumbersome in comparison with our SIM-based approach, yet providing a less general view, and would be particularly demanding when analyzing the behavior for a large variety of parameter sets.

With the progress in systems biology in recent decades it has become clear that cell function depends on the functioning of complex networks. Experimentally it has become possible to approach such networks and this has led to avalanches of data. To analyze these data, models are being constructed and analyzed. There is however

a time lag between the collection of data and the model construction and it will take a while until we have constructed mathematical models of equally high complexity as the data. Once the models have been produced, the more important challenge remains, *i.e.* that of understanding the actual behavior of the network. For this it may be essential to achieve simplified views of the behavior of the network without losing the essence of its behavior. The ZDP approach developed here may be one of the methods that can be developed further to do this.

The analysis described in this chapter has shown that interesting biochemical information may be achieved by ZDP reduction and, accordingly, offers an example of the usefulness of ZDP in the biochemical context. It also opens up for further investigations into the reasons for this behavior and the biological consequences of the grouping on the functioning of the cells.

Appendix

5.A Parameter sets

Here we report two of the parameter sets used in Section 5.4.2. The units of the parameter values are arbitrary. For simplicity we use the same notation for the parameters as in the PTS model given in Appendix 3.A although these parameters concern signal transduction pathways in general and not the particular PTS pathway.

Parameter set A: $[\text{Glc}] = 1000, [\text{Glc·P}] = 50, [\text{Pyr}] = 87, [\text{PEP}] = 1, k_{1f} = 10, k_{1r} = 0.005, k_{2f} = 18, k_{2r} = 50, k_{3f} = 10, k_{3r} = 0.001, k_{4f} = 10, k_{4r} = 1, k_{5f} = 10, k_{5r} = 82, k_{6f} = 10, k_{6r} = 7, k_{7f} = 10, k_{7r} = 88, k_{8f} = 10, k_{8r} = 1, k_{9f} = 100, k_{9r} = 1, k_{10f} = 10, k_{10r} = 1, [\text{EI}]_{tot} = 1, [\text{HPr}]_{tot} = 1, [\text{EIIA}]_{tot} = 1,$ and $[\text{EIICB}]_{tot} = 1$

Parameter set B: $[\text{Glc}] = 80, [\text{Glc·P}] = 50, [\text{Pyr}] = 70, [\text{PEP}] = 40, k_{1f} = 10, k_{1r} = 1, k_{2f} = 100, k_{2r} = 1, k_{3f} = 16, k_{3r} = 6, k_{4f} = 10, k_{4r} = 1, k_{5f} = 60, k_{5r} = 5, k_{6f} = 10, k_{6r} = 5, k_{7f} = 50, k_{7r} = 5, k_{8f} = 18, k_{8r} = 3, k_{9f} = 100, k_{9r} = 7, k_{10f} = 10, k_{10r} = 5, [\text{EI}]_{tot} = 10, [\text{HPr}]_{tot} = 30, [\text{EIIA}]_{tot} = 10,$ and $[\text{EIICB}]_{tot} = 10.$

Chapter 6

Discussion

In this chapter, we summarize the achievements reached by means of the two main approaches to simplification of biochemical models taken in this thesis: balancing and ZDP. We then compare the properties of the two methods and the type of models to which they are applicable and we discuss the use of input and output variables in biochemical models, which are needed for the application of balancing. We also relate our results on balancing to work on this topic that appeared whilst our work was performed. We then summarize future directions of research that the simplification approaches treated in this thesis suggest and, finally, we give a more general outlook on the role of simplifications in the field of systems biology.

6.1 Simplification approaches taken in this thesis

In this thesis we have explored methods to simplify biochemical models and our aim has been to find ways to construct simplified descriptions which realistically account for the complex dynamics in the biochemical systems. Two main directions have been taken. Our first approach was to explore the well-known linear method of balancing and truncation—a natural first step due to the central role this method has played for model reduction within the area of control theory and for reduction of models in other sciences. The second reduction method we studied, which we explored in much more depth, is based on the zero-derivative principle (ZDP) and derives from geometric singular perturbation theory, a field within applied mathematics. The latter method had not been used in a biochemical context before and in this thesis we have demonstrated various aspects of its usefulness for simplification and analysis of realistic biochemical models.

During the work on this thesis, the question has been raised whether the ZDP used here is related to the concept of zero dynamics encountered in control theory. The theory underlying the ZDP is presented in detail in Chapter 3 of this thesis. In short, the ZDP aims at identifying accurate approximations of low-dimensional, slow invariant manifolds (SIMs) embedded in the state space of a multiscale system. Zero dynamics, on the other hand, is a concept used for the design of feedback control laws. In particular, it is the name given to the dynamics of a (nonlinear) control system for which the input has been set to a function (depending on time) that renders the output function zero at all times. Although both concepts involve the extraction and study of the dynamics on low-dimensional, invariant submanifolds of the state space, this is where the similarities between them end. Indeed, zero dynamics is a product of the control exercised on a system and not of an intrinsic timescale separation present in the system. Hence, the concept of zero dynamics seems loosely related, at best, to geometric singular perturbation theory and thus also to ZDP.

6.2 Aims achieved

As was discussed in the Introduction to this thesis, simplification of biochemical models is useful for many reasons. In this thesis we have particularly addressed the issues of reduction of computation times, construction of simple yet accurate rate laws, and, perhaps most importantly, gathering information that leads to better understanding about the biochemical system. Below we briefly describe the means by which these goals have been achieved.

The method of balancing and truncation was first used to reduce a model of glycolysis in yeast with the aim to reduce the computation times. This however resulted in a substantial trade-off in accuracy due to the linearization preceding and required for the reduction. We also employed the information obtained from the balancing procedure to draw conclusions about the importance of the various concentrations for the dynamics of the glycolytic pathway. This analysis was based on the coefficients in the linear combinations that constituted the balanced state variables; since these variables are ordered according to the importance for the dynamics, the terms that contribute most to the first state variables have a strong influence on the dynamics.

We found that the concentrations of NADH and acetaldehyde have little influence on the dynamics in the glycolysis model.

We derived a rate law for a reversible enzyme-catalyzed reaction which is accurate also in cases when the common Michaelis–Menten expression for the same reaction fails; this was achieved by applying the first order ZDP analytically to the mass action kinetic expressions of this reaction. We also showed that the computation times for numerical integration over a model of the phosphotransferase system (PTS) could be substantially reduced by numerical application of ZDP and the resulting time courses approximated those of the original model with high accuracy. The approximations of SIMs resulting from the application of ZDP also provided simplified views of the dynamics, contributing to further insight into the behavior of the system. In particular, these manifolds demonstrated that the reaction rates in the PTS exhibit an interesting collective behavior: certain rates assume the same magnitudes during the slow phase, independent of the initial conditions.

6.3 Comparison of the balancing and ZDP approaches

The two types of simplification approaches studied in this thesis, based on balancing and ZDP, respectively, are of essentially different nature. As already mentioned, balancing is a linear method while ZDP a nonlinear one. Consequently, the former requires linearization of the biochemical model which for the often highly nonlinear models in biochemistry may yield inaccurate results, as demonstrated in Chapter 2. Further, because balancing originates from control theory, it is applicable to models for which input and output functions are defined and it aims at approximating a map from the input to the output. The state variables of the resulting, simpler model are linear combinations of the old state variables, which are formed by balancing the reachability and observability Grammians such that the degrees of reachability and observability of the new state variables in the balanced system become equal. Hence, the structure of the biochemical reaction network is not recognizable from the simpler model. The ZDP method is applicable to models defined solely by the ODEs describing the dynamics of the state variables, without input and output. Reduction methods deriving from the field of dynamical systems, such as the ZDP, aim at approximating the dynamics of the state variables instead of the map from input to output. The state variables in a model reduced by ZDP is a subset of the state variables in the full model and approximations of the eliminated state variables are provided in terms of algebraic expressions. Reduction by ZDP hence preserves the biochemical network structure.

In addition to the application of ZDP to a biochemical network as a whole by formulating algebraic equations that define a SIM and then employing these relations to obtain the dynamics on this SIM, we have demonstrated that simplification may also be performed by application of ZDP-based rate laws to describe the kinetics of enzymatic reactions—in this setting, the ZDP is used implicitly. Naturally, also then, the method is applicable to models without input and output variables and the network structure is preserved, *i.e.*, the variables in the resulting model are again a subset of the original state variables.

Another difference between the two methods is that the ZDP requires the decomposition of the state into one fast and one slow component while balancing, on the other hand, does not require any other *a priori* information than the model itself. The decomposition of the state vector is typically based on experience stemming from experiments and, possibly also, from simulations of the model. Such an approach has efficaciously been used for the determination of the fast variables as a preparation for the quasi-steady state approximation (QSSA), widely used in biochemistry. For ZDP, the decomposition should be based on the same considerations as those employed for QSSA: a slow component which is suitable for QSSA is also expected to be suitable for ZDP.

In spite of the differences between the two methods with respect to the types of models that they are formulated for, they may both be applied to the same biochemical ODE models if, in the case of applying balancing and truncation, input and output functions are added to the model. The suitability of addition of input and output variables to a biochemical model differs depending on the purpose of the model. For models used in traditional engineering sciences, *i.e.*, the models that balancing mainly has been applied to, the choice of input and output variables is often relatively straight-forward: *e.g.*, for a model used for the cruise control of a car, the obvious input is the torque of the engine and the output the speed of the car. For biochemical models, on the contrary, this choice is often much less obvious. In biochemistry, the aim is often to understand the behavior of a system. The output variables should then be the variables that are of interest to study, *e.g.*, variables that are of high importance for the biological function performed by the system. Which these variables are is often not known *a priori*; one way to define the output is then to define all state variables as output variables. In these situations, *i.e.*, when understanding is the aim, the input variables should be chosen as variables that depend on environmental changes. In biochemical models, a large fraction of the parameters may have this property and could hence all be chosen as input variables. The use of input and output variables in this situation however becomes somewhat artificial, although possible, and employment of models without input and output may then perhaps be preferred.

There are however also cases when the choice of input and output variables for biochemical systems may be much more natural than in the situation discussed above. This may be the case when the model describes an experimental system: the parameters varied in the experiment may be modeled as input and the experimentally measured variables as output. In summary, the suitability of the presence of input and output differs depending on the aim of the model and, consequently, the sets of cases to which the two methods treated in this thesis are applicable differ slightly but overlap.

For the balancing approach, we used a model of the glycolysis in yeast for the demonstration of the method since this model is thoroughly validated and hence highly realistic. When later choosing a realistic model for the demonstration of the ZDP approach, we found that the same glycolysis model was less suitable for this purpose: in the glycolyis model, the two slowest eigenvalues only differed by a factor 3, which indicates that there is no one-dimensional SIM in this model or, at best, a very weakly attractive one; a comparison of one-dimensional ZDP manifolds with trajectories of the model indeed showed that none of these manifolds was attractive (we investigated

all the 13 possible ZDP_1 manifolds). A similar analysis showed that this model has a two-dimensional SIM which attracted trajectories, although this attraction visually was relatively unclear. For the demonstration of the ZDP approach, we preferred to work with a model with a clearly attractive one- or two-dimensional manifold in order to make the presentation transparent and to reduce computational costs associated with tabulation of the manifold. Hence, we decided to work with the PTS model, which has a distinct one-dimensional SIM and which also is a well validated and highly realistic model. In order to enable a more accurate comparison of the performance in approximating time courses between the two reduction approaches, balancing and ZDP, it could be of interest to make this comparison for the same model; this however falls outside the scope of this thesis.

6.4 Relating our work on balancing to work by others

The method of balancing and truncation has been applied previously to biochemical models in an article by Liebermeister *et al* which appeared whilst our work was performed [80]; our work on this method however focuses on other issues than that article did.

In our work on balancing in Chapter 2, we put substantial focus on the idea behind the method, which we described in much detail for a biochemical readership (an issue not treated in [80]). In particular, we describe the notion of 'importance for the dynamics', *i.e.*, the property that the reduction method aims to preserve in the reduced model, in terms of input and output energies. To the best of our knowledge, this theory has earlier only been available in more mathematical/theoretical literature.

We also focus much on the biochemical interpretation of the linear combinations that define the balanced variables in terms of the importance of the various metabolites for the dynamics of the pathway—a major reason that we put much emphasis on the theory behind the reduction method, as the theory should assist in the interpretation of these linear combinations. The issue of the importance of the various state variables was also treated in [80], although much less focus was devoted to it there. The analysis approach used in that article differed from ours in that it was based on the coefficients of the inverse of the transformation matrix in stead of the transformation matrix itself that we used; the authors did not discuss the interpretation of their approach. The model to which this analysis was applied was a model of the glycolysis (of an unspecified organism) constructed using a network structure obtained from the KEGG database and by assuming mass action kinetics and setting all kinetic constants equal to 1. The model that we investigated was a model of the glycolysis in yeast which was based on experimental measurements of the enzyme kinetics and kinetic constants [122] and hence likely a more realistic model. Further, in [80], 1 input and 2 output variables were used in the analysis. We have also earlier performed our analysis using only few input and output variables [51, 14], since in engineering applications such small numbers of inputs and outputs is common practice. However, later we discovered that the weighting of the variables depends much on the choice of input and output variables and, therefore, in order to investigate the biochemical importance of the various state variables for the over-all dynamics of the

yeast glycolysis model that we studied, we used all the 13 state variables as output variables, and all the 92 parameters as input variables in our analysis in Chapter 2. The high accuracy of the reduced model that we constructed by eliminating the variables that were estimated as least important by our analysis supports the adequacy of this choice.

In [80], a methodology was presented of splitting a biochemical model into two modules denoted the subsystem and the environment, and of defining the input variables as the concentrations of metabolites on the boundary between the two modules and the output variables as the reaction rates on this boundary; the idea was to reduce the environment module by linearization, balancing, and truncation, while keeping the subsystem module as it is, as an alternative to approximating the environment by constant values. The authors illustrated their procedure on a model of a reaction chain with four state variables. This model was arbitrarily divided into a subsystem and an environment module, each containing two state variables. The environment module was replaced by a linear model with one state variable obtained by linearization, balancing and truncation of this module. The resulting model thus contained three coupled state variables: two (pertaining to the subsystem) dictated by the original, nonlinear dynamics and one (representing the environment) following linear dynamics. It was shown that the dynamics of the two state variables in the subsystem is accurately reproduced by this coupled model.

In our work, we instead investigated the performance of the method of linearization, balancing, and truncation for the realistic model of glycolysis in yeast [122], which has 13 state variables. Our results show that the application of linearization to this model however resulted in a highly inaccurate reduced system. Similar issues with inaccuracy were observed for several sets of input and output variables and also for the slightly simpler, yet realistic model of the PTS. These results suggest that the linearization of realistic, complex biochemical models is unsatisfactorily inaccurate.

The high accuracy of the reduced model obtained by reduction of the environment module of the simple reaction chain in [80] raises the question whether the modularization approach used in that article would be suitable also for larger, more realistic biochemical models. In our reduced model of glycolysis in yeast the pyruvate concentration becomes negative when the input deviates by 40% from its reference level (Figure 2.2B); this result indicates that coupling this model to a model of *e.g.* the citric acid cycle (in which a derivate of pyruvate, acetyl CoA, enters) may give less accurate results than modeling pyruvate as a constant in that model. This fact suggests that the modularization approach would be inappropriate in this case, at least for perturbations of the input of 40% or more from its reference level. Our results hence suggest that the method of linearization, balancing and truncation has to be used with caution when applied to realistic biochemical models, also when the modularization approach of [80] is to be taken.

6.5 Future perspectives

The theory of balancing has been extended to the nonlinear case; this work was pioneered in 1993 by Scherpen [107] and since then many results on the topic have

been reported, *e.g.* [35, 36, 37, 38, 48, 73, 90, 108]. Nevertheless, computational issues remain and for the complex models that occur in systems biology these methods are not yet practicable. These methods may however become interesting for reduction of biochemical systems when further developed.

In this thesis we have shown that the ZDP may be used for simplification of biochemical models in several different ways. Several aspects of this method and its biochemical findings are of interest to explore further. Rate laws based on ZDP may be developed for other reaction mechanisms than the reversible enzyme-catalyzed reaction with one substrate and one product considered in this thesis. The numerical calculation of SIMs by ZDP may be used to explore the slow dynamics in other biochemical systems than the PTS studied here. In particular, it is of interest to investigate whether the collectivization of the rates that we observed in the PTS also occurs in other systems. It is also of interest to explore how this collective behavior arises from the interactions between the molecules and to understand in more depth how it depends on parameter values and model structure. Further, this behavior—which shows that the slow dynamics of the rates is simpler than it possibly could be in the sense that rates within the same collective are attracted to the same low-dimensional curves in stead of each rate being attracted to a different curve—suggests simplification of the model based on this information; algebraic constraints obtained by setting the rate expressions of the reaction rates within each collective equal to each other may be employed to reduce the model. Such a reduction approach may be nearly as simple as the well-known QSSA (which is equivalent to zeroth order ZDP) while even more accurate than first-order ZDP since an assumption of equal rates may be even closer to reality than the ZDP condition.

6.6 An outlook on systems biology: as simple as possible, but not simpler

The complexity of biochemical models has increased enormously since the first simple models of enzyme kinetic reactions appeared in the beginning of the twentieth century [56, 88, 12] and today most biochemical models contain dozens—the largest models thousands—of dynamic variables [19, 28, 58, 91, 111]. The complexity of the models that appear still increases rapidly: only during the period that the doctoral studies presented in this thesis have been performed (from 2005 until now), the complexity of the models that have appeared has increased significantly and this development is seemingly not about to stagnate—rather the opposite seems to be the case due to the continuous accumulation of biological data that needs to be understood.

In contrast to the complex models in systems biology, the mathematical models used in physics have contained relatively few variables, often only a couple, or at least less than a dozen. There, the paradigm of Occam's razor has been prevailing—complexity should not be incorporated into a model unless necessary—and this strategy has been successful. The question may arise whether biochemical models then need to be so complex: after all, these systems consist of the same type of matter and follow the same scientific laws as physical systems. Furthermore, systems biology partly uses scientific methods common with physics, *i.e.*, formulation of general

principles and quantitative laws [136]; why not also make the models as simple as possible? Indeed, the idea of Occam's razor has been applied to biological systems, often without motivation but accepted due to its paradigmatic status in physics; however, simple models have proven inappropriate as compared to more complex ones when comparing their outcome to the now available high-dimensional data [29, 136]. The reason for this is that life—*i.e.*, the object under study—is inherently complex. As was outlined in the Introduction to this thesis, a minimum of more than 300 genes is required for life [31, 42]. Accordingly, complex models are seemingly necessary in systems biology. These issues on complexity versus simplicity are discussed in Westerhoff *et al* [136].

It goes without saying that biochemical models, although complex, should not be made unnecessarily complex—in this sense Occam's razor is applied also in systems biology. However, when 'as simple as possible' amounts to hundreds of variables in order to account for environmental regulations and various special cases, Occam's razor as a paradigm loses impact. In [136], a new paradigm in systems biology, replacing Occam's razor, was proposed: based on the requirement of 300 genes for life, it is argued that a model describing the interactions of less than 300 genes is less likely to be true and complete than one including more than 300 genes.

Because of the necessity of modeling biological systems with complex models, the question of how to deal with these models is gaining increasing attention and ways to simplify them are investigated [59, 120, 125]. The issue of simplification of biochemical models is however paradoxical: as was argued above, much information needs to be included in the biological models in order for them to make sense. On the other hand, although complexity is needed to describe the inherently complex biological systems, there is seemingly also complexity in these systems which is not always necessary for understanding certain aspects of their biological function. For instance, as was demonstrated in Chapter 5 of this thesis, much of the dynamics in the virtually 13-dimensional PTS takes place in one single dimension and an interesting collective behavior of the reaction rates was discovered when zooming in on this dimension. Examples of well-known methods that have contributed to the construction of simplified views of biochemical systems already for a couple of decades are metabolic control analysis [17, 54] and flux balance analysis [8, 127].

Systems biology is a relatively new field that constantly changes in focus and there is not yet a roadmap, or recipe, telling how to perform this science, analogous to the scientific method used in physics, although some approaches have been suggested [131, 136]. Hence, it remains to see which role simplifications will play in systems biology. Our expectation, shared by many others, is that their use will increase since the growing complexity of models and the accumulation of high-throughput data lead to an increasingly apparent need of understanding and possibly also an increasing need of reducing simulation times—the latter perhaps only temporarily as the speed of computers also develops at a fast pace. During a first phase, simplifications may also serve as indications as to where we should start to tackle the huge amount of information that is available; an example of an approach towards this end is given in [136] where the authors use flux balance analysis to investigate which reactions in the yeast metabolome are most important and hence should be examined first. Even at a later stage, when detailed, mechanistic models of entire cells are available, we

expect that simplifications will continue to play an important role in systems biology for the extraction of information from the complex models. Emergent properties from the interactions of thousands of molecules will not be possible to understand without simplifications that can elucidate different aspects of their dynamics. Simplifications may also become integrated into a future systems biology methodology, as a part of a spiraling loop between theory and practice, in order to render the biochemical models as simple as possible, but not simpler.

With this thesis, we—the author and her coworkers—hope to have provided some convincing examples of the usefulness of simplification of biochemical models.

Bibliography

[1] Antoulas AC (2005) *Approximation of large-scale dynamical systems.* Number DC06 in Advances in Design and Control. SIAM, Philadelphia.

[2] Bakker BM, Michels PAM, Opperdoes FR & Westerhoff HV (1997) Glycolysis in bloodstream form *Trypanosoma brucei* can be understood in terms of the kinetics of the glycolytic enzymes. *J Biol Chem* **272**, 3207–3215.

[3] Benner P, Quintana-Ortí ES & Quintana-Ortí G (2003) State-space truncation methods for parallel model reduction of large-scale systems. *Parallel Computing* **29**, 1701–1722.

[4] Bentley GE (2008) Biological timing: Sheep, Dr. Seuss, and mechanistic ancestry. *Curr Biol* **18**, R736–R738.

[5] Blüthgen N, Bruggeman FJ, Legewie S, Herzel H, Westerhoff HV & Kholodenko BN (2006) Effects of sequestration on signal transduction cascades. *FEBS J* **273**, 895–906.

[6] Bodenstein M (1913) Eine Theorie der photochemischen Reaktionsgeschwindigkeiten. *Z physik Chem* **85**, 329–397.

[7] Bodenstein M & Lütkemeyer H (1924) Die photochemische Bildung von Bromwasserstoff und die Bildungsgeschwindigkeit der Brommolekul aus den Atomen. *Z physik Chem* **114**, 208–236.

[8] Bonarius HPJ, Schmid G & Tramper J (1997) Flux analysis of underdetermined metabolic networks: The quest for the missing constraints. *Trends Biotech* **15**, 308–314.

[9] Boyde TRC (1980) *Foundation stones in biochemistry.* Voile et Aviron, Hong Kong.

[10] Boulware MJ & Marchant JS (2008) Timing in cellular Ca^{2+} signaling. *Curr Biol* **18**, R769–R776.

[11] Bowen JR, Acrivos A & Oppenheim AK (1963) Singular perturbation refinement to quasi-steady state approximation in chemical kinetics. *Chem Eng Sci* **18**, 177–188.

[12] Briggs GE & Haldane JB (1925) A note on the kinetics of enzyme action. *Biochem J* **19**, 338–339.

[13] Browning G & Kreiss H-O (1982) Problems with different time scales for nonlinear partial differential equations. *SIAM J Appl Math* **42**, 704–718.

[14] Bruggeman FJ, Härdin HM, van Schuppen JH & Westerhoff HV (2007) Silicon cell models: Construction, analysis, and reduction. In *Biosimulation in drug development* (Bertau M, Mosekilde E & Westerhoff HV, eds), pp. 403–423. Wiley–VCH, Weinheim, Germany.

[15] Bruggeman FJ, Snoep JL & Westerhoff HV (2008) Control, responses and modularity of cellular regulatory networks: a control analysis perspective. *IET Syst Biol* **2**, 397–410.

[16] Bruggeman FJ, Westerhoff HV, Hoek JB & Kholodenko B (2002) Modular response analysis of cellular regulatory networks. *J Theor Biol* **218**, 507–520.

[17] Burns JA, Cornish–Bowden A, Groen AK, Heinrich R, Kacser H, Porteous JW, Rapoport SM, Rapoport TA, Stucki JW, Tager JM, Wanders RJA & Westerhoff HV (1985) Control analysis of metabolic systems. *Trends Biochem Sci* **10**, 16.

[18] Calder MS & Siegel D (2008) Properties of the Michaelis–Menten mechanism in phase space. *J Math Anal Appl* **339**, 1044–64.

[19] Chen WW, Schoeberl B, Jasper PJ, Niepel M, Nielsen UB, Lauffenburger DA & Sorger PK (2009) Input–output behavior of ErbB signaling pathways as revealed by a mass action model trained against dynamic data. *Mol Syst Biol* **5**, 239.

[20] Chu D, Zabet NR & Mitavskiy B (2009) Models of transcription factor binding: Sensitivity of activation functions to model assumptions. *J Theor Biol* **257**, 419–429.

[21] Cornish–Bowden A (2004) *Fundamentals of enzyme kinetics (3rd. Ed.)*. Portland Press, London.

[22] Crick FHC (1958) On protein synthesis. *Symp Soc Exp Biol* **XII**, 139–163.

[23] Crick FHC (1970) Central dogma of molecular biology. *Nature* **227**, 561–563.

[24] Danø S, Madsen MF, Schmidt H & Cedersund G (2006) Reduction of a biochemical model with preservation of its basic dynamic properties. *FEBS J* **273**, 4862–4877.

[25] Debnam PM, Shearer G, Blackwood L & Kohl DH (2004) Evidence for channeling of intermediates in the oxidative pentose phosphate pathway by soybean and pea nodule extracts, yeast extracts, and purified yeast enzymes. *FEBS J* **246**, 283–290.

[26] Deutscher J, Francke C & Postma PW (2006) How phosphotransferase system-related protein phosphorylation regulates carbohydrate metabolism in bacteria. *Microbiol Mol Biol Rev* **70**, 939–1031.

[27] Einstein A (1934) On the method of theoretical physics. *Phil Science* **1**, 163–169.

[28] Feist AM, Henry CS, Reed JL, Krummenacker M, Joyce AR, Karp PD, Broadbelt LJ, Hatzimanikatis V & Palsson BØ (2007) A genome-scale metabolic reconstruction for *Escherichia coli* K-12 MG1655 that accounts for 1260 ORFs and thermodynamic information. *Mol Syst Biol* **3**, 121.

[29] Fell DA (2007) How can we understand metabolism? In *Systems biology: Philosophical foundations* (Boogerd FC, Bruggeman FJ, Hofmeyr J-HS & Westerhoff HV, eds), pp. 87–102. Elsevier, Amsterdam.

[30] Fowler S & Thomashow MF (2002) Arabidopsis transcriptome profiling indicates that multiple regulatory pathways are activated during cold acclimation in addition to the CBF cold response pathway. *The Plant Cell* **14**, 1675–1690.

[31] Fraser CM, Gocayne JD, White O, Adams MD, Clayton RA, Fleischmann RD, Bult CJ, Kerlavage AR, Sutton G, Kelley JM, Fritchman JL, Weidman JF, Small KV, Sandusky M, Fuhrmann J, Nguyen D, Utterback TR, Saudek DM, Phillipps CA, Merrick JM, Tomb JF, Dougherty BA, Bott KF, Hu P, Lucier TS, Peterson SN, Smith HO, Hutchison CA & Venter JC (1995) The minimal gene complement of *Mycoplasma genitalium*. *Science* **270**, 397–403.

[32] Frenzen CL & Maini PK (1988) Enzyme kinetics for a two-step enzymic reaction with comparable initial enzyme–substrate ratios. *J Math Biol* **26**, 689–703.

[33] de la Fuente A, Snoep JL, Westerhoff HV & Mendes P (2002) Metabolic control in integrated biochemical systems. *Eur J Biochem* **269**, 4399–4408.

[34] Friedmann HC (editor, 1981) *Enzymes*. Hutchinson Ross, Stroudburg, Pennsylvania.

[35] Fujimoto K & Scherpen JMA (2001) Balancing and model reduction for nonlinear systems based on the differential eigenstructure of Hankel operators. In *Proc 40th IEEE Conf on Decision and Control*, pp. 3253–3257.

[36] Fujimoto K & Scherpen JMA (2003) Nonlinear balanced realization based on singular value analysis of Hankel operators. In *Proc 42nd IEEE Conf on Decision and Control*, pp. 6072–6077.

[37] Fujimoto K & Scherpen JMA (2005) Nonlinear input-normal realizations based on the differential eigenstructure of Hankel operators. *IEEE Trans Automat Contr* **50**, 2–18.

[38] Fujimoto K & Tsubakino D (2007) Computation of nonlinear balanced realization and model reduction based on Taylor series expansion. *Systems & Control Letters* **57**, 283–289.

[39] Gao H, Wang Y, Liu X, Yan T, Wu L, Alm E, Arkin A, Thompson DK & Zhou J (2004) Global transcriptome analysis of the heat shock response of *Shewanella oneidensis*. *J Bacteriology* **186**, 7796–7803.

[40] Gear CW, Kaper TJ, Kevrekidis IG & Zagaris A (2005) Projecting to a slow manifold: Singularly perturbed systems and legacy codes. *SIAM J Appl Dyn Syst* **4**, 711–732.

[41] Gjuvsland AB, Plahte E & Omholt SW (2007) Threshold-dominated regulation hides genetic variation in gene expression networks. *BMC Syst Biol* **1**, 57.

[42] Glass JI, Assad-Garcia N, Alperovich N, Yooseph S, Lewis MR, Maruf M, Hutchison CA, Smith HO & Venter JC (2006) Essential genes of a minimal bacterium. *Proc Natl Acad Sci* **103**, 425–430.

[43] Glass L & Kauffman SA (1973) The logical analysis of continuous, non-linear biochemical control networks. *J Theor Biol* **39**, 103–129.

[44] Goldbeter A (2008) Biological rhythms: Clocks for all times. *Curr Biol* **18**, R751–R753.

[45] Gorban AN & Karlin IV (2005) *Invariant manifolds for physical and chemical kinetics.* Springer, Berlin.

[46] Gosset G, Zhang Z, Nayyar S, Cuevas WA & Saier MH Jr (2004). Transcriptome analysis of Crp-dependent catabolite control of gene expression in *Escherichia coli. J Bacteriology* **186**, 3516–3524.

[47] Guldberg CM & Waage P (1879). Concerning chemical affinity. *Erdmann's Journal für Practische Chemie* **127**, 69–114.

[48] Hahn J & Edgar TF (2002) An improved method for nonlinear model reduction using balancing of empirical gramians. *Comput Chem Eng* **26**, 1379–1397.

[49] Hairer E, Nørsett SPN & Wanner G (1987) *Solving ordinary differential equations I: Nonstiff problems.* Springer, Berlin.

[50] Hairer E & Wanner G (1991) *Solving ordinary differential equations II: Stiff and differential-algebraic problems.* Springer, Berlin.

[51] Härdin HM & van Schuppen JH (2006) System reduction of nonlinear positive systems by linearization and truncation. In *Positive systems—Proceedings of the second multidisciplinary symposium on positive systems: theory and applications (POSTA 06)* (C. Commault and N. Marchand, eds), pp. 431–438. Springer-Verlag, Berlin Heidelberg.

[52] Härdin HM, Zagaris A, Krab K & Westerhoff HV (2009) Simplified yet highly accurate enzyme kinetics for cases of low substrate concentrations. *FEBS J* **276**, 5491–5506.

[53] Hartwell LH, Hopfield JJ, Leibler S & Murray AW (1999) From molecular to modular cell biology. *Nature* **402**, C47-C52.

[54] Heinrich R, Rapoport SM & Rapoport TA (1977) Metabolic regulation and mathematical models. *Prog Biophys Mol Biol* **32**, 1–82.

[55] Heinrich R & Schuster S (1996) *The regulation of cellular systems.* Chapman and Hall, New York.

[56] Henri V (1902) Théorie générale de l'action de quelques diastases. *Comptes Rendus Hebdomadaires des Séances de l'Académie des Sciences de Paris* **135**, 916–919. Reprinted in pages 140–143 of [9] and in English translation in pages 130–135.

[57] Henri V (1903) *Lois générales de l'action des diastases.* Hermann, Paris. Pages 85–93 are reprinted in pages 258–266 of [34].

[58] Herrgård MJ, Swainston N, Dobson P, Dunn WB, Arga KY, Arvas M, Blüthgen N, Borger S, Costenoble R, Heinemann M, Hucka M, Le Novère N, Li P, Liebermeister W, Mo ML, Oliveira AP, Petranovic D, Pettifer S, Simeonidis E, Smallbone K, Spasić I, Weichart D, Brent R, Broomhead DS, Westerhoff HV, Kirdar BI, Penttilä M, Klipp E, Palsson BØ, Sauer U, Oliver SG, Mendes P, Nielsen J & Kell DB (2008) A consensus yeast metabolic network reconstruction obtained from a community approach to systems biology. *Nature Biotech* **26**, 1155–1160.

[59] Hlavacek WS (2009) How to deal with large models? *Mol Syst Biol* **5**, 240.

[60] Huang X, Holden HM & Raushel FM (2001). Channeling of substrates and intermediates in enzyme-catalyzed reactions. *Annu Rev Biochem* **70**, 149–180.

[61] Hynne F, Danø S & Sørensen PG (2001) Full-scale model of glycolysis in *Saccharomyces cerevisiae. Biophys Chem* **94**, 121–163.

[62] International Human Genome Sequencing Consortium (2004) Finishing the euchromatic sequence of the human genome. *Nature* **431**, 931–945.

[63] Kaper TJ (1999) An introduction to geometric methods and dynamical systems theory for singular perturbation problems. *Proc Sympos Appl Math* **56**, 85–131.

[64] Keizer J (1987) *Statistical thermodynamics of nonequilibrium processes.* Springer, Berlin.

[65] Kelley CT (1995) *Iterative methods for linear and nonlinear equations, Frontiers in applied mathematics 16.* SIAM Publications, Philadelphia. (Also available at http://www.siam.org/books/textbooks/fr16_book.pdf.)

[66] Kholodenko BN, Demin OV, Moehren G & Hoek JB (1999) Quantification of short term signaling by the epidermal growth factor receptor. *J Biol Chem* **274**, 30169–30181.

[67] King EL & Altman C (1956) A schematic method of deriving the rate laws for enzyme-catalyzed reactions. *J Phys Chem* **60**, 1375–1378.

[68] Kitano H (2001) *Foundations of systems biology.* The MIT Press, Camebridge, MA.

[69] Kitano H (2002) Systems biology: A brief overview. *Science* **295**, 1662–1664.

[70] Kofahl B & Klipp E (2004) Modelling the dynamics of the yeast pheromone pathway. *Yeast* **21**, 831–850.

[71] Kreiss H-O (1979) Problems with different time scales for ordinary differential equations. *SIAM J Numer Anal* **16**, 980–998.

[72] Kreiss H-O (1985) Problems with different time scales. In *Multiple Time Scales* (Brackbill JH & Cohen BI, eds), pp. 29–57. Academic Press, New York.

[73] Krener A (2006) Model reduction for linear and nonlinear control. The Bode Lecture in the *45th IEEE Conf on Decision and Control*.

[74] Laub AJ, Heath MT, Paige CC & Ward RC (1987) Computation of system balancing transformations and other application of simultaneous diagonalization algorithms. *IEEE Trans Automat Contr* **34**, 115–122.

[75] Larhlimi A & Bockmayr A (2009) A new constraint-based description of the steady-state flux cone of metabolic networks. *Discrete Applied Mathematics* **157**, 2257–2266.

[76] Lee E, Salic A, Krüger R, Heinrich R & Kirschner MW (2003) The roles of APC and axin derived from experimental and theoretical analysis of the Wnt pathway. *PLoS Biol* **1**, e10.

[77] van Leemput P, Vanroose W & Roose D (2007) Mesoscale analysis of the equation-free constrained runs initialization scheme. *Multiscale Model Simul* **6**, 1234–1255.

[78] Leloup J-C & Goldbeter A (2003) Toward a detailed computational model for the mammalian circadian clock. *Proc Natl Acad Sci* **100**, 7051–7056.

[79] Liao JC & Lightfoot EN Jr (1988) Lumping analysis of biochemical reaction systems with time scale separation. *Biotech Bioeng* **31**, 869–879.

[80] Liebermeister W, Baur U & Klipp E (2005) Biochemical network models simplified by balanced truncation. *FEBS J* **272**, 4034–4043.

[81] Lorenz EN (1980) Attractor sets and quasi-geostrophic equilibrium. *J Atmos Sci* **37**, 1685–1699.

[82] Maas U & Pope SB (1992) Simplifying chemical kinetics: Intrinsic low-dimensional manifolds in composition space. *Combustion and Flame* **88**, 239–264.

[83] Mease KD, Bharadwaj S & Iravanchy S (2003) Timescale analysis for nonlinear dynamical systems. *J Guidance Control Dyn* **26**, 318–330.

[84] Mease KD, Topcu U & Aykutlug E (2008) Characterizing two-timescale nonlinear dynamics using finite-time Lyapunov exponents and vectors. arXiv:0807.0239v1. Available at http://arxiv.org/abs/0807.0239

[85] van der Meer R, Westerhoff HV & Van Dam K (1980) Linear relation between rate and thermodynamic force in enzyme-catalyzed reactions. *BBA Bioenergetics* **591**, 488–493.

[86] Mendes P, Kell DB & Westerhoff HV (1992) Channelling can decrease pool size. *Eur J Biochem* **204**, 257–266.

[87] Moore BC (1981). Principal component analysis in linear systems: Controllability, observability, and model reduction. *IEEE Trans Automat Contr* **26**, 17–32.

[88] Michaelis L & Menten ML (1913) Die Kinetik der Invertinwirkung. *Biochem Z* **49**, 333–369.

[89] Morgunov I & Srere PA (1998) Interaction between citrate synthase and malate dehydrogenase: Substrate channeling of oxaloacetate. *J Biol Chem* **273**, 29540–29544.

[90] Newman AJ & Krishnaprasad PS (1998) Computation for nonlinear balancing. In *Proc 37th IEEE Conf on Decision and Control*, pp. 4103–4104.

[91] Nordling TEM, Hiroi N, Funahashi A & Kitano H (2007) Deduction of intracellular sub-systems from a topological description of the network. *Mol BioSyst* **3**, 523–529.

[92] O'Malley RE Jr (1991) *Singular perturbation methods for ordinary differential equations.* Springer, New York.

[93] Okino MS & Mavrovouniotis ML (1998) Simplification of mathematical models of chemical reaction systems. *Chem Rev* **98**, 391–408.

[94] Palsson BØ (2006) *Systems biology: Properties of reconstructed networks.* Camebridge University Press, New York.

[95] Park DJ (1974) The hierarchical structure of metabolic networks and the construction of efficient metabolic simulators. *J Theor Biol* **46**, 31–74.

[96] Postma PW, Lengeler JW & Jacobson GR (1993) Phosphoenolpyruvate:carbohydrate phosphotransferase systems of bacteria. *Microbiol Mol Biol Rev* **57**, 543–594.

[97] Reder C (1988) Metabolic control theory: A structural approach. *J Theor Biol* **135**, 175–201.

[98] Reich JG & Sel'kov EE (1981) *Energy metabolism of the cell.* Academic Press, Bristol, UK.

[99] Rohwer JM, Meadow ND, Roseman S, Westerhoff HV & Postma PW (2000) Understanding glucose transport by the bacterial phosphoenolpyruvate:glycose phosphotransferase system on the basis of kinetic measurements *in vitro*. *J Biol Chem* **275**, 34909–34921.

[100] Saavedra E, Marín-Hernández A, Encalada R, Olivos A, Mendoza-Hernández G & Moreno-Sánchez R (2007) Kinetic modeling can describe *in vivo* glycolysis in *Entamoeba histolytica*. *FEBS J* **274**, 4922–40.

[101] Salazar C & Höfer T (2000) Kinetic models of phosphorylation cycles: A systematic approach using the rapid-equilibrium approximation for protein–protein interactions. *Biosystems* **83**, 195–206.

[102] Sauro HM & Kholodenko BN (2004) Quantitative analysis of signaling networks. *Prog Biophys Mol Biol* **86**, 5–43.

[103] Savageau MA (1969) Biochemical systems analysis, I. Some mathematical properties of the rate law for the component enzymatic reactions. *J Theor Biol* **25**, 365–369.

[104] Savageau MA (1969) Biochemical systems analysis, II. The steady–state solutions for an n-pool system using a power-law approximation. *J Theor Biol* **25**, 370–379.

[105] Savageau MA (1970) Biochemical systems analysis, III. Dynamic solutions using a power-law approximation. *J Theor Biol* **26**, 215–226.

[106] Savageau MA (1976) *Biochemical systems analysis: A study of function and design in molecular biology.* Addison–Wesley, Reading, MA.

[107] Scherpen JMA (1993) Balancing for nonlinear systems. *Syst Contr Lett* **21**, 143–153.

[108] Scherpen JMA & Gray WS (2000) Minimality and local state decompositions of a nonlinear state space realization using energy functions. *IEEE Trans Automat Control* **45**, 2076–2086.

[109] Schmidt H, Madsen MF, Danø S & Cedersund G (2008) Complexity reduction of biochemical rate expressions. *Bioinformatics* **24**, 848–854.

[110] Schneider KR & Wilhelm T (2000) Model reduction by extended quasi-steady-state approximation. *J Math Biol* **40**, 443–450.

[111] Schoeberl B, Eichler–Jonsson C, Gilles ED & Müller G (2002) Computational modeling of the dynamics of the MAP kinase cascade activated by surface and internalized EGF receptors. *Nat Biotech* **20**, 370–375.

[112] Segel IH (1993) *Enzyme kinetics: behavior and analysis of rapid equilibrium and steady-state enzyme systems.* Wiley, New York.

[113] Segel LA (1988) On the validity of the steady state assumption of enzyme kinetics. *Bull Math Biol* **50**, 579–593.

[114] Segel LA (1972) Simplification and scaling. *SIAM Review* **14**, 547–571.

[115] Segel LA & Slemrod M (1989) The quasi-steady-state assumption: A case study in perturbation. *SIAM Review* **31**, 446–477.

[116] Shampine LF & Reichelt MW (1997) The MATLAB ODE suite. *SIAM J Sci Comput* **18**, 1–22.

[117] Schuster S, Kahn D & Westerhoff HV (1993) Modular analysis of the control of complex metabolic pathways. *Biophys Chem* **48**, 1–17.

[118] Small JR & Fell DA (1990) Covalent modification and metabolic control analysis: Modification to the theorems and their application to metabolic systems containing covalently modifiable enzymes. *Eur J Biochem* **191**, 405–411.

[119] Snoep JL, Bruggeman F, Olivier BG & Westerhoff HV (2006) Towards building the silicon cell: A modular approach. *Biosystems* **83**, 207–216.

[120] Surovtsova I, Sahle S, Pahle J & Kummer U (2006) Approaches to complexity reduction in a systems biology research environment (SYCAMORE). *Proc Wint Sim Conf* 1683–1689.

[121] Surovtsova I, Simus N, Lorenz T, König A, Sahle S & Kummer U (2009) Accessible methods for the dynamic time-scale decomposition of biochemical systems. *Bioinformatics* **25**, 2816–2823.

[122] Teusink B, Passarge J, Reijenga CA, Esgalhado E, van der Weijden CC, Schepper M, Walsh MC, Bakker BM, van Dam K, Westerhoff HV & Snoep JL (2000) Can yeast glycolysis be understood in terms of *in vitro* kinetics of the constituent enzymes? Testing biochemistry. *Eur J Biochem* **267**, 5313–5329.

[123] Teusink B, Walsh MC, Van Dam K & Westerhoff HV (1998) The danger of metabolic pathways with turbo design. *Trends Biochem Sci* **23**, 162–169.

[124] Turányi T, Tomlin AS & Pilling MJ (1993) On the error of the quasi-steady-state approximation. *J Phys Chem* **97**, 163–172.

[125] Vallabhajosyula RR & Sauro HM (2006) Complexity reduction of biochemical networks. *Proc Wint Sim Conf* 2006, 1690–1697.

[126] Vandekerckhove C, van Leemput P & Roose D (2008) Accuracy and stability of the coarse time-stepper for a lattice Boltzmann model. *J Algor Comp Tech* **2**, 249–273.

[127] Varma A & Palsson BØ (1994) Metabolic flux balancing: Basic concepts, scientific and practical use. *Nature Biotech* **12**, 994–998.

[128] Visser D & Heijnen JJ (2002) The mathematics of metabolic control analysis revisited. *Metabol Eng* **4**, 114–123.

[129] Visser D & Heijnen JJ (2003) Dynamic simulation and metabolic redesign of a branched pathway using lin–log kinetics. *Metabol Eng* **5**, 164–176.

[130] Welch JJ, Watts JA, Vakoc CR, Yao Y, Wang H, Hardison RC, Blobel GA, Chodosh LA & Weiss MJ (2004) Global regulation of erythroid gene expression by transcription factor GATA-1. *Blood* **104**, 3136–3147.

[131] Westerhoff HV & Kell DB (2007) The methodologies of systems biology. In *Systems biology philosophical foundations* (Boogerd FC, Bruggeman FJ, Hofmeyr J-HS & Westerhoff HV, eds), pp. 23–70. Elsevier, Amsterdam.

[132] Westerhoff HV, Kolodkin A, Conradie R, Wilkinson SJ, Bruggeman FJ, Krab K, van Schuppen JH, Hardin H, Bakker BM, Moné MJ, Rybakova KN, Eijken M, van Leeuwen HJ & Snoep JL (2009) Systems biology towards life in silico: mathematics of the control of living cells. *J Math Biol* **58**, 7–34.

[133] Westerhoff HV, Koster JG, van Workum M & Rudd KE (1989) On the control of gene expression. In *Control of metabolic processes* (Cornish–Bowden A & Cardenas ML, eds), pp. 399–413. Plenum Press, New York.

[134] Westerhoff HV & Palsson BØ (2004) The evolution of molecular biology into systems biology. *Nat Biotech* **22**, 1249–1252.

[135] Westerhoff HV & Van Dam K (1987) *Thermodynamics and control of biological free-energy transduction.* Elsevier, Amsterdam.

[136] Westerhoff HV, Winder C, Messiha H, Simeonidis E, Adamczyk M, Verma M, Bruggeman FJ & Dunn W (2009) Systems Biology: The elements and principles of Life. *FEBS L* **583**, 3882–3890.

[137] Westermark PO & Lansner A (2003) A model of phosphofructokinase and glycolytic oscillations in the pancreatic β-cell. *Biophys J* **85**, 126–139.

[138] Zagaris A, Gear CW, Kaper TJ & Kevrekidis IG (2009) Analysis of the accuracy and convergence of equation-free projection to a slow manifold. *ESAIM: M^2AN*, **43**, 757–784.

[139] Zagaris A, Kaper HG & Kaper TJ (2005) Two perspectives on reduction of ordinary differential equations. *Mathematische Nachrichten* **278**, 1629–1642.

[140] Zagaris A, Vandekerckhove C, Gear CW, Kaper TJ & Kevrekidis IG. Stability and stabilization of the constrained runs schemes for equation-free projection to a slow manifold. In preparation.

[141] Zobeley J, Lebiedz D, Kammerer J, Ishmurzin A & Kummer U (2005) A new timedependent complexity reduction method for biochemical systems. *Trans Comp Syst Biol* **1**, 90–110.

[142] JWS Online is a database for biochemical models accessible at http://jjj.biochem.sun.ac.za/database/index.html.

Summary

Mathematical modeling and analysis of biochemical systems contribute to a better insight in the functional properties of cellular networks, facilitate drug development, and assist in experimental design. Many of the models used are relatively simple, because they have been made with as few assumptions as possible according to the idea of Occam's razor and with the objective to make them tractable by simple mathematics. In recent years however, the development of more realistic models of much higher complexity has been stimulated due to the improved understanding of the components of inherently complex biochemical systems and the development of experimental techniques to verify the models. Indeed, the great advance of biochemistry and molecular biology enabling the understanding of how individual macromolecules work, together with the advances in functional genomics enabling the identification, quantification and purification of virtually all molecules of any living organism, are now increasing the pressure to take the ultimate step to understand the molecular basis of the functioning of organisms. Such understanding should be founded on realistic models of all the components of living organisms together (so-called silicon cells/organisms). The high complexity of the already existing exemplars of parts of such realistic models however often hampers the understanding of what they model and restrains the mathematical analysis. Indeed, a complete realistic model of reality is not yet the understanding of that reality. Mathematical analyses to achieve simplified descriptions of the dynamics are amongst the tools that help such understanding. In this thesis we explore methods to make the realistic biochemical models as tractable as possible while aiming for an accurate description of the complex behavior of the biochemical systems.

The work presented in this thesis concerns two main approaches towards the simplification of biochemical models. First, we study one of the best-known reduction methods deriving from the area of control theory, consisting of so-called balancing and truncation. This is a linear method, *i.e.* it is applicable to linear models only and the resulting simpler models are also linear. This method has been widely used for reduction of models in other sciences but its application to biochemical models has not been explored much. The second method, which the main part of the work in this thesis is related to, is a nonlinear method (*i.e.*, applicable to and resulting in nonlinear models) based on the so-called zero-derivative principle (ZDP). This method has been applied to only few models before, mainly for theoretical analysis and demonstration of the method. In this thesis we develop a framework for the use of this method in a biochemical and systems biological context.

Balancing and truncation is a method which is applicable to models which are formulated in terms of dynamic input and output variables in addition to the state variables, *i.e.*, the dynamic variables that describe the state of the system. Balancing is the reformulation of a model in terms of new state variables that are linear combinations of the old ones such that the new model, expressed in these new variables, achieves certain properties: the so-called reachability and observability Grammians of the model, *i.e.*, the matrices pertaining to the maps from input to state and state to output, respectively, become equal and diagonal, with the eigenvalues arranged in decreasing order. This implies that the new state variables become ordered according to their importance for the dynamics of the map from input to output. The truncation is the subsequent elimination of those variables that have least importance for this dynamics. In Chapter 2 we apply this method to a realistic nonlinear model of glycolysis in yeast with 13 state variables. Since the method is a linear method, the glycolysis model had to be linearized, *i.e.* approximated by a linear model. This approximation however resulted in relatively large errors when comparing the time courses of the linear model with those of the original, nonlinear one. We then employed information obtained implicitly from the balancing procedure to estimate the importance of the state variables for the dynamics of the model. Because the analysis was based on linearization, which had proved to yield inaccurate time courses, we performed the analysis at several points of linearization in order to account for possible effects of the nonlinearities. We found, in particular, that the state variables representing the concentrations of NADH and acetaldehyde have little influence on the dynamics of the model. Reducing the nonlinear model by approximating these state variables by their steady state values resulted in a nonlinear reduced model which accurately approximates the original model. Apparently, information obtained from analysis of ill-fitting linear models can still be of use in designing good non-linear approximations of the original models.

In Chapters 3–5 we treat simplifications obtained by implementing the ZDP. These simplifications are based on the fact that biochemical systems often exhibit a large variety of timescales at which the various processes in the system proceed: certain processes change very quickly during a short initial phase while others are almost stagnant. At the end of this phase, the initially fast variables have slowed down and in the view of the fast timescale, the state resembles a steady state although still changing, but now at the slow timescale. In the state space, this behavior amounts to attraction of trajectories by a low-dimensional manifold (subspace) on which the dynamics is slow, a so-called slow invariant manifold (SIM). As a consequence of this behavior, the system spends a large part of the time close to the SIM and, therefore, simplified models describing only the dynamics on this manifold would assist to approximate the behavior of the system. Simplifications of this type are not new to biochemistry; the same idea rests behind the quasi-steady-state approximation (QSSA) which has been widely used in biochemistry for almost a century. The QSSA has been used to derive the well-known enzyme kinetic rate laws of Michaelis–Menten type from mass action kinetics. These rate laws are highly useful for the modeling of enzymatic reactions in cases when the concentration of the enzyme is much lower than that of its substrate since the timescale separation is large under this condition. However, *in vivo*, this condition often does not hold and the timescale separation is

only moderate. The ZDP method is an extension of the QSSA which provides high accuracy, also in the cases when the timescale separation is moderate.

The ZDP is the principle of setting the time derivatives of any given order of the state variables that change quickly during the short initial phase, equal to zero. The resulting set of algebraic equations defines a manifold in the state space which is an approximation of a SIM. A simplified model is given by the differential equations that describe the dynamics of the slow state variables together with these algebraic constraints for the fast variables. The zeroth order ZDP, *i.e.*, the condition obtained from setting the first-order time derivatives to zero, is equivalent with the QSSA. The use of higher order derivatives provides higher accuracy of the approximation of the SIM and of the simplified system.

In Chapter 3 we first outline the behavior of systems exhibiting timescale disparities and we describe the theory of ZDP for a biochemical readership. We then apply first-order ZDP (*i.e.* the case when second derivatives are set to zero) to the mass action kinetic expressions for a reversible reaction and derive an enzyme kinetic rate law. We show that under conditions of realistic yet low substrate concentrations, the Michaelis–Menten rate expression may readily be off by more than a factor of four when predicting the variation of concentrations with time while our first-order ZDP based kinetics gives a much more accurate description of the true enzyme dynamics.

We then use ZDP to explore the dynamics in a model of the phosphotransferase system (PTS) involved in glucose uptake, metabolism, and signalling in enteric bacteria. This model has nine state variables. We find that this system can be understood accurately in terms of the behavior of a single state variable with the remaining eight constrained to follow that behavior, a clear example of an extensive simplification of a complex system without loss of understanding. The one-dimensional SIM in this model was given by eight algebraic equations which were hard to solve analytically and hence we determined the SIM numerically. We also employed this manifold to integrate numerically over the reduced model and in this way reduce the simulation time by a factor between 5 and 25, depending on the initial condition, as compared to integrating with a standard stiff integrator over the full model. The algorithm that we developed for the numerical calculation of approximations of SIMs based on ZDP, which uses Newton's method to solve for points on the manifolds over a grid, is described in Chapter 4 where also the Mathematica code is provided.

In Chapter 5 we further explore the slow dynamics of the PTS by investigating the values of the reaction rates along the manifolds. We find that the rates in this network exhibit a behavior which is much simpler than it could have been: the rates are partitioned into collectives within each of which all rates assume the same magnitude during the slow phase, while rates belonging to different collectives assume different magnitudes. Such relaxation behavior of the rates was observed also upon a large variety of perturbations of the parameter set albeit other constitutions of the collectives was obtained. These results indicate that grouping of the rates is likely to be encountered for different environmental conditions and, also, in other signal transduction pathways possessing structures similar to that of the PTS. Moreover, the difference between the constitutions of the collectives suggests that biological evolution may have involved this behavior in the regulation of cell function. The observed behavior also suggests new reduction procedures that utilize inherent, possibly functional sim-

plicity of the system and calls for further investigations in order to understand the dynamics in more depth.

In summary, the simplification approaches taken in this thesis facilitate the handling of the realistic, complex models in systems biology in several different ways. One issue that we have approached is the need of new rate laws to describe the cellular reaction mechanisms for which traditional enzyme kinetics is inappropriate. We derived a rate law based on ZDP for a reversible enzyme-catalyzed reaction which describes the reaction kinetics accurately also in cases of low substrate concentrations when the traditional enzyme kinetics fails to describe the dynamics; rate laws for other mechanisms which hold under similar conditions may be derived by the same principle. We also addressed the issue of long computation times. In particular, we showed that for the model of the PTS, we reduced the times it takes to integrate over the model, substantially. Last, and perhaps most importantly, we demonstrated that simplified models may contribute to further insight into the unintuitive dynamics of complex biochemical systems: we explored the behavior on different timescales in the PTS and we found that the rates in this pathway exhibit an interesting relaxation behavior on the slow timescale.

Samenvatting in het Nederlands

De Nederlandse vertaling van de titel van dit proefschrift is:

Biologische complexiteit hanteren:
zo eenvoudig mogelijk maar niet eenvoudiger

Wiskundig modelleren van biochemische systemen en wiskundige analyse van de modellen dragen bij tot een beter inzicht in de functionele eigenschappen van cellulaire netwerken, vergemakkelijken de ontwikkeling van geneesmiddelen en helpen bij het ontwerpen van experimenten. Veel van de gebruikte modellen zijn betrekkelijk eenvoudig, doordat ze gemaakt zijn met zo min mogelijk veronderstellingen volgens het principe van Ockhams scheermes, en met het doel hanteerbaar te zijn middels eenvoudige wiskunde. In de afgelopen jaren echter, heeft de ontwikkeling van meer realistische modellen van veel hogere complexiteit een impuls gekregen, door het verbeterde inzicht in de componenten van inherent complexe biochemische systemen en door de ontwikkeling van experimentele technieken om de modellen te verifiëren. Inderdaad, de belangrijke vooruitgang in de biochemie en de moleculaire biologie op het gebied van de werking van individuele macromoleculen, samen met de recente ontwikkelingen in de functionele genomica die de identificatie, kwantificatie en zuivering van vrijwel alle moleculen van elk levend organisme mogelijk maken, voeren nu de druk op om de uiteindelijke stap te maken inzicht te verkrijgen in de moleculaire grondslag van de werking van organismen. Zulk inzicht moet worden gebaseerd op realistische modellen van alle componenten van levende organismen tezamen (zogeheten silicon cells/organisms). De hoge complexiteit van de reeds bestaande voorbeelden van delen van dergelijke realistische modellen, belemmert echter vaak het begrip van wat zij modelleren en beperkt de mogelijkheden tot wiskundige analyse. Inderdaad, een volledig realistisch model van de werkelijkheid is nog niet hetzelfde als volledig inzicht in die werkelijkheid. Wiskundige analyses om vereenvoudigde beschrijvingen van de dynamica te krijgen, zijn middelen die helpen bij het verkrijgen van zulk inzicht. In dit proefschrift onderzoeken we methoden om de realistische biochemische modellen zo hanteerbaar mogelijk te maken, terwijl tegelijkertijd wordt gestreefd naar een nauwkeurige beschrijving van het complexe gedrag van de biochemische systemen.

Het in dit proefschrift gepresenteerde werk betreft twee methoden voor de vereenvoudiging van biochemische modellen. Ten eerste onderzoeken we een van de bekendste reductiemethoden die voortkomt uit de regeltheorie, die bestaat uit balanceren en afsnijden. Dit is een lineaire methode, d.w.z. zij is alleen van toepassing op lin-

eaire modellen en de daaruit voortkomende eenvoudigere modellen zijn ook lineair. Deze methode wordt veelvuldig gebruikt voor de reductie van modellen in andere wetenschappen, maar naar de toepassing op biochemische modellen is nog niet veel onderzoek gedaan. De tweede methode, waaraan het grootste deel van het werk in dit proefschrift gerelateerd is, is een niet-lineaire methode (d.w.z. van toepassing op en resulterend in niet-lineaire modellen), gebaseerd op het zogenaamde nuldifferentiaalquotiëntprincipe (NDP). Deze methode is eerder toegepast op slechts enkele modellen, voornamelijk voor theoretische analyse en illustratie van de methode. In dit proefschrift ontwikkelen we een kader voor het gebruik van deze methode in een biochemische en systeembiologische context.

Balanceren en afsnijden is een methode die van toepassing is op modellen die geformuleerd zijn in termen van dynamische ingangs- en uitgangssignalen in aanvulling op de toestandsvariabelen, d.w.z. de dynamische variabelen die de toestand van het systeem beschrijven. Balanceren is de herformulering van een model in termen van nieuwe toestandsvariabelen die lineaire combinaties zijn van de oude, zodanig dat het nieuwe model, uitgedrukt in deze nieuwe variabelen, aan bepaalde eigenschappen voldoet: de zogenaamde regelbaarheids- en waarneembaarheids-Gram-matrices van het model, d.w.z. de matrices die betrekking hebben op de afbeeldingen van ingangssignaal naar toestand en van toestand naar uitgangssignaal respectievelijk, worden gelijk aan elkaar en diagonaal, met de eigenwaarden gerangschikt in dalende volgorde. Hieruit volgt dat de nieuwe toestandsvariabelen worden geordend in volgorde van hun mate van belangrijkheid voor de dynamica van de afbeelding van ingangs- naar uitgangssignaal. Het afsnijden is de daaropvolgende eliminatie van de variabelen die het minst belangrijk zijn voor deze dynamica. In Hoofdstuk 2 passen we deze methode toe op een realistisch model van de glycolyse in gist met 13 toestandsvariabelen. Doordat de methode een lineaire methode is, moest het glycolysemodel gelineariseerd worden, d.w.z. benaderd worden door een lineair model. Deze benadering resulteerde echter in relatief grote fouten, d.w.z. grote verschillen tussen het verloop in de tijd van het lineaire model en dat van het oorspronkelijke model. Vervolgens hebben we de informatie die impliciet was verkregen uit het proces van balanceren, gebruikt om de mate van belangrijkheid van de toestandsvariabelen voor de dynamica van het model in te schatten. Omdat de analyse was gebaseerd op linearisatie, welke methode het verloop in de tijd onnauwkeurig bleek te beschrijven, hebben we om rekening te houden met eventuele gevolgen van de niet-lineariteiten, het systeem gelineariseerd in verschillende punten in de toestandsruimte en de analyse vervolgens uitgevoerd op deze gelineariseerde systemen. We hebben in het bijzonder geconstateerd dat de toestandsvariabelen die de concentraties van NADH en aceetaldehyd beschrijven, weinig invloed hebben op de dynamica van het model. Reductie van het niet-lineaire model door deze toestandsvariabelen te benaderen met hun stabiele-toestandswaarden, leidde tot een gereduceerd model dat het oorspronkelijke model nauwkeurig benadert. Blijkbaar kan informatie die verkregen wordt uit het analyseren van slecht fittende lineaire modellen, toch bruikbaar zijn voor het ontwerpen van goede niet-lineaire benaderingen van de oorspronkelijke modellen.

In de Hoofdstukken 3–5 behandelen we vereenvoudigingen die verkregen zijn door toepassing van het NDP. Deze vereenvoudigingen zijn gebaseerd op het feit dat biochemische systemen vaak grote verschillen in tijdschalen vertonen waarop de verschil-

lende processen in het systeem voortschrijden: sommige processen veranderen zeer snel gedurende een korte initiële fase, terwijl andere vrijwel stilstaan. Aan het eind van deze fase zijn de aanvankelijk snelle variabelen langzamer geworden en lijkt de toestand vanuit het oogpunt van de snelle tijdschaal een stabiele toestand te zijn geworden, alhoewel het systeem dan nog steeds verandert, maar nu op de langzame tijdschaal. In de toestandsruimte komt dit gedrag neer op aan aantrekkingskracht van banen door een laagdimensionale variëteit (deelruimte) waarop de dynamica traag is, een zogenaamde langzame invariante variëteit (LIV). Als een gevolg van dit gedrag bevindt het systeem zich een groot deel van de tijd in de buurt van de LIV; daardoor zouden vereenvoudigde modellen die alleen de dynamica op deze variëteit beschrijven, helpen om het gedrag van het systeem te benaderen. Vereenvoudigingen van deze soort zijn niet nieuw voor de biochemie; hetzelfde idee ligt ten grondslag aan de quasi-steady-state benadering (QSSB), die al bijna een eeuw veelvuldig gebruikt wordt in de biochemie. De QSSB is gebruikt bij het afleiden van de welbekende enzymkinetische snelheidsuitdrukkingen van Michaelis–Menten-type uit de massawerkingskinetiek. Deze snelheidsuitdrukkingen zijn zeer nuttig voor het modelleren van enzymatische reacties in gevallen waarin de concentratie van het enzym veel lager is dan die van zijn substraat, doordat het verschil in tijdschalen groot is onder deze voorwaarde. Niettemin, *in vivo* is deze voorwaarde vaak niet vervuld en is het verschil in tijdschalen slechts matig. De NDP-methode is een uitbreiding van de QSSB die hoge nauwkeurigheid biedt, ook in de gevallen waarin het verschil in tijdschalen matig is.

Het NDP is het principe van het nulstellen van de tijdsafgeleiden van een gegeven orde van de toestandsvariabelen die snel veranderen tijdens de korte initiële fase. Het resulterende stelsel van algebraïsche vergelijkingen omschrijft een variëteit in de toestandsruimte die een benadering van een LIV is. Een vereenvoudigd model wordt gegeven door de differentiaalvergelijkingen die de dynamica van de langzame toestandsvariabelen beschrijven, tezamen met deze algebraïsche vergelijkingen voor de snelle variabelen. Het NDP van nulde orde, d.w.z. de voorwaarde verkregen door de tijdsafgeleide van eerste orde gelijk aan nul te stellen, is equivalent met de QSSB. Het gebruik van afgeleiden van hogere orde biedt een hogere nauwkeurigheid van de benadering van de LIV en van het vereenvoudigde systeem.

In Hoofdstuk 3 schetsen we eerst het gedrag van systemen die verschillen in tijdschalen vertonen en beschrijven we de theorie van NDP voor een biochemisch publiek. Vervolgens passen we NDP van eerste orde (d.w.z. het geval waarin de tweede afgeleiden gelijk aan nul worden gesteld) toe op de massawerkingskinetische uitdrukkingen voor een omkeerbare reactie en leiden we een enzymkinetische snelheidsuitdrukking af. We tonen aan dat, onder voorwaarden van realistische maar lage substraatconcentraties, de Michaelis–Menten-formule snel meer dan een factor vier kan afwijken bij het voorspellen van de variatie van concentraties in de tijd, terwijl onze kinetiek gebaseerd op NDP van eerste orde, een veel nauwkeurigere beschrijving geeft van de werkelijke enzymdynamica.

We gebruiken vervolgens NDP om de dynamica te onderzoeken in een model van het fosfotransferasesysteem (FTS), dat betrokken is bij de opname van glucose, metabolisme en het seinen in darmbacteriën. Dit model heeft negen toestandsvariabelen. We zien dat dit systeem nauwkeurig beschreven kan worden in termen van

het gedrag van een enkele toestandsvariabele, terwijl de resterende acht dat gedrag volgen, een duidelijk voorbeeld van een verregaande vereenvoudiging van een complex systeem zonder verlies van begrip. De ééndimensionale LIV in dit model werd gegeven door acht algebraïsche vergelijkingen die moeilijk analytisch opgelost konden worden; daarom hebben we de LIV numeriek berekend. We hebben deze variëteit ook gebruikt om numeriek te integreren over het vereenvoudigde model en op deze manier de simulatietijd te verkorten met een factor tussen de 5 en de 25, afhankelijk van de begintoestand, in vergelijking met integratie over het volle model met een standaard stiff integrator. Het algoritme dat we hebben ontwikkeld voor de numerieke berekening van benaderingen van LIVen gebaseerd op NDP, dat gebruikmaakt van de methode van Newton om punten op de variëteiten te bepalen over een rooster, wordt beschreven in Hoofdstuk 4, waar ook de Mathematica-code ter beschikking wordt gesteld.

In Hoofdstuk 5 onderzoeken we de langzame dynamica van het FTS verder door de waarden van de reactiesnelheden op de variëteiten te bekijken. We zien dat de snelheden in dit netwerk een gedrag vertonen dat veel eenvoudiger is dan het had kunnen zijn: de snelheden kunnen worden ingedeeld in groepen waarbinnen alle snelheden dezelfde waarde aannemen tijdens de langzame fase, terwijl snelheden die behoren tot verschillende groepen, verschillende waarden aannemen. Dit relaxatiegedrag van de snelheden werd ook geobserveerd voor een grote verscheidenheid aan veranderingen in de parameterverzameling, hoewel andere groepsindelingen verkregen werden. Deze resultaten duiden erop dat dit relaxatiegedrag waarschijnlijk voorkomt onder verschillende milieuomstandigheden en ook in andere signaaltransductiesystemen die structuren hebben die vergelijkbaar zijn met die van het FTS. Bovendien suggereert het verschil in groepsindelingen dat biologische evolutie dit gedrag met zich mee heeft gebracht in de regulatie van de celfunctie. Het geobserveerde gedrag suggereert ook nieuwe vereenvoudigingsprocedures die gebruikmaken van inherente, mogelijk functionele eenvoud van het systeem en pleit voor verder onderzoek om de dynamica diepgaander te begrijpen.

Samenvattend, de vereenvoudigingsmethoden die behandeld zijn in dit proefschrift, vergemakkelijken het hanteren van de realistische, complexe modellen in de systeembiologie in verschillende opzichten. Een kwestie die we hebben besproken, is de noodzaak van nieuwe snelheidsuitdrukkingen om de cellulaire reactiemechanismen te beschrijven waarvoor traditionele enzymkinetiek ongeschikt is. We hebben een snelheidsuitdrukking gebaseerd op NDP afgeleid voor een omkeerbare enzymreactie die de reactiekinetiek nauwkeurig beschrijft, ook in gevallen van lage substraatconcentraties wanneer de traditionele enzymkinetiek er niet in slaagt de dynamica te beschrijven; snelheidsuitdrukkingen voor andere mechanismen die onder dezelfde voorwaarden gelden, kunnen worden afgeleid met behulp van hetzelfde principe. We hebben ook de kwestie van lange berekeningstijden behandeld. In het bijzonder hebben we voor het FTS-model laten zien, dat we de tijden die nodig zijn om over het model te integreren, aanzienlijk hebben verlaagd. Als laatste, en misschien wel belangrijkste, hebben we laten zien dat vereenvoudigde modellen kunnen bijdragen aan verder inzicht in de onintuïtieve dynamica van complexe biochemische systemen: we hebben het gedrag op verschillende tijdschalen onderzocht in het FTS-model en we hebben gezien dat de

snelheden in dit systeem een interessant gegroepeerd gedrag vertonen op de langzame tijdschaal.

Sammanfattning på svenska

Den svenska översättningen av titeln till denna avhandling är

Hantering av biologisk komplexitet:
så enkelt som möjligt men inte enklare

Matematisk modellering och analys av biokemiska system bidrar till bättre förståelse för funktionella egenskaper hos dessa system samt är till nytta för experimentell design och läkemedelsutveckling. Många biokemiska modeller är relativt enkla eftersom de har konstruerats med så få antaganden som möjligt i enlighet med Ockhams rakkniv och med målsättningen att göra dem matematiskt lätthanterliga. De senaste åren har dock utvecklingen av mer realistiska och därmed mycket mer invecklade modeller stimulerats på grund av den ökade kunskapen om komponenterna i de komplexa biokemiska systemen, samt utvecklingen av experimentella tekniker som kan verifiera modellerna. De stora framstegen inom biokemi och molekylärbiologi, som bidragit till förståelse för hur individuella makromolekyler fungerar, i kombination med framstegen inom funktionell genomik, vilka möjliggjort identifiering, kvantifiering och rening av i stort sett alla molekyler som förekommer i levande organismer, ökar nu trycket för att ta det avgörande steget till att förstå den molekylära grunden för hur organismer fungerar. En sådan förståelse bör baseras på realistiska modeller som beskriver hur komponenterna hos levande organismer samverkar (så kallade silicon cells/organisms). Nu befintliga modeller – som utgör delar av sådana kompletta, realistiska modeller – är dock ofta så invecklade att det är svårt att förstå vad de modellerar och att matematiskt analysera dem. Med andra ord, en realistisk modell av verkligheten är i sig inte tillräcklig för att förstå verkligheten. En typ av verktyg som dock kan bidra till förståelse är matematiska metoder som ger förenklade beskrivningar av dynamiken i modellerna. I denna avhandling undersöker vi metoder för att göra de realistiska biokemiska modellerna så begripliga och lätthanterliga som möjligt medan vi samtidigt inriktar oss på att försöka få en noggrann beskrivning av det komplexa beteendet hos de biokemiska systemen.

Arbetet som presenteras i denna avhandling rör två olika typer av förenkling av biokemiska modeller. Först studerar vi den mest kända reduktionsmetoden inom reglerteknik vilken består av så kallad balansering och trunkering. Detta är en linjär metod, dvs den kan tillämpas enbart på linjära modeller och de resulterande enklare modellerna är också linjära. Denna metod har använts i stor utsträckning för att reducera modeller inom många vetenskaper; dess tillämpning på biokemiska mod-

eller har dock endast skett i mycket liten omfattning. Den andra metoden, vilken huvuddelen av arbetet i denna avhandling handlar om, är en icke-linjär metod (dvs tillämpbar på och resulterande i icke-linjära modeller) som baseras på den så kallade noll-derivata-principen (NDP). Denna metod har endast applicerats på ett fåtal modeller tidigare och då i huvudsak i teoretiskt syfte och för demonstration av metoden.

Balansering och trunkering är en metod som kan appliceras på modeller som är formulerade i termer av dynamiska in- och utsignaler. Balansering är omformuleringen av en modell i termer av nya tillståndsvariabler, som är linjärkombinationer av de gamla, på så sätt att den nya modellen, uttryckt i dessa nya variabler, erhåller vissa egenskaper: de så kallade nåbarhets- och observerbarhetsgrammianerna för modellen (vilka är matriser relaterade till avbildningar från insignaler till tillståndsvariabler respektive från tillståndsvariabler till utsignaler) blir lika och diagonala med egenvärdena i dalande ordning. Detta resulterar i att de nya tillståndsvariablerna ordnas efter deras betydelse för dynamiken hos avbildningen från insignal till utsignal. Trunkering är den påföljande elimineringen av de variabler som har minst betydelse för denna dynamik. I Kapitel 2 tillämpar vi denna metod på en realistisk icke-linjär modell med 13 tillståndsvariabler som beskriver glykolysen i jästceller. Eftersom metoden är linjär var det nödvändigt att linjärisera den olinjära glykolysmodellen, dvs approximera den med en linjär modell. Detta resulterade dock i ett relativt stort fel, dvs en stor skillnad mellan den linjära modellen och originalmodellen vad det gällde simuleringsresultat. Vi använde sedan information som vi erhållit implicit vid balanseringen för att uppskatta betydelsen av de olika tillståndsvariablerna för modellens dynamik. Eftersom denna analys var baserad på linjärisering, som ju hade visat sig resultera i oprecisa simuleringar, upprepade vi analysen vid flera tillstånd för att ta möjliga effekter av olinjäriteter i beaktande. Vi fann speciellt att tillståndsvariablerna som representerade koncentrationer av NADH och acetaldehyd hade liten påverkan på modelldynamiken. Reducering av den icke-linjära modellen, genom att approximera dessa tillståndsvariabler med dess värden vid stationärt tillstånd, resulterade i en icke-linjär reducerad modell som noggrant approximerar originalmodellen. Detta visar att information som erhållits vid analys av dåligt anpassade linjära modeller likväl kan vara till användning för att bilda bra icke-linjära approximationer av originalmodellen.

I Kapitel 3–5 behandlar vi förenklingar baserande på NDP. Denna familj av metoder utnyttjar det faktum att biokemiska system ofta uppvisar stora skillnader mellan de tidsskalor på vilka de olika processerna i systemet framskrider: vissa processer framskrider väldigt fort under en kort initial fas, medan andra nästan står still. I slutet av denna fas har de initialt snabba variablerna saktat in och från den snabba tidsskalans perspektiv liknar tillståndet ett stationärt tillstånd, fastän det fortfarande förändras, men nu i ett långsammare tempo. I tillståndsrummet motsvaras detta beteende av att trajektorier attraheras mot en lågdimensionell mångfald (ett delrum) på vilken dynamiken är långsam, en så kallad långsam invariant mångfald (LIM). Som en konsekvens av detta beteende tillbringar systemet en stor del av tiden nära LIMen; förenklade modeller som beskriver dynamiken på denna mångfald kan därför användas för att approximera beteendet hos systemet. Förenklingar av detta slag är inte nya inom biokemi; samma idé ligger bakom den så kallade quasi-steady-state-approximationen (QSSA) vilken har använts vida inom biokemi under nästan ett århundrade. QSSA har använts för att härleda de välkända enzymkinetiska hastighet-

suttrycken av Michaelis-Menten-typ från kinetiska uttryck givna av massverkans lag. Michaelis-Menten-uttrycken är mycket användbara för modellering av enzymatiska reaktioner i de fall då koncentrationen av enzymet är mycket lägre än den av dess substrat eftersom tidsskaleseparationen är stor under denna betingelse. Ofta uppfylls dock inte detta villkor *in vivo* och tidsskaleseparationen är då endast måttlig. Den NDP-baserade metod som vi behandlar här är en utvidgning av QSSA; denna metod tillhandahåller hög noggrannhet, även i de fall då tidsskaleseparationen är måttlig.

NDP är principen att sätta tidsderivator (av någon given ordning) av vissa tillståndsvariabler lika med noll; de tidsvariabler vars derivator sätts till noll är de som förändras snabbt under den korta initiala fasen. Den resulterande mängden av algebraiska ekvationer definierar en mångfald i tillståndsrummet vilket är en approximation av en LIM. Dessa algebraiska ekvationer, tillsammans med de differentialekvationer som beskriver dynamiken hos de långsamma tillståndsvariablerna, utgör en förenklad modell av systemet. Nollte ordningens NDP, dvs det villkor som fås då första ordningens derivator sätts till noll, är ekvivalent med QSSA. Användningen av högre ordningens derivator resulterar i högre noggrannhet hos approximationen av LIMen och av den förenklade modellen.

I Kapitel 3 skissar vi först beteendet hos system med tidsskaleseparation och beskriver teorin bakom NDP för en läsekrets med bakgrund inom biokemi/systembiologi. Sedan använder vi första ordningens NDP (dvs fallet då andraderivator sätts till noll) för att förenkla massverkanskinetiska uttryck för en reversibel reaktion och härleda ett enzymkinetiskt hastighetsuttryck. Vi visar att då substratkoncentrationen är låg, dock fortfarande realistisk, kan Michaelis-Menten-ekvationen slå fel med en faktor fyra medan vår första ordningens NDP-baserade kinetik ger en noggrann beskrivning av den sanna enzymdynamiken.

Vi använder sedan NDP för att undersöka dynamiken hos en modell av fosfotransferassystemet (FTS) involverat i glukosupptag, metabolism och signalering i bakterier. Denna modell har nio tillståndsvariabler. Vi finner att detta system kan förstås i termer av beteendet hos en enda tillståndsvariabel med de övriga åtta tvingade att följa det beteendet – ett tydligt exempel på en omfattande förenkling av ett komplext system utan att gå miste om förståelse. Den endimensionella LIMen i denna modell gavs av åtta algebraiska ekvationer vilka var svåra att lösa analytiskt varför vi istället beräknade LIMen numeriskt. Vi använde denna mångfald för att numeriskt integrera över den reducerade modellen och på detta sätt minska simuleringstiden med en faktor 5 till 25, beroende på initialvillkoret, i jämförelse med att lösa den fulla modellen med en styv differentialekvationslösare. Den NDP-baserade algoritm som vi utvecklade för numerisk beräkning av approximationer av LIMer, vilken använder Newtons metod för att beräkna punkter på mångfalderna för en given mängd av värden för de långsamma variablerna, beskrivs i Kapitel 4 där även Mathematica-koden ges.

I Kapitel 5 fortsätter vi att utforska den långsamma dynamiken hos FTS genom att undersöka värdena av reaktionshastigheterna längsmed mångfalderna. Vi finner att hastigheterna i detta system uppvisar ett beteende som är mycket enklare än vad det kunde ha varit: hastigheterna är uppdelade i grupper och inom var och en av dessa antar alla hastigheter samma värde under den långsamma fasen, medan hastigheter som tillhör olika grupper kan anta olika värden. Detta grupperingsbeteende hos hastigheterna observerades även för ett stort antal perturbationer av parametermäng-

den ehuru andra grupperingar då erhölls. Dessa resultat indikerar att gruppering av reaktionshastigheterna troligen kan äga rum under varierande miljöförhållanden samt att detta grupperingsbeteende även skulle kunna förekomma i andra signaltransduktionsnätverk med strukturer liknande FTSs struktur. Vidare tyder skillnaderna mellan konstitutionen av grupperna på att biologisk evolution kan ha involverat detta beteende i regleringen av cellfunktion. Det observerade beteendet öppnar även upp för nya reduktionsmetoder som utnyttjar den inbyggda, möjligtvis funktionella, enkelheten hos systemet samt inbjuder till vidare utforskning av systemet för att mer ingående förstå dess dynamik.

Sammanfattningsvis underlättar förenklingsmetoderna utvecklade i denna avhandling hanteringen av realistiska, komplexa modeller inom systembiologi på flera olika sätt. En fråga som vi har behandlat är behovet av hastighetsuttryck för att beskriva de cellulära reaktionsmekanismer för vilka traditionella enzymkinetiska hastighetsuttryck inte är lämpliga. Vi härledde ett enzymkinetiskt uttryck baserat på NDP för en reversibel enzym-katalyserad reaktion som med hög noggrannhet beskriver reaktionskinetiken även i fall då substratkoncentrationen är låg och traditionell enzymkinetik inte lyckas beskriva dynamiken; hastighetslagar för andra mekanismer som gäller under liknande betingelser kan härledas utifrån samma princip. Vi har också behandlat problemet med långa beräkningstider. Särskilt visade vi att simuleringstiden för FTS-modellen kunde reduceras avsevärt med hjälp av ZDP. Till sist, och kanske av mest betydelse, demonstrerade vi att förenklade modeller kan bidra till bättre insikt i den långtifrån intuitiva dynamiken hos komplexa biologiska system: vi utforskade beteendet hos FTS på olika tidsskalor och fann att hastigheterna i detta reaktionsnätverk uppvisar ett intressant grupperingsbeteende på den långsamma tidsskalan.

Acknowledgements

I would like to thank a number of people that have been involved in the work behind this thesis. First of all, I want to thank my advisors Hans, Jan, Klaas, and Antonios for giving me the opportunity to perform this interesting project. It has been a privilege to work with advisors from different backgrounds, contributing to this interdisciplinary project with expertise from their respective fields. I am also very grateful to NWO for providing the financial means for this project.

I would also like to thank our secretary Jeannet, my colleague Marijke, and my paranimfs and good friends Tim and Katja for their helpfulness with practical issues during the preparation of this thesis. Tim has also helped me out with the Dutch translation of the summary of this thesis, which I am very grateful for. My father has given me useful comments on the Swedish translation of the summary. I also want to cordially thank everybody at the MCF department at the VU and my colleagues at CWI for interesting scientific discussions, help with many practical things, and for making my PhD years in Amsterdam really enjoyable and unforgettable.

I would also like to express my gratitude to Bo Wahlberg and Elling Jacobsen for enabling me to work at the Automatic Control Lab at KTH during my visits to Stockholm. I am also grateful to Camilla and Torbjörn for our inspiring scientific discussions and to the whole group for the nice company.

Also many people outside work have helped me much with the work on this thesis, directly or indirectly. Tim, Jens, Marieke, Maria, Ilona, Vincent, and many other friends in the Netherlands have helped me with both practical and work-related matters, but in particular they have helped me to take my mind off from work and contributed to make my years as a PhD student in Amsterdam a beautiful time to remember. My Swedish friends Eva, Sara, Sarangi, and Johanna, my aunts Sonja and Eva, my cousins, and many other friends and relatives have given me enormously much support during these years. Vivi, thank you for making my father happier, your joy and helpfulness has made also me happier and has facilitated the work on this thesis. Marre and pappa, I very much appreciate our open discussions that help me to develop my thoughts. Thanks also for consideration, support and help during the years. I am also indescribably grateful to my mother for everything she has given me, for her interest in what I have done, and for the patience, consideration, and love she showed me. Although she is not here anymore she has played a major role in the work on this thesis, because what she gave me remains vivid inside of me and helps to guide me in what I am doing.